A HIERARCHICAL MULTISCALE APPROACH TO HISTORY MATCHING AND OPTIMIZATION FOR RESERVOIR MANAGEMENT IN MATURE FIELDS

A Dissertation

by

HAN-YOUNG PARK

Submitted to the Office of Graduate Studies of
Texas A&M University
in partial fulfillment of the requirements for the degree of

DOCTOR OF PHILOSOPHY

August 2012

Major Subject: Petroleum Engineering

A Hierarchical Multiscale Approach to History Matching and Optimization for Reservoir Management in Mature Fields

A HIERARCHICAL MULTISCALE APPROACH TO HISTORY MATCHING AND OPTIMIZATION FOR RESERVOIR MANAGEMENT IN MATURE FIELDS

A Dissertation

by

HAN-YOUNG PARK

Submitted to the Office of Graduate Studies of
Texas A&M University
in partial fulfillment of the requirements for the degree of

DOCTOR OF PHILOSOPHY

Approved by:

Chair of Committee,	Akhil Datta-Gupta
Committee Members,	Michael J. King
	Eduardo Gildin
	Yalchin Efendiev
Head of Department,	A. Daniel Hill

August 2012

Major Subject: Petroleum Engineering

ABSTRACT

A Hierarchical Multiscale Approach to History Matching and Optimization for Reservoir Management in Mature Fields. (August 2012)

Han-Young Park, B.S., Hanyang University, Seoul, Korea;

M.S., Texas A&M University, College Station, Texas, USA

Chair of Advisory Committee: Dr. Akhil Datta-Gupta

Reservoir management typically focuses on maximizing oil and gas recovery from a reservoir based on facts and information while minimizing capital and operating investments. Modern reservoir management uses history-matched simulation model to predict the range of recovery or to provide the economic assessment of different field development strategies. Geological models are becoming increasingly complex and more detailed with several hundred thousand to million cells, which include large sets of subsurface uncertainties. Current issues associated with history matching, therefore, involve extensive computation (flow simulations) time, preserving geologic realism, and non-uniqueness problem. Many of recent rate optimization methods utilize constrained optimization techniques, often making them inaccessible for field reservoir management. Field-scale rate optimization problems involve highly complex reservoir models, production and facilities constraints and a large number of unknowns.

We present a hierarchical multiscale calibration approach using global and local updates in coarse and fine grid. We incorporate a multiscale framework into hierarchical updates: global and local updates. In global update we calibrate large-scale parameters to match global field-level energy (pressure), which is followed by local update where we match well-by-well performances by calibration of local cell properties. The inclusion of multiscale calibration, integrating production data in coarse grid and successively finer grids sequentially, is critical for history matching high-resolution geologic models through significant reduction in simulation time.

For rate optimization, we develop a hierarchical analytical method using streamline-assisted flood efficiency maps. The proposed approach avoids use of complex optimization tools; rather we emphasize the visual and the intuitive appeal of streamline method and utilize analytic solutions derived from relationship between streamline time of flight and flow rates. The proposed approach is analytic, easy to implement and well-suited for large-scale field applications.

Finally, we present a hierarchical Pareto-based approach to history matching under conflicting information. In this work we focus on multiobjective optimization problem, particularly conflicting multiple objectives during history matching of reservoir performances. We incorporate Pareto-based multiobjective evolutionary algorithm and Grid Connectivity-based Transformation (GCT) to account for history matching with conflicting information.

The power and effectiveness of our approaches have been demonstrated using both synthetic and real field cases.

DEDICATION

I dedicate this dissertation to my beloved family: Hyunmi, Jiwon, and Chanmin.

ACKNOWLEDGEMENTS

I would like to show my greatest appreciation to my academic advisor, Dr. Akhil Datta-Gupta, for his continuous enlightenment, trust, academic guidance, and financial support. His remarkable knowledge and insightful view have guided me to successfully complete this work.

I would like to express sincere gratitude to Dr. Michael J. King for his inspiring ideas and valuable advice. Deepest gratitude is also due to the members of the committee, Dr. Eduardo Gildin and Dr. Yalchin Efendiev, for their valuable comments and suggestions that have shaped this dissertation.

I am so grateful for my colleagues and all senior graduate friends with whom I have worked at Texas A&M University, especially MCERI group friends; Jonguk Kim for motivating me to this study and his friendship, Jichao Yin for his assistance and co-work on technical papers, Eric Bhark, Alvaro Rey, Mohan Sharma, Song Du, Jiang Xie, Satyajit Taware, Jeongmin Kim, Suksang Kang, Zheng Zhang, Shingo Watanabe, Yanbin Zhang, Shusei Tanaka, Dongjae Kam, Changdong Yang, Jichao Han, Peerapong Ekkawong, Feyisayo Olalotiti-Lawal for their assistance and for making my graduate years memorable.

My special thanks go to my supervisors and colleagues in KOGAS, especially Dr. Myeongnam Kim, Heungbog Lee, Yunsaeng Kim, and Jungho Park for their encouragement and support that really helped me in completion of this work.

Lastly, I wish to express my love and gratitude to all my beloved families including my parents in law; for their understanding and endless love, through the duration of my studies.

NOMENCLATURE

GA = Genetic algorithm

RSM = Response surface methodology

DOE = Design of experiments, experimental design

$\mathbf{m}_i$ = A genome of model multipliers

T = Temperature in heat-bath algorithm

S_w = Water saturation

F_w = Fractional flow of water

$\Delta\tilde{\mathbf{t}}$ = Optimal generalized travel time (GTT) shift

$\delta\mathbf{R}$ = Permeability update needed in local update

$\mathbf{S}$ = Sensitivity matrix of GTT w.r.t. permeability

$\mathbf{L}$ = Second spatial-difference operator

β_1 = Weight for norm penalty term in LSQR

β_2 = Weight for roughness penalty term in LSQR

PV_c = Pore volume for coarse cell

PV_f = Pore volume for fine cell

K_c = Permeability for coarse cell

K_f = Permeability for fine cell

$TRANX_c$ = Transmissibility in X-direction for coarse cell

$TRANX_f$ = Transmissibility in X-direction for fine cell

$\bar{\tau}_{ij}$ = Average total TOF for the connection between well i and j

α_{ij} = Global update coefficient for the connection between well i and j

β_{ij} = Local update coefficient for the connection between well i and j

q_{ij} = Total flux for the connection between well i and j

$n_{sl,ij}$ = Number of streamlines for connecting well i and j

τ_{ijk} = k^{th} streamline' total TOF in the connection between well i and j

α_{ijk} = k^{th} streamline's global update coefficient in the connection between well i and j

α_{ijl} = l^{th} streamline's global update coefficient in the connection between well i and j

S_{ij} = Sensitivity coefficient: changes in arrival time at producer i with respect to change in flow rate of well j

$N_{fsl,i}$ = Number of fast streamlines between well i and j

S_w = Water saturation, fraction

S_{wf} = Water flood front saturation, fraction

f_w = Fractional flow, dimensionless

$\boldsymbol{S}$ = Parameter space

O = Objective space

$\forall$ = Logic symbol meaning 'for all'

$\exists$ = Logic symbol meaning 'there exists'

$\wedge$ = Logic symbol meaning 'and'

$\mathbf{T_{ij}}$ = Trade-off between objective i an j

ω = Weight factor

TABLE OF CONTENTS

Page

Page

LIST OF FIGURES

Page

Page

Page

Page

Page

Page

CHAPTER I

INTRODUCTION AND STUDY OBJECTIVES

1.1 Introduction

The purpose of reservoir management is to maximize oil and gas recovery from a reservoir on the basis of facts and information while minimizing capital investment and operating expenses. Modern reservoir management using reservoir simulation model uses history matched model to predict the range of recovery or to provide the economic assessment of different field development strategies. Geologic models are becoming more complex with millions of grid cells where large sets of subsurface uncertainties including faults, flow channels, and barriers are embedded. Current issues about history matching are: extensive computation time associated with flow simulations, preserving geological realism, and non-uniqueness issues. Rate optimization is also receiving interests in the area of reservoir management, which is generally preceded by history matching. Most history matching and optimization problems in petroleum industry have several (potentially conflicting) objectives to be satisfied. These problems are typically treated as single objective optimization problem by aggregating all objectives into a scalar function resulting in incomplete exploration of the solution space. The motivation of this research is to develop novel and efficient approaches for history matching and rate optimization, specifically for large-scale application in mature fields and for handling conflicting multiobjectives.

This dissertation follows the style of *SPE Journal*.

1.2 Overview of History Matching and Rate Optimization

Reservoir simulation models are becoming more complex and detailed with several hundred thousand to millions cells. The full field models often consist of many wells and include decades of production history. The complexity of the models results in a large number of model parameters that are directly related to the problem of significant computational expense of deriving sensitivities of model parameters to production response. It often limits the use of assisted history matching techniques and application of probabilistic methods because of long simulation time. Excessive reservoir simulation run time is a key obstacle specifically for history matching such large and complex reservoir models.

There have been many studies related to reconciling high resolution geological models to production data. They can be classified broadly into three categories: gradient-based methods, sensitivity-based methods, and derivative-free methods. Gradient-based methods have been widely used for automatic history matching but it converges typically slow (Gill et al. 1981; McCormick and Tapia 1972). Sensitivity-based method uses computed sensitivities that are simply partial derivatives that define the change in production response because of small changes in reservoir parameters. Sensitivity-based methods have been known to be attractive because of faster convergence compared to gradient-based methods (Bissell et al. 1992). In particular, the streamline-assisted generalized travel time inversion (GTTI) technique has proven to be an efficient means for computing the parameter sensitivities (Cheng et al. 2005; Cheng et al. 2004; Datta-Gupta et al. 2001) because the sensitivities are obtained in a single forward simulation run. The GTTI history matching approach has been applied successfully to several field cases (Cheng et al. 2004; Hohl et al. 2006; Qassab et al. 2003; Rey et al. 2009). The derivative-free methods such as simulated annealing and genetic algorithms are relatively simple to implement but are limited to applications with small number of parameters because of the computational burden (Oliver et al. 2001).

Because reservoir simulation models deal with substantial modeling uncertainties, stochastic approaches are necessary to quantify the uncertainties using multiple realizations rather than generating one unique solution. Deterministic approach itself can be not sufficient for such complex reservoirs embedded with lots of uncertainties. If the initial model does not capture large-scale structural and stratigraphic features appropriately, the solution from the deterministic approach can result in unrealistic updates to the reservoir model. Stochastic search techniques have, therefore, become more popular in the history matching process to avoid the problem of convergence to local optimum nearest to the initial starting point (Cheng et al. 2008). Global search techniques include simulated annealing (SA) (Galassi et al. 2009; Kirkpatrick et al. 1983; Ouenes et al. 1994), Markov chain Monte Carlo (MCMC) (Ma et al. 2008; Sambridge and Mosegaard 2002) and genetic algorithms (GA) (Holland 1992) , which have been known to be effective for history matching problems (Bittencourt and Horne 1997; Floris et al. 2001; Romero and Carter 2001; Schulze-Riegert et al. 2002; Williams et al. 2004). Computational inefficiency is an issue for these methods because they require large number of flow simulation runs. It becomes computationally prohibitive for long simulation run times when the parameter space is very large and when the simulation run time is long.

In the sense, the use of multiscale approach has been getting much attention in both forward simulation and dynamic data integration because of its nature of computational efficiency. The multiscale history matching approach may start with the largest (coarser) scale and successively refines the grid to finer grid. In each stage, the parameters are adjusted to corresponding grid scale and are calibrated accordingly. Multiscale approach reduces the computational effort and/or improves the quality of the match as compared to history matching directly on the fine scale. Besides, the multiscale approach avoids solutions getting trapped in local minimum because of fewer parameters and decomposition by scale (Aanonsen 2008; Kim et al. 2010; Yoon et al. 2001).

In previous work (Yin et al. 2010), a hierarchical assisted history matching framework was demonstrated, which combines elements of both stochastic and

deterministic approaches to history match different levels of reservoir responses. At the first step, global parameters were calibrated to match reservoir response in terms of field pressures and cumulative liquid production using genetic algorithm. It was followed by local parameter calibration that uses a sensitivity-based model calibration for fine scale permeability changes to match flood front progression and individual well responses.

3-D streamlines provide an effective tool for reservoir management because of their ability to display reservoir flow and well connections in a physically intuitive manner. Streamlines have been extensively used to investigate the interaction between heterogeneity and well patterns and also for rate allocation and pattern balancing. More recently, streamlines have been used in conjunction with constrained optimization techniques for improving waterflood performance via rate control (Alhuthali et al. 2008). Field-scale rate optimization problems, however, involve highly complex reservoir models, production and facilities constraints and a large number of unknowns, making them inaccessible for routine waterflood management.

Most history matching and optimization problems in petroleum industry have multiple (or many) objectives to be satisfied. These objectives are potentially conflicting each other, often including dynamic data of the reservoir such as pressure and multiphase production data and 4D time-lapse seismic data, for example, acoustic impedance and saturation displacement. Those multiobjective problems are typically treated as single objective optimization problems by aggregating all objectives into a scalar function (weighted-sum) resulting in incomplete exploration of the solution space. The problem is particularly severe if the objectives are conflicting.

1.3 Objectives and Dissertation Outline

We will now outline the stages of this research and the specific objectives associated to each phase.

1.3.1 Hierarchical multiscale approach to history matching

In the first part of this dissertation, we propose a hierarchical multiscale calibration approach using global and local updates in multiscale grids. We closely follow a previously proposed approach (Cheng et al. 2008; Yin et al. 2010) of updating global and local parameters recursively, however, we incorporate multiscale approach where we integrate production data in coarse grids and finer grids sequentially. The proposed approach utilizes different levels of parameter space (global and local) and geometric space (coarse and fine). The inclusion of multiscale approach is critical to history matching large reservoir models in the sense that integration process in coarse grid allows for reduction of simulation time significantly, resulting in dramatic improvement of computational efficiency. Because there is much uncertainty in the large-scale static and dynamic parameters, we at first identify key parameters and calibrate those using an evolutionary algorithm. The global parameter calibration, matching and balancing field level energy, is followed by streamline assisted multiscale inversion to calibrate local parameter to match well by well production history. For local parameter calibration, we utilize a grid coarsening function embedded in commercial finite difference simulators to shorten simulation time significantly at a small loss of accuracy. Multi-dimensional penalized objective function is formed according to levels of coarsening, which facilitates minimization and avoids local minima. The proposed approach takes advantage of the multiscale framework in both simulation and inversion.

1.3.2 Hierarchical analytical approach to rate optimization

In the second part of this dissertation, we develop a rate optimization method using streamline-assisted time of flight and flux distribution maps. Streamline technologies have been widely used for reservoir management because of its powerful flow visualization capabilities that allow us to analyze rate allocation, pattern balance and waterflood performance. The connected flux volumes and its relative distribution can be

easily obtained in terms of allocation factors from the streamlines. We follow-up on the previous work of Alhuthali et al. (2007; 2010) and propose a rapid and easy to use method to optimize production/injection rates. The goal here is to avoid use of complex optimization tools; rather we emphasize the visual and the intuitive appeal of the streamline method. The basic underlying principle relies on two main ideas: (i) equalizing 'average time of flight' to all producers (ii) and minimizing the 'time of flight variance' within the streamline bundle. To accomplish this, we propose an easy to implement method for rate optimization utilizing streamline-based flood efficiency map. The main advantage of the proposed approach is that it is analytic, easy to implement and well-suited for large-scale field applications. Another advantage is its intuitive nature; we can visually examine the flow patterns as the calculations progress.

1.3.3 Hierarchical Pareto-based approach to history matching

In the third part of this dissertation, we propose to use a Pareto-based multi-objective evolutionary algorithm (MOEA) focusing on finding a set of optimal solutions during history matching of reservoir performances. Pareto-based techniques unlike aggregation-based technique make direct use of the dominance relation for fitness assignment, where actually Pareto ranks are used as a measure of success for finding good solutions instead of fitness score. For history matching purpose, we develop a Pareto-based multiobjective hierarchical history matching with Grid Connectivity-based Transformation (GCT) (Bhark, E.W. et al. 2011) technique. We use GCT basis coefficients as parameters for calibration using the gradient-free evolutionary optimization algorithm. The effectiveness of proposed approach is presented through applications to history matching of reservoir performances where 4D time-lapse seismic data (saturation displacement data) and production data have been matched.

1.4 Software Prototype

The primary deliverable of this work will be a software prototype called ‘DESTINY’ equipped with an improved history matching and optimization algorithms in conjunction with streamline tracing algorithms. The proposed methods in this dissertation such as multiscale streamline-assisted inversion and hierarchical production/injection rate optimization using flood efficiency maps are all implemented in this software. The object-oriented programming language (C++) is used and multiple attributes including well-based, reservoir objects are saved in a dynamic hierarchical framework. The developed graphical user interface (GUI) can be easily used to applications. The applications presented in this dissertation have been carried out using DESTINY. The more information about DESTINY, its instruction on how to use, and application examples are provided in appendix.

CHAPTER II

HIERARCHICAL MULTISCALE APPROACH TO HISTORY MATCHING

In this chapter, we present a hierarchical history matching approach in conjunction with multiscale inversion that follows a sequence of calibrations from global to local parameters in coarse and fine scales. We utilize grid coarsening to reduce total number of active cells and preserve flux distribution at small loss in accuracy but significant savings in computation time. First, we identify the heavy hitters in the large scale static and dynamic parameters and calibrate them using an evolutionary algorithm. This global parameter calibration, matching of regional and field level a reservoir energy, is followed by a streamline assisted multiscale inversion to match well by well production history by updating local parameters. Starting with coarse grid, we match the production data at the wells by gradually refining the reservoir grid. This multiscale data integration results in significant improvement in computation efficiency and an effective iterative minimization.

We have applied the proposed history matching strategy to an offshore carbonate field in India with about 300 wells and more than 25 years of production history. Regional oil and water production were first history matched by global coarse scale update. The global update greatly facilitated next step of local parameter calibration matching well bottom-hole pressure and water cut production history. Because streamline-assisted multiscale approach allows for parameter sensitivities to be computed analytically during simulation runs, it further improved a computational speed. History matching and model updating can be now accomplished in days rather than months. Most importantly, the updated models are found to be geologically consistent.

2.1 Introduction

Reservoir simulation models are becoming increasingly complex and more detailed with several hundred thousand to millions cells. Full field models very often consist of a large number of wells and decades of production history. The calibration of large number of model parameters is directly related to computational expenses associated with deriving sensitivities of model parameters to production response. It often limits the use of assisted history matching techniques. Long simulation run time is a key obstacle in history matching such large and complex reservoir models.

There are numerous studies in the literature related to reconciling high resolution geological models to production data. These can be classified broadly into three categories: gradient-based methods, sensitivity-based methods, and derivative-free methods. Gradient-based methods typically converge slowly (Gill et al. 1981; McCormick and Tapia 1972) but they have been widely used for automatic history matching; The derivative-free methods such as simulated annealing and genetic algorithms are simple to implement but limited to relatively small number of parameters because of the computational burden (Oliver et al. 2001). Sensitivity-based method uses computed sensitivities which are partial derivatives that define the change in production response because of small changes in reservoir parameters. Several techniques have been used for calculating the sensitivities: perturbation method, adjoint methods, and streamline-based sensitivities. The perturbation method is computationally prohibitive for large number of parameters. Adjoint methods (Li et al. 2003) use the optimal control theory and mathematically complex and typically require access to the source code of the forward simulator which may not be available (Rey et al. 2009). Streamline based sensitivities can be obtained very efficiently in a single forward simulation run. Sensitivity-based methods are generally attractive because of faster convergence compared to gradient-based methods (Bissell et al. 1992). The streamline-based generalized travel time inversion (GTTI) technique has proven to be an efficient means for computing the parameter sensitivities (Cheng et al. 2005; Cheng et al. 2004; Datta-

Gupta et al. 2001). The GTTI history matching approach has been applied successfully to several field cases (Cheng et al. 2004; Hohl et al. 2006; Qassab et al. 2003; Rey et al. 2009).

There is an increasing acknowledgement that because reservoir simulation model deals with lots of uncertainties, stochastic approaches are necessary to quantify the uncertainties using multiple realizations rather than relying on a single solution. It might be obvious that if the initial model does not capture large-scale structural and stratigraphic features appropriately, the solution can be unrealistic updates to the reservoir model. Stochastic search techniques have therefore become more popular in the history matching, particularly for identifying large-scale parameter uncertainties (Cheng et al. 2008). Global search techniques such as simulated annealing (SA) (Galassi et al. 2009; Kirkpatrick et al. 1983; Ouenes et al. 1994), Markov chain Monte Carlo (MCMC) (Ma et al. 2008; Sambridge and Mosegaard 2002) and genetic algorithms (GA) (Holland 1992) , have been successfully applied to history matching problems (Bittencourt and Horne 1997; Floris et al. 2001; Romero and Carter 2001; Schulze-Riegert et al. 2002; Williams et al. 2004). However, these techniques require typically a large number of simulation runs and can become computationally prohibitive if the parameter space is very large and the simulation run time is very long.

The use of multiscale approach is getting increased attention in both forward simulation and dynamic data integration for inverse problems. For history matching applications, Yoon et al. (2001) proposed a multiscale history matching method that starts with the largest scale and gradually progresses to finer grid. Use of optimal coarsening was proposed to streamline-assisted dual scale inversion by Kim et al. (2010). They reported significant savings in computational costs and avoidance of local minimum because of fewer parameters and decomposition by scale. However, although the history matching was done at coarse scale, they used the underlying fine-scale grid for forward simulation. Aanonsen (2008) showed that multiscale approach reduces the computational effort and/or improve the quality of the match as compared to history matching directly on the fine scale through synthetic examples. In his approach a

commercial history-matching tool which is based on gradient simulator with a Levenberge-Marquardt optimizer was used to minimize objective function. Taware et al. (2011) showed a practical approach for assisted history matching using grid coarsening where they reconstruct flux at fine scale from coarse scale in order to trace streamline along fine grid cells, and also compute sensitivities and model updates at the fine scale.

In a previous work Yin et al. (2010) demonstrated a hierarchical assisted history matching framework which combines elements of both stochastic and deterministic approaches to history match different levels of reservoir responses. First, global parameters were calibrated to match global reservoir response in field pressures and cumulative liquid production by use of genetic algorithm. It was followed by local parameter calibration which uses a sensitivity-based model calibration for fine scale permeability changes to match flood front progression and individual well responses.

In this dissertation we incorporate a multiscale framework to the previous work (Yin et al. 2010) for application to large reservoir models. Because of the orders to magnitude improvement in computation efficiency, the uncertainty can be explored in greater detail. The organization of this paper is as follows. First, we outline the procedure for the proposed hierarchical and multiscale approach with global and local updates. Next, we discuss background and mathematical formulation underlying our proposed method. We illustrate multiscale streamline-based inversion method with the benchmark Brugge field model. Finally, we demonstrate the practical feasibility of our approach using application to an offshore carbonate reservoir.

2.2 Approach

In this chapter, we propose a hierarchical multiscale calibration approach using global and local updates in coarse and fine grid. We follow a previously proposed approach (Yin et al. 2010) of updating global and local parameters recursively, however, we incorporate a multiscale framework where we integrate production data in coarse grid and successively finer grids sequentially. The proposed approach utilizes different

parameter space (global and local) and geometric space (coarse and fine). The inclusion of multiscale framework is critical for history matching high resolution reservoir models with hundreds of wells through significant reduction in simulation time. Because there can be considerable uncertainty in the large-scale static and dynamic parameters, we at first identify the key parameters and calibrate those using an evolutionary algorithm. This global parameter calibration, matching and balancing field level energy, is followed by streamline assisted multiscale inversion to calibrate local parameters to match well by well production history. For local parameter calibration, we utilize a grid coarsening function embedded in commercial finite difference simulators to shorten simulation time significantly at small loss of accuracy. The workflow for the proposed hierarchical multiscale inversion is shown in Fig. 2-1. We first discuss briefly the major steps in our approach, followed by details on each step including the background and mathematical formulation.

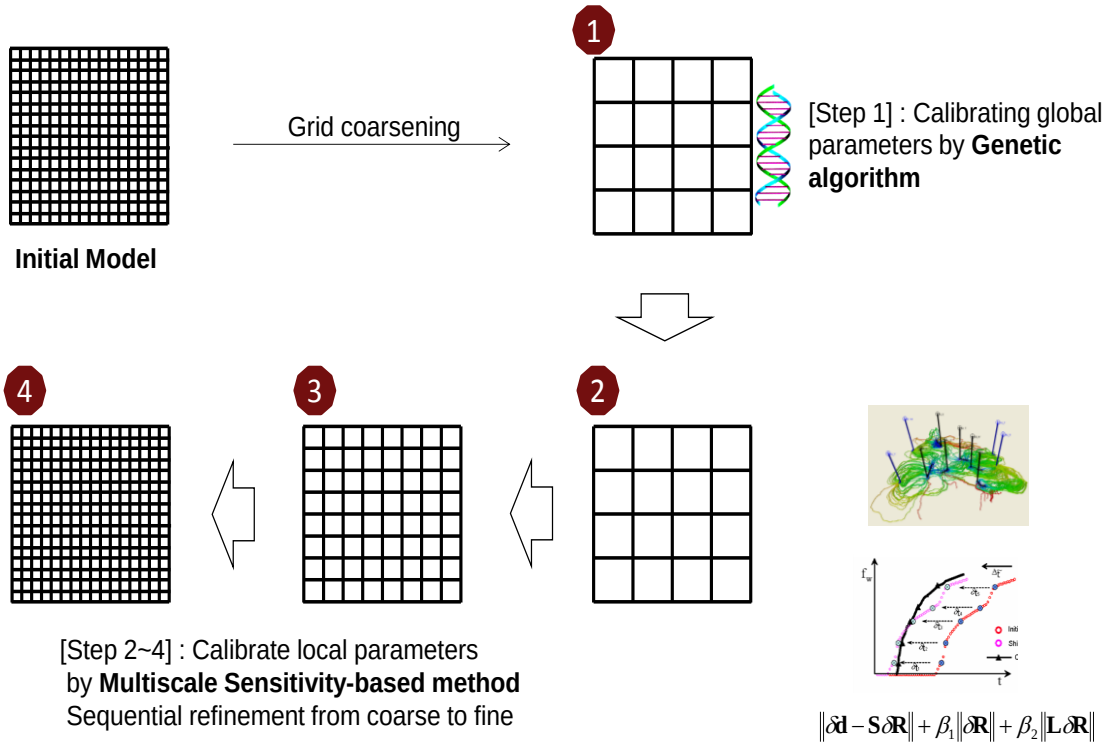

Fig. 2-1 Overview of workflow for hierarchical multiscale inversion

2.2.1 Global parameter calibration in coarse grid

Global parameter calibration process, shown as Step 1 in Fig. 2-1, includes sensitivity analysis and updating of large-scale parameters by a genetic algorithm. The global parameters are adjusted to match the global reservoir responses in terms of a field energy (pressure) and total liquid production. Simulation in coarsened grid is used at this stage for computational efficiency and also allow examination of large scale uncertainties in the model.

- ***Construction of objective function.*** The objective function is defined as a mismatch between observed (or history) data and the simulated response. The objective function is established considering the availability and the resolving power of the data. The minimization of this objective function is the goal of history matching.
- ***Sensitivity analysis*.** A small set of key global parameters is first identified via a sensitivity analysis and a low-level experimental design using high-low values for each of the potential parameters. A proxy of the objective function with respect to selected key global parameters is constructed using a detailed experimental design and response surface methodology (Pan and Horne 1998; Yeten et al. 2002). This proxy model is used to prescreen models before an actual simulation is carried out. We use kriging for constructing proxy model.
- ***Calibrating global parameters.*** A genetic algorithm with a proxy check and a stretched heat bath fitness function (Sen et al. 1995) is used to generate updated ensemble of models conditioned to total liquid production and a field level energy (pressure). A set of representative models is selected via a cluster analysis for further updates in local parameter calibration stage.

2.2.2 Local parameter calibration in coarse and fine grids: multiscale inversion

Each selected model from the globally calibrated ensemble is further calibrated to individual well's production history using multiscale sensitivity-based method in this

stage. A multiscale framework allows decomposing parameter estimation problem by scales. As illustration shown in Fig. 2-2**,** we start from very coarse grid and gradually refine the grid to calibrate grid cell properties. The calibration at the coarse-scale grid takes advantages of increased computational efficiency. The sequential updating approach allows to capture different levels of uncertainties (large and small scales), calibrates the model parameters of each stage, and successively improves the quality of match. A multiscale streamline-based inversion technique is applied for well-level matching via local changes in parameters.

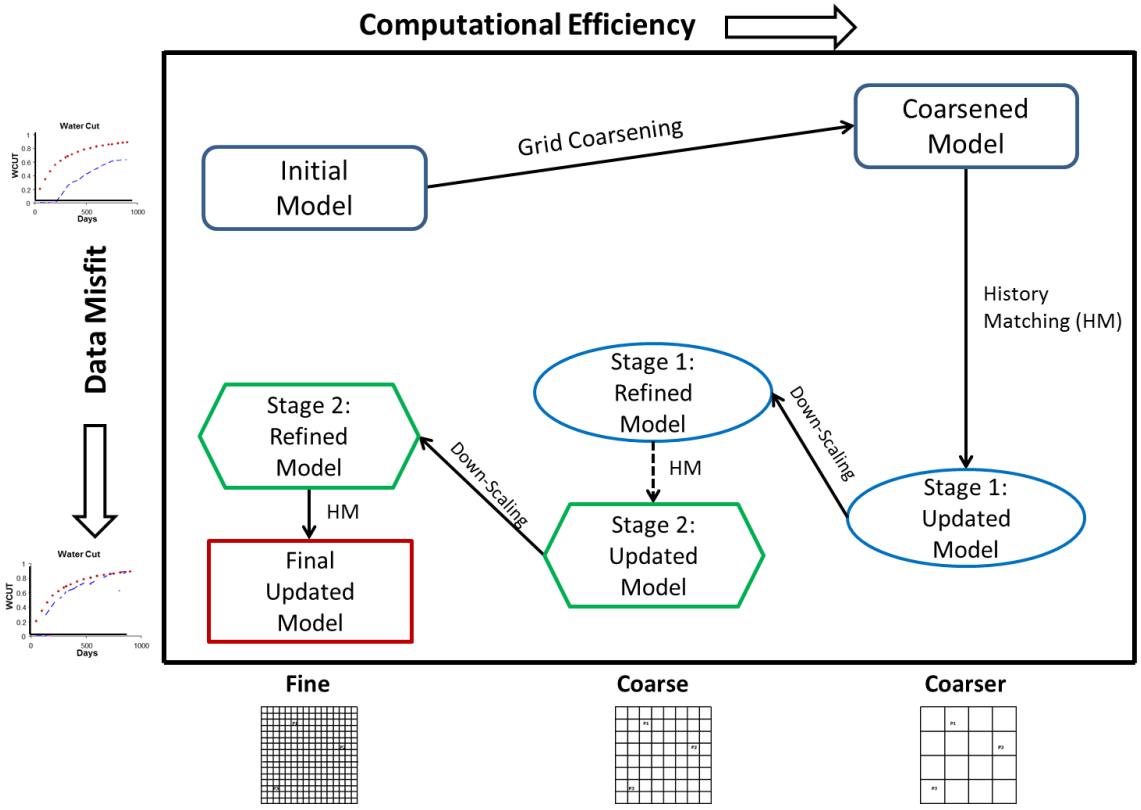

Fig. 2-2 Overview of multiscale inversion framework

2.3 Background and Mathematical Formulation

Our global matching approach closely follows the method outlined by Cheng et al. (2008) and Yin et al. (2010). Design of Experiments (DOE), Genetic Algorithm (GA) and Response Surface Methodology (RSM) are used for calibrating reservoir geological features at the global and regional scales. The global objective (misfit) function is defined as:

$$f(\mathbf{m}) = f(m_1, m_2, \ldots, m_N) = \ln|\Delta p_{MDT}| + \ln|\Delta Q| + \ln|\Delta p_{SBHP}| + \cdots \quad \ldots\ldots\ldots\ldots(2.1)$$

where multiple objectives are handled by using the logarithm of the absolute misfit in Eq.2.1. In multiobjective optimization problem, all objectives are typically aggregated into a scalar function (weighted-sum) based on their measurement errors, which are not readily available. The determination of the correct weights is one of major difficulties, we are not aware of which weights are the most appropriate to retrieve a satisfactorily solution (Hajizadeh et al. 2011). The selection of the weights using aggregation-based method is typically subjective and potentially biased as a result of the different scales/magnitudes of the data types (Yin et al. 2010). The use of production of the individual data-type components can mitigate this problem. Moreover, it is still allowable to assign a weight to each log objective in order to subjectively emphasize or degrade its relative importance.

2.3.1 Grid coarsening

Utilizing grid coarsening module, cells are amalgamated to reduce the total number of active cells in the global grid. The properties for coarse cell is obtained from simple upscaling from fine to coarse in a single coarse cell amalgamation. The formulation

typically used in commercial simulators, for upscaling key properties including pore volume and permeability is explained below.

Pore volume for coarse cell is just summation of pore volume of fine cells as follows:

$$PV_c = \sum_f PV_f \qquad \text{……(2.2)}$$

Permeability for coarse cell is computed by following.

$$K_c = \frac{\sum_f PV_f K_f}{PV_c} \qquad \text{……(2.3)}$$

Coarsened model can preserve most of the heterogeneity of the initial geological model depending on levels and types of coarsening (King et al. 2006). Use of coarsening is very efficient means to evaluate the sensitivities of global parameters as it can significantly reduce simulation runtimes which is vital for deriving parameter sensitivities (Mamonov et al. 2007). The tradeoff with regard to accuracy can be more than compensated by the reduction in simulation run time.

- ***Optimal coarsening algorithm.*** The coarsening geologic model typically loses a level of accuracy and introduces biased performance predictions: the calculation of coarsened cell properties cannot retain the variance in transit time across the column of cells because the different flow velocities in each cell will be replaced by a single average cell (King et al. 2006). There are many related publications that address optimal coarsening algorithms to minimize the inaccuracy of flow simulation. For example, King et al. (2006) proposed a statistical analysis for optimal layer coarsening where the arithmetic averaging of the velocity is used because it provides an unbiased estimator of the mean. In next section, we will show the effects of optimal coarsening on the performance of history matching. In this paper, we are not

focusing on the development of coarsening algorithms; instead, we will focus on the use of those optimal coarsening algorithms for the proposed hierarchical multiscale approach.

2.3.2 Global model calibration using the genetic algorithm with proxy

We have used the Genetic Algorithm (GA), one of the evolutionary algorithms, for calibration of global parameters. The genetic algorithm imitates biological principals of evolution – survival of the fittest. It has been extensively applied to the history matching problem (Bittencourt and Horne 1997; Floris et al. 2001; Romero and Carter 2001; Schulze-Riegert et al. 2002; Williams et al. 2004). Usually, solutions are represented as binary strings of 0's and 1's. The full binary string containing all variables is called a genome or chromosome. The evolution starts from a population of randomly generated individuals. In each generation, the fitness of every individual in the population is evaluated. Multiple individuals are stochastically selected from the current population (based on their fitness), and modified (recombined and possibly randomly mutated) to form a new population. The new population is then used in the next iteration of the algorithm. Commonly, the algorithm terminates when either a maximum number of generations has been produced, or a satisfactory fitness level has been reached for the population.

For history matching problems, we minimize an objective function $f(\mathbf{m}_i)$ while maximizing the fitness of genomes, as in Eq.2.4. This is equivalent to maximizing a fitness function $\exp(-f(\mathbf{m}_i))$. In our implementation of the GA, we incorporate a stretching of the fitness function to facilitate the selection process. Specifically, the 'heat bath' algorithm is a fitness scaling method that increases the probability of samples around the solution while speeding up the convergence (Sen et al. 1995). The selection probability of model $\mathbf{m}_i$ is given by:

$$P(\mathbf{m}_i) = \frac{\exp[-f(\mathbf{m}_i)/T_n]}{\sum_i \exp[-f(\mathbf{m}_i)/T_n]}; \quad T_n = \alpha^n T_0; \quad 0 < \alpha < 1 \qquad \text{……(2.4)}$$

In Eq. 2.4 T_n is a 'temperature' like parameter, which is gradually reduced at regular intervals (n is incremented after a fixed number of generations) by a ratio of α as the population evolves, much like the simulated annealing algorithm (Kirkpatrick et al. 1983). To evaluate the objective function and thus the fitness of a newly generated genome, we first check the proxy value for that genome. If it has a value smaller than a predefined threshold then a flow simulation will be carried out. Otherwise it is assigned a large objective score with zero fitness and will be discarded in the next GA generation. Heat-bath accelerates convergence and thus requires fewer simulations to reduce the objective function to a same level. This completes the description of each stage of the global history matching process. A flowchart with all the steps is shown in Fig. 2-3.

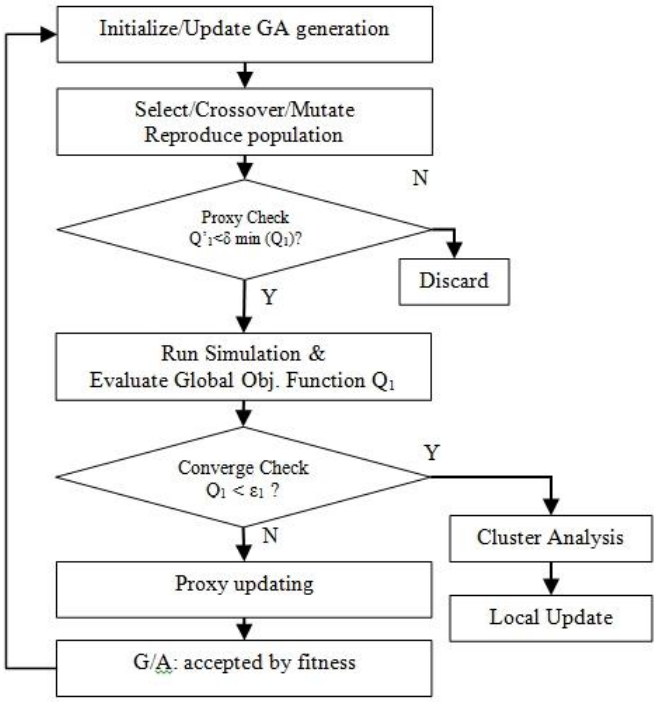

Fig. 2-3 Flowchart of GA with proxy

2.3.3 Local parameter calibration using streamline assisted multiscale inversion

In this approach we decompose the inverse problem by scale and integrate production data by a scale-by-scale inversion. We utilize the grid coarsening module available in many commercial reservoir simulators, where different scales of coarsening can be easily applied. Starting with coarser grid, we integrate the production data at the wells by gradually refining the grid. Simulation using grid coarsening provides with coarsen-scale flux information that is then used to trace streamline in coarsened cells or geometry. In Fig. 2-4, we compare tracing in fine grid and coarsened grid geometry. After tracing, we obtain from streamline properties coarsen-scale sensitivity that relates change in reservoir performance to small perturbations in reservoir parameters. For the sensitivity we follow the formulation proposed by Vasco et al. (1999). After sensitivity computation, we carry out streamline based generalized travel time inversion (GTTI) to match the production response for each well. The details on this GTTI method can be found in many publications (Cheng et al. 2006; He et al. 2002).

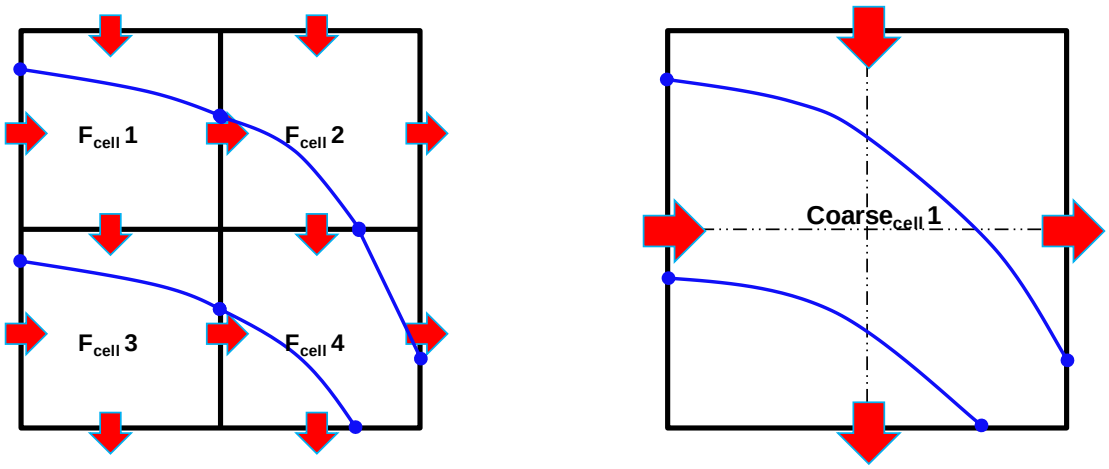

Fig. 2-4 Streamline tracing in fine grid (left) and coarsened grid (right)

In this part we present how to obtain parameter sensitivities at various scales and integrate production data to geologic models in a multiscale framework. We demonstrate its effectiveness and suitability through application to a mature offshore carbonate

reservoir. As we proceed to finer scale, we have a large number of parameters compared to the amount of data. The inverse problem becomes underdetermined and ill-posed, and the solution can be unstable (Yoon et al. 2001). Following Fig. 2-5 shows our proposed multiscale streamline sensitivity-based inversion workflow. We now discuss about each step in the workflow.

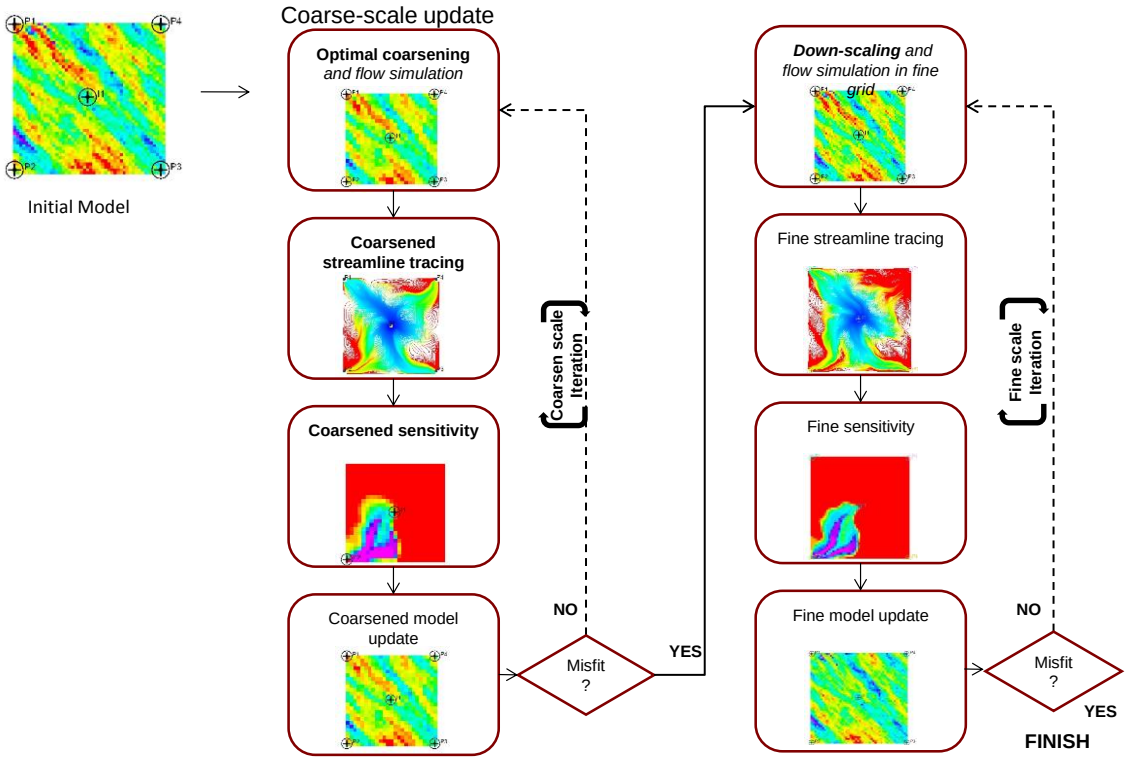

Fig. 2-5 Overview of streamline-assisted multiscale inversion

- ***Grid coarsening.*** This step is explained in the previous section.
- ***Coarsened tracing.*** The module of grid coarsening in finite difference simulator provides coarse scale fluxes which are used for tracing streamline through coarse cells. In the past approach (Taware et al. 2010), the authors reconstructed fine scale fluxes from coarse scale fluxes and traced streamline through fine geometry. It resulted in fine scale inversion with coarse scale simulation. In contrast, in the proposed approach both flow simulation and history matching are conducted at same

scale. A critical element in this approach is streamline tracing using coarse fluxes as it allows for speed-up in tracing and upscaled sensitivity directly from the streamlines.

- ***Coarsened sensitivity.*** Sensitivity defines the relationship between production data and small perturbation in reservoir properties. The sensitivity is simply the partial derivatives of the production response with respect to reservoir parameters like permeability.

$$\sum_{J=1}^{M}\sum_{j=1}^{n(J)} S_{ij}\delta m_j = \varepsilon_i$$

$$\sum_{j=1}^{n(J)} S_{ij}\delta m_j = S_{iJ}\delta m_J$$

$$S_{iJ} = \sum_{j=1}^{n(J)} S_{ij}$$

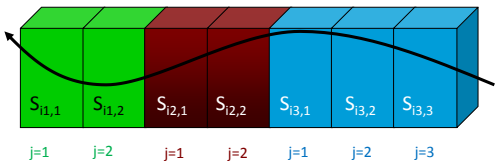

(a) Previous approach

$$\sum_{J=1}^{M} S_{iJ}\delta m_J = \varepsilon_i$$

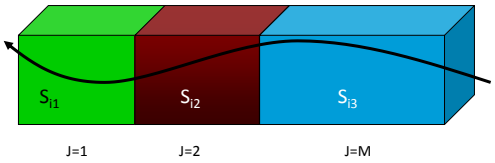

(b) Our proposed approach

Fig. 2-6 Approaches to coarsened sensitivity for travel time inversion; previous approach (a) and our proposed approach (b)

Unlike previous approaches (Kim et al. 2010; Yoon et al. 2001) that involve integrating fine scale sensitivities embedded within each coarse scale cell, we compute coarse-scale sensitivity directly from coarsened grids. As explained in previous

publications (Vasco et al., 1999, Cheng et al., 2007), the sensitivity from streamline relates the travel time of water front to the cell permeability. It is notable that the sensitivity can be obtained from a single simulation run, which is very advantageous over other methods in terms of efficiency of computation. Fig. 2-6 shows the difference of sensitivity formulation between previous approach and our proposed method, where J denotes coarsen cell index and j is for fine cell index. Also, n(J) denotes the number of fine cells within a coarsen cell and S_{iJ} represents sensitivity of J^{th} coarsen cell for i-th production data.

In the past approaches, the change of production response of ith production data was obtained by summing fine cell sensitivities. It is assumed that the magnitude of the change of fine cell parameters is the same as the change of coarse cell parameters ($\delta m_j = \delta m_J$). In contrast, we compute coarsened sensitivity directly from the coarse-scale streamline properties.

The streamline-assisted sensitivity relates the travel time of water front arrival time to cell permeability (Vasco et al., 1999, Cheng et al., 2007). The time of flight is simply the travel time of a neutral tracer along streamlines and is obtained by integrating slowness (s(x)) which is the reciprocal of the total interstitial velocity.

$$\tau = \int_{\psi} s(x)dx \quad \text{and} \quad s(x) = \frac{1}{|v(x)|} \qquad \text{.....(2.5)}$$

The water saturation equation in two-phase flow can be written in streamline time of flight coordinates as follows.

$$\frac{\partial}{\partial t}\left(\frac{S_w}{B_w}\right) + \frac{\partial}{\partial \tau}\left(\frac{F_w}{B_w}\right) = 0 \qquad \text{.....(2.6)}$$

We can obtain the travel-time sensitivity of water saturation front to reservoir parameters, *m*, from the above equation. It defines the relationship between water front arrival time, t_a , and coarse scale cell parameter, m_c.

$$\frac{\partial t_a}{\partial m_c} = \frac{\dfrac{\partial}{\partial m_c}\left(\dfrac{S_w}{B_w}\right)}{\dfrac{\partial}{\partial t}\left(\dfrac{S_w}{B_w}\right)} = \frac{\dfrac{\partial \tau}{\partial m_c}\cdot\dfrac{\partial}{\partial \tau}\left(\dfrac{S_w}{B_w}\right)}{\dfrac{\partial}{\partial t}\left(\dfrac{S_w}{B_w}\right)} \approx \frac{\dfrac{\partial \tau}{\partial m_c}}{\dfrac{\partial F_w}{\partial S_w}} \qquad \text{……..……(2.7)}$$

The computed sensitivity is placed in the penalized objective function as specified in the Eq. 2.8 and Eq. 2.9.

- ***Update coarsen model.*** For production data integration, we minimize a penalized objective function as given below.

$$\left\|\Delta\tilde{\mathbf{t}} - \mathbf{G}\delta m_c\right\| + \beta_1\left\|\delta m_c\right\| + \beta_2\left\|\mathbf{L}\delta m_c\right\| \qquad \text{……(2.8)}$$

The minimization of the equation above is equivalent to solving the following augmented linear system ($\mathbf{Ax} = \mathbf{b}$) in a least square sense. We use an iterative minimization method via the LSQR algorithm (Paige and Saunders, 1982).

$$\begin{pmatrix} \mathbf{G} \\ \beta_1\mathbf{I} \\ \beta_2\mathbf{L} \end{pmatrix}\delta m_c = \begin{pmatrix} \Delta\tilde{\mathbf{t}} \\ \mathbf{0} \\ \mathbf{0} \end{pmatrix} \qquad \text{……(2.9)}$$

For solving Eq. 2.9, we use an iterative minimization method, the LSQR algorithm (Paige and Saunders, 1982). The first term in Eq. 2.8 represents the data misfit as quantified by the generalized travel time (GTT) misfit, which allows for minimizing the difference between production responses and our model predictions. The GTT, $\Delta\tilde{\mathbf{t}}$

corresponds to the optimal generalized travel time shift required to achieve a maximum correlation between observed and simulated production responses (He et al. 2002). Also, $\delta \mathbf{m}_c$ stands for the change in reservoir coarse model parameter (for example, permeability at each coarse grid cell). The symbol **G** denotes the coarse-scale sensitivity of the GTT at each well with respect to the grid permeability. Because the travel time sensitivity is derived for every producing well and the sensitivity is a function of reservoir parameter, the size of G matrix is M×N, which is dependent on the number of wells (M) and reservoir parameter (N). We note that as a result of coarsening, the size of whole matrix is significantly reduced. The second and third term in Eq. 2.8 are about norm penalty and roughness penalty respectively. They ensure that our final model is not significantly far apart from the initial or starting model and spatial continuity is preserved. The relative strength of the prior model is determined with weighting factor β_1 while for roughness weighting β_2 is used. The symbol **I** denotes the identity matrix and **L** represents a spatial difference operator; for example the second spatial derivative of parameters measuring the model roughness.

The impact of the reduction of matrix (A) size from coarsening in improving the computational efficiency becomes apparent if we examine the operation count per LSQR iteration. LSQR iteration requires the number of operation given by 2nz(A) + 5col(A) + 3row(A), where nz(A) is the number of nonzero element in A, col(A) is the number of columns, and row(A) is the number of rows (BjÖrck et al, 1998).

- ***Fine scale inversion.*** Once we reach satisfactory convergence in coarse scale inversion, we sequentially move to finer scale inversion and follow same procedure as in the coarse scale inversion.

2.4 Streamline-assisted Multiscale Inversion

In this section we illustrate the proposed multiscale streamline-assisted inversion approach using application to the Brugge field. We highlight the benefits of the multiscale inversion approach through this illustration. In particular, a special focus is

given to the use of optimal coarsening algorithms to maximize the efficiency of the proposed workflow.

As part of an SPE Applied Technology Workshop (ATW) the Brugge field example was set up to evaluate various production optimization methods. The model properties are designed based on a North sea brent-type field. The model consists of about 60,000 grid cells with 9 layers. We applied our multiscale inversion approach for matching 10 years of oil and water production history for this field. The details of Brugge field can be found in the paper by Peters et al. (2009) .

To start with, we performed grid coarsening by uniformly merging 2 blocks in I, J, and K directions. As a result, the number of total grid cells and active cells are significantly reduced while preserving major features of heterogeneity of the initial fine-scale model as shown in Fig. 2-7**.** For instance 44,464 active cells are reduced to 6,343 active cells (approx. 14% compared to the fine model).

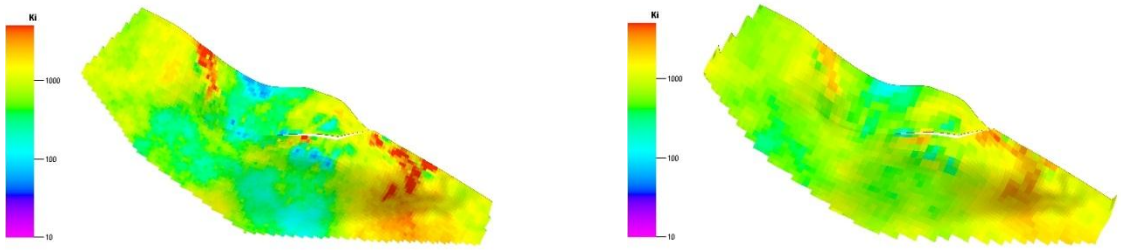

Fig. 2-7 Fine scale permeability model (left) and coarse scale permeability model (right)

We simulated the coarsened model and obtained coarse scale dynamic results including pressure and fluxes to trace streamline through the coarsened cells. Fig. 2-8 compares streamlines traced in coarsened grid and fine grid based on a velocity field of a certain time step. The streamlines path and time of flight look very similar with little loss of accuracy. We note that the coarse grid streamlines have been generated based on coarsened flux information while fine grid streamlines are based on fine-scale simulation

results. Also, coarse grid tracing saves time because of smaller number of cells to trace compared to the fine cells.

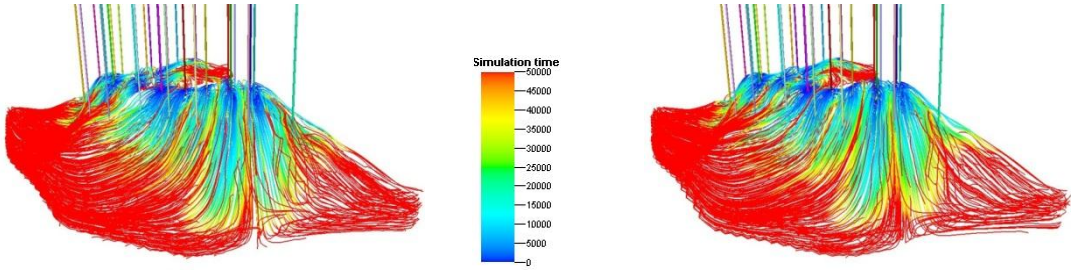

Fig. 2-8 Traced streamline in fine grid (left) and coarse grid (right)

After tracing streamlines, we compute the sensitivities for integration of production data. Fig. 2-9 shows, for example, streamline-derived analytic coarse-scale sensitivities where the color of grid cell shows the magnitude of the sensitivity.

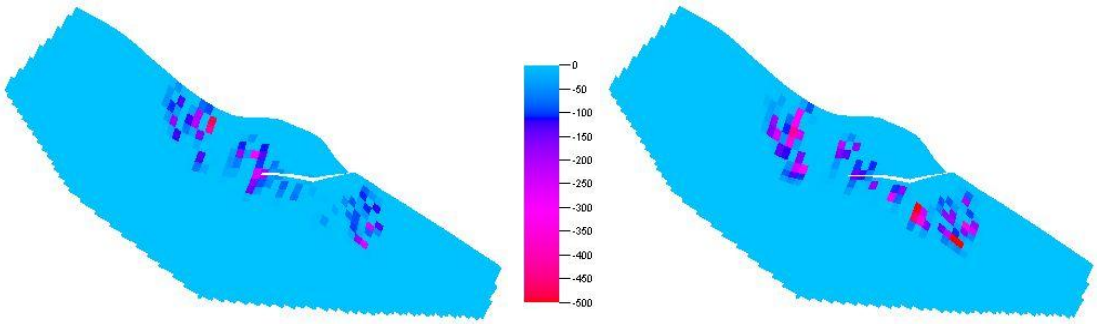

Fig. 2-9 Computed coarsen sensitivity viewed for different layers (k=5, left and k=8, right)

Next, we construct the penalized objective function in Eq. 2.8 by including all sensitivities, followed by minimization using the iterative minimization solver (LSQR). Once we have new model through minimization, we simulate it, check the misfit, and evaluate the objective function. We continue the updating process until it satisfies convergence criteria, typically, defined in terms of acceptable data misfit.

After coarse-scale inversion, we scaled down to original fine grid scale to further calibrate the reservoir parameters in fine grid scale. At this stage, not many iterations are needed to achieve satisfactory convergence because coarse-scale calibration takes us to the vicinity of the solution. Fig. 2-10 shows the final updated permeability field and the figures below are showing calibrated regions (permeability changes) during coarse-scale inversion and fine-scale inversion (Fig. 2-11). We observe that most of the changes were made during coarse-scale inversion where large-scale uncertainties were captured and updated accordingly. The fine-scale calibration resulted in fine-tuning after major change in coarse-scale inversion.

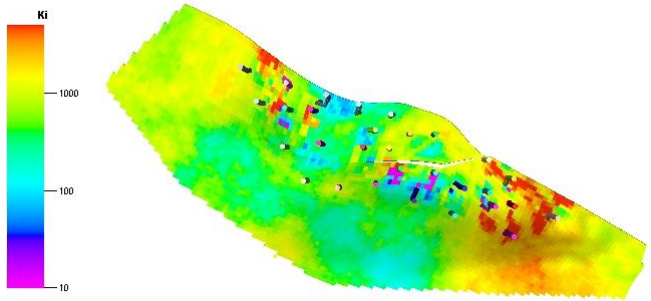

Fig. 2-10 Final updated permeability model

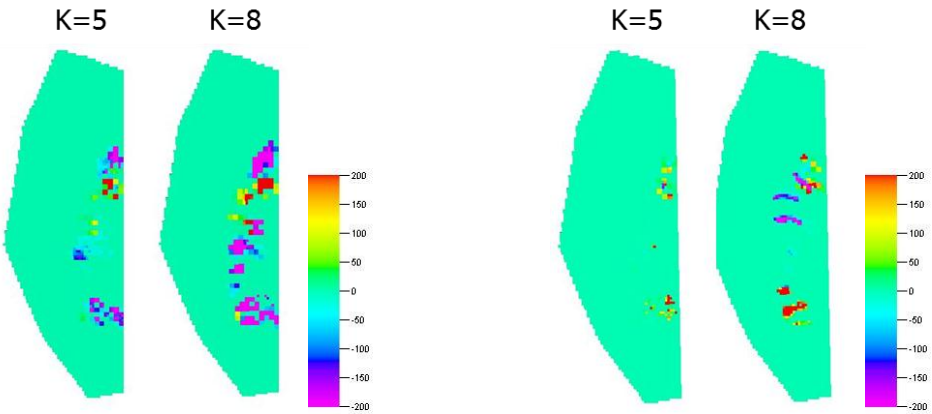

Fig. 2-11 Calibrated regions at coarse scale inversion (left) and at fine scale inversion (right)

We demonstrated here streamline-assisted multiscale inversion approach with two scale updates: coarse and fine scale inversion. We can extend the approach to multiple scales as needed. For example, we can start from much coarser grid (for example, 3×3×3 coarsening), down to a medium level of coarse grid (2×2×2 coarsening), and finally to a fine grid. It constitutes three (3) scale updates.

Next, we used optimal coarsening algorithm rather than uniform coarsening for multiscale approach. The optimal layer coarsening algorithm (King et al. 2006) relies on sequential coarsening of the fine-scale geological model. It uses static parameters as 'heterogeneity measure' and sequentially performs layer coarsening such that variation of the measure within the layers is minimized and variation of the measure between the layers is maximized. We note that the layer optimal coarsening is performed in the vertical direction only. The difference between optimal layer coarsening and uniform coarsening is about vertical layering (k direction) with the optimal coarsening leading to non-uniform coarsening in the vertical direction. As a result of the optimal layering for Brugge field, we obtained the optimal layering shown in Fig. 2-12, which is compared with uniform coarsening. Both have 5 layers but different layering schemes. As shown below, the optimal case merges the first through fourth layer as one, fifth and sixth as the second layer, rest of the layers are not merged. In comparison, the uniform coarsening merged every two layers.

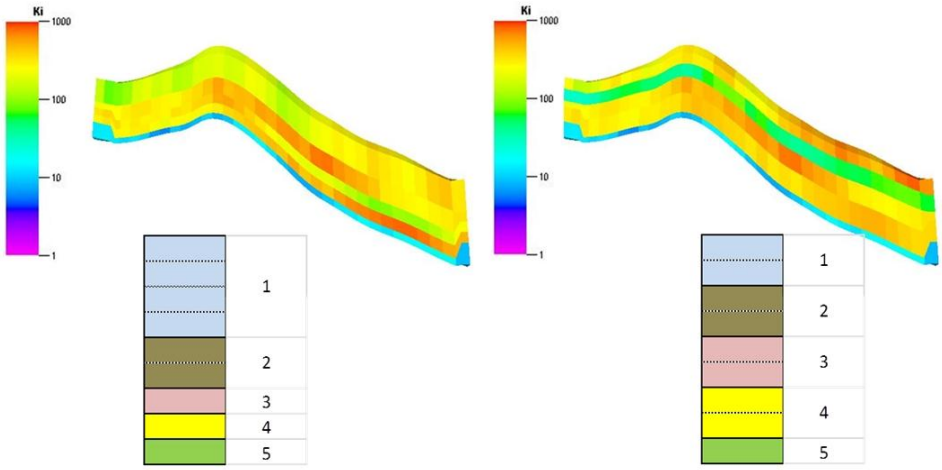

Fig. 2-12 Optimal layering (left) and uniform layering (right)

To examine the benefits of the multiscale approach, we compare multiscale approach and direct fine scale approach in terms of convergence and computation time. The first benefit is obviously savings in computation time. The Fig. 2-13 compares the computation time between fine scale and multiscale approaches. We notice that not only the savings are from forward simulation run and but also additional computational savings are from tracing and iterative minimization processes during history matching. The differences should be much larger for real field case, which will be discussed in the next section. In addition, from Fig. 2-14 we notice that multiscale inversion performed better than direct fine scale inversion, less misfit, and better convergence.

The effects of optimal coarsening algorithm are also apparent. In Fig. 2-13, both coarsening models (uniform and optimal) required similar amount of computation time. However, optimal coarsening gives better convergence compared to uniform vertical coarsening.

Looking at the objective function behaviors in Fig. 2-14, we make two observations. First, multiscale approaches converge very fast in the beginning. As soon as we switch to fine-grid inversion, which is at 11^{th} iteration, we see that the objective function increases. As we discussed in previous section, that is because of bias included when it is uniformly coarsened without in consideration of the variance of geologic properties. However, we recover within a couple of iterations and improve further in fine-scale inversion. There is not noticeable increase in optimal coarsening model calibration because the optimally coarsened cells better preserve original heterogeneity. Second, the use of coarsening avoids local minima resulting in better solutions.

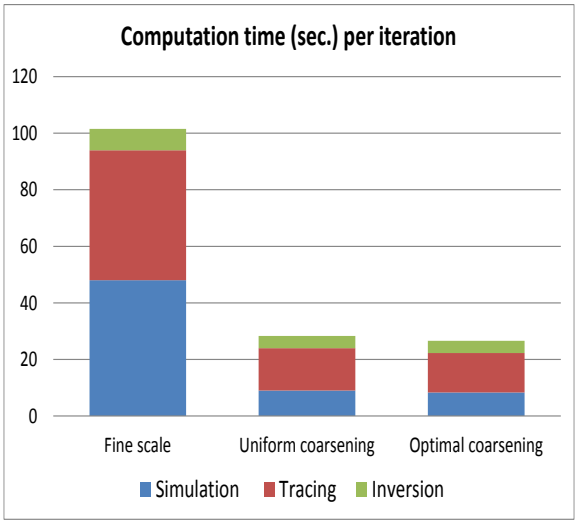

Fig. 2-13 Comparison of computation time

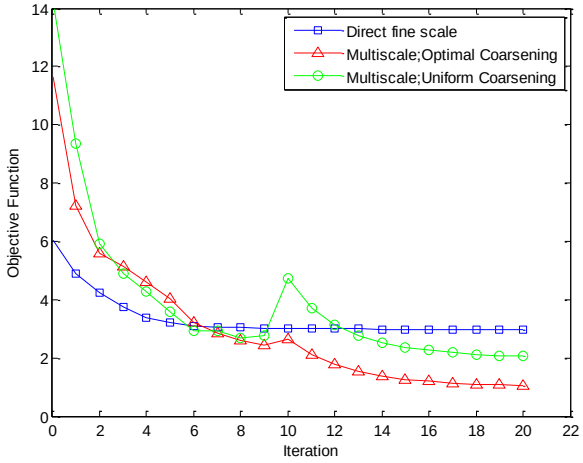

Fig. 2-14 Comparison of objective function behavior

2.5 Field Application

In this section we demonstrate the effectiveness and suitability of the proposed hierarchical multiscale approach through application to history matching an offshore carbonate field in India.

2.5.1 Field description

The Heera field is highly heterogeneous carbonate reservoir located in the western coast of India in the vicinity of the giant Mumbai High field. It is the second largest field of the western offshore basin off the west coast of the Indian peninsula and started commercial production in 1984. The development history of Heera field is shown in Fig. 2-15. The development includes 3 phases during 1984-2002 and additional development during 2002-2003. Many platforms including lots of wells were developed during those periods. For example 161 wells in 14 platforms were commissioned in the field during the first 3 phases.

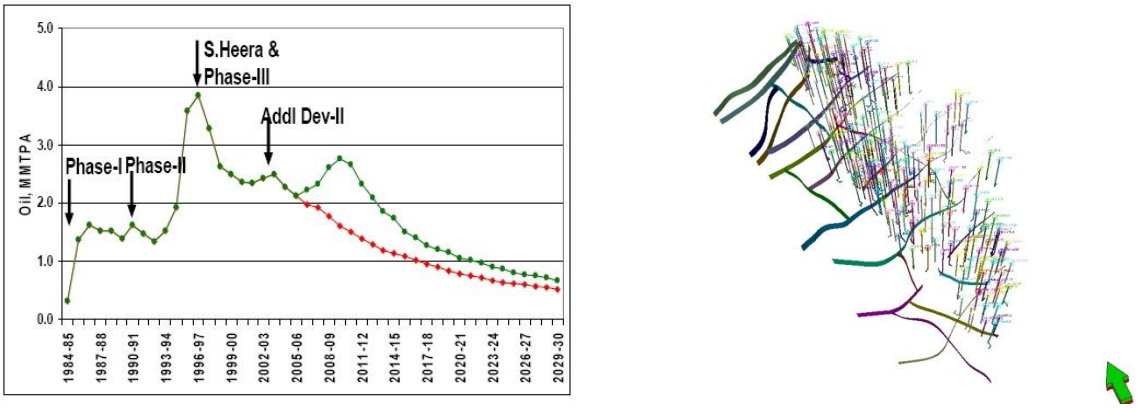

Fig. 2-15 The development history of Heera field (Mitra and Kumar 2008) (left) and complex faults in the field (right)

The Heera field has been producing over 20 years and is currently producing with a substantial water-cut. The redevelopment plan was drawn in 2006 to improve oil recovery factor of main reservoir (i.e. Bassein). A major redevelopment effort is ongoing to sustain and improve production from these fields through selective infill drilling, optimization of well trajectories and state-of-the-art reservoir management practices.

Heera simulation model consists of approximately 1 million grid cells with 24 layers. It contains many faults in the field of which some are following I direction and some lie across J direction as shown in Fig. 2-15. Average permeability for this field is about 73

md, relatively low permeable because of carbonate reservoir. Permeability fields and initial oil saturations are shown in Fig. 2-16 and Fig. 2-17 respectively. Those are pretty much representative of other layers since the layers between are similar to them. We observe that high saturation oil zones, layer 5th through 13th, are embedded in high permeability zones around the field.

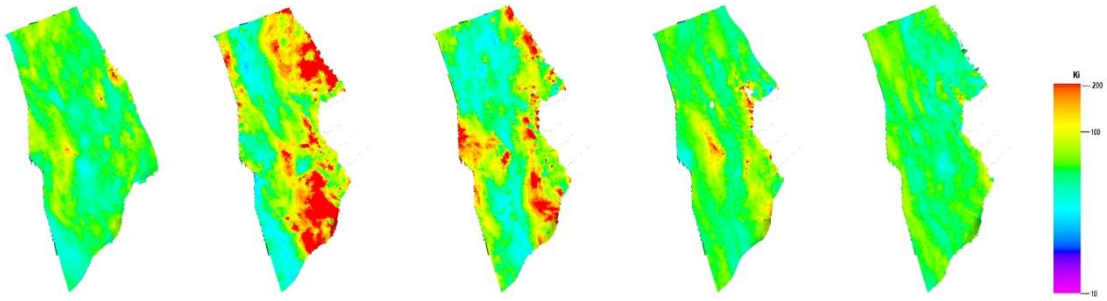

Fig. 2-16 Permeability field by layer (1st , 5th, 11th, 13th, 21st layer from left to right)

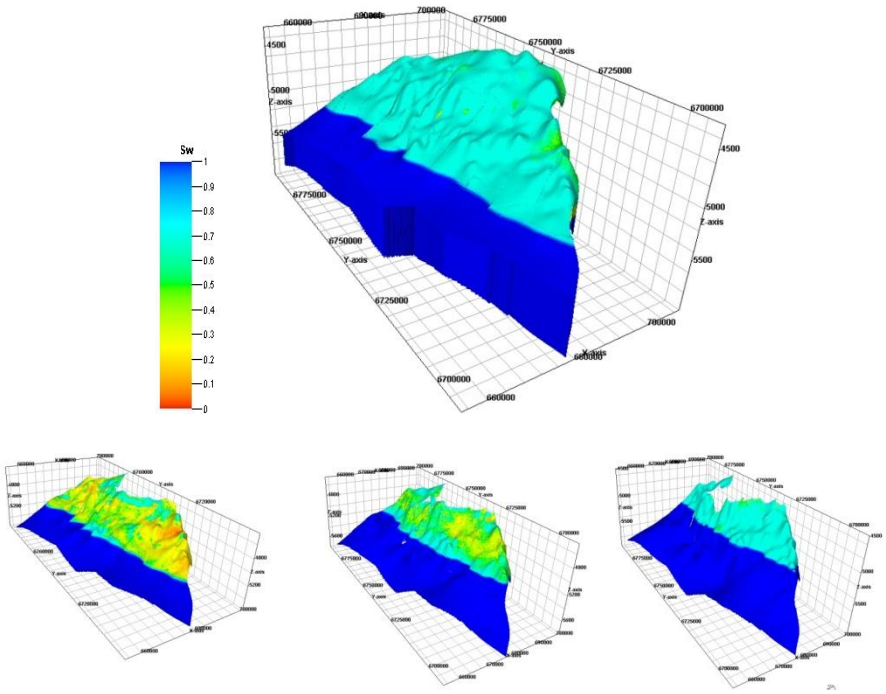

Fig. 2-17 Initial oil saturation field (top) and by layer (5th, 13th, 24st layer from left to right)

2.5.2 Multiscale history matching using global and local parameters updates

The objective of this history matching study was matching water-cut and bottom hole pressures for about 30 years of production history. Because initial reservoir model is large and requires long simulation run time (about 24 hours), grid coarsening module was used for calibrating global parameters. The history matching workflow for this field is shown in Fig. 2-18. First, we match field wide pressure (energy) and total production volumes, using pore volume multipliers. It followed by matching of bottom hole pressures. In this second step, we match regional energy and adjust platform wise production by calibrating regional permeability multiplier and aquifer strengths. At the final step, we update local parameter (permeability) to match well by well water-cut, where we used our proposed streamline-assisted multiscale inversion method.

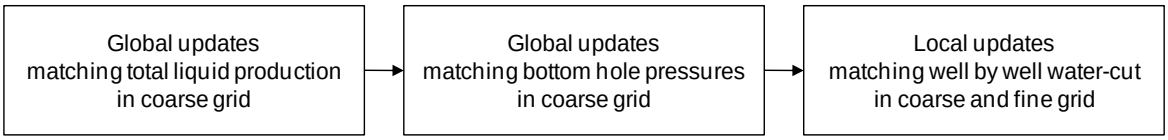

Fig. 2-18 Strategy and workflow for history matching Heera field

Multiscale models were analyzed to see how well it preserves heterogeneity of reservoir by the level of coarsening. More importantly, we examined how much it can reduce computational load and at the same time how much we may lose in terms of accuracy. We considered the trade-off between accuracy and computational efficiency. We have shown in Fig. 2-19, different levels of coarsened permeability fields; 2 by 2 uniform coarsening (X2) model and 3 by 3 uniform coarsening (X3) model. We see that the main features and heterogeneity of reservoir are kept in both coarsened models. The comparison of pointed area between multiscale models shows clearly that we lose a bit detail of heterogeneity but it still maintains key characteristics of the model. The number of grid cells for coarsened models becomes just 13% (for X2 model) and about 4% (for X3 model) of fine grid cells.

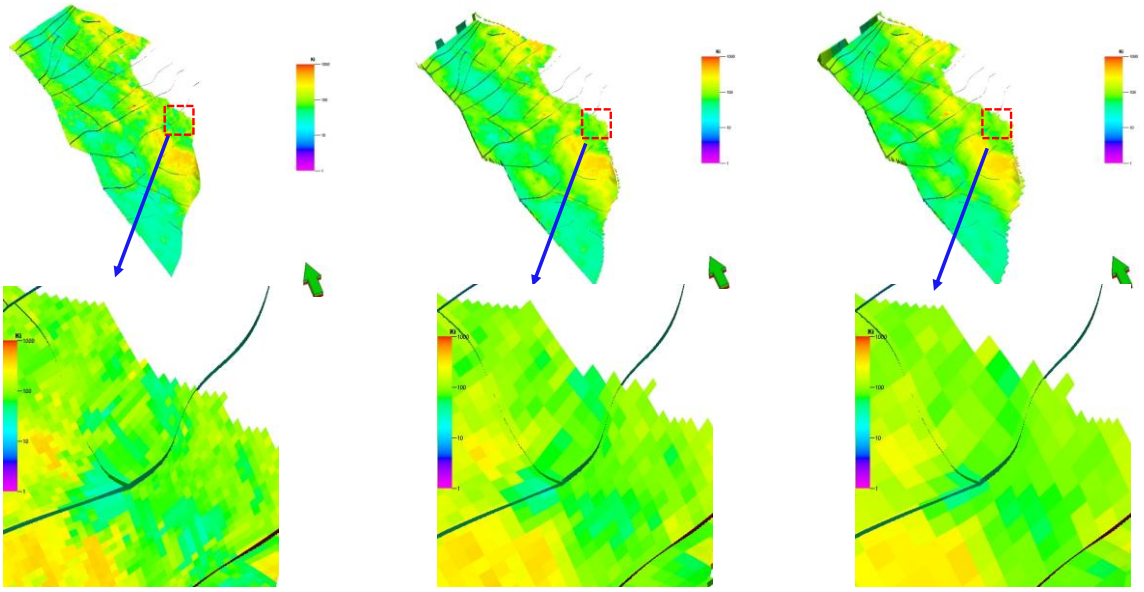

(a) fine scale (b) coarse scale (2 by 2 uniform coarsening) (c) coarser scale (3 by 3 uniform coarsening)

Fig. 2-19 Permeability field by size of coarsening

We lose minor accuracy in terms of simulation results because of coarsening but it is compensated by the reduction in simulation runtime. Fig. 2-20 shows field oil and water production rates for different levels of coarsening. We note that water production rate becomes little different in around 5000 days. However, generally production responses including oil rate are quite satisfactory for use in global parameter update. It is more important to update large-scale features during initial stage of history matching such as global update. In terms of simulation runtime the benefit is significant as shown in Fig. 2-21 if we use coarsened model. Because we need typically many simulation runs during global updates process, the use of coarse model is reasonable choice.

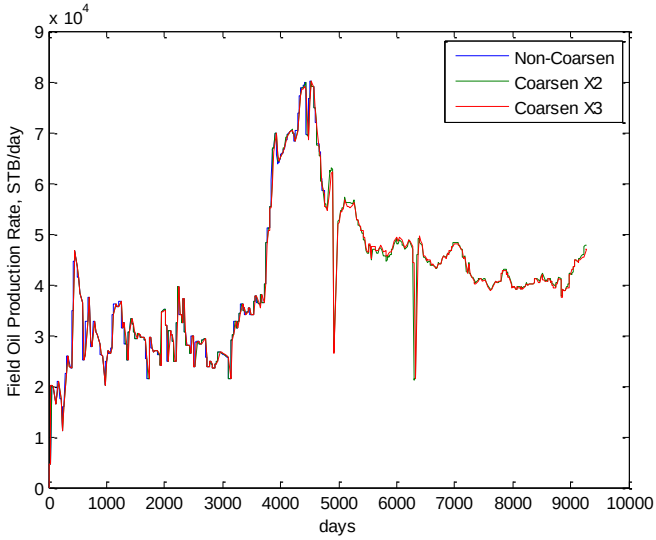

(a) Field oil production rate

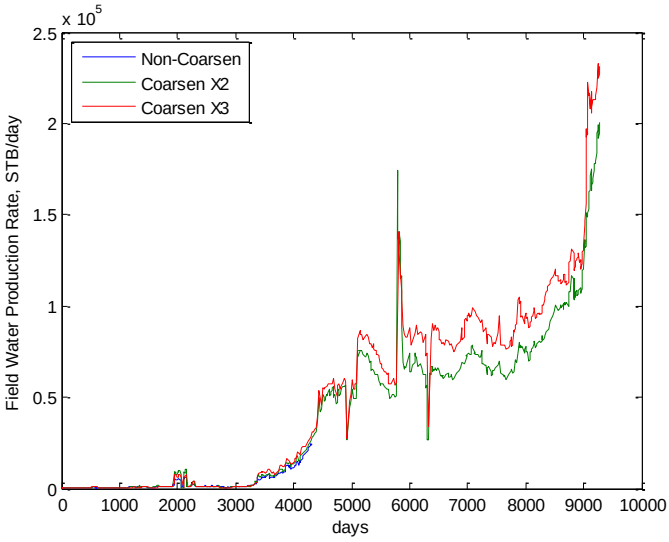

(b) Field water production rate

Fig. 2-20 Field oil production rate (a) and water rate (b) for different coarsening levels

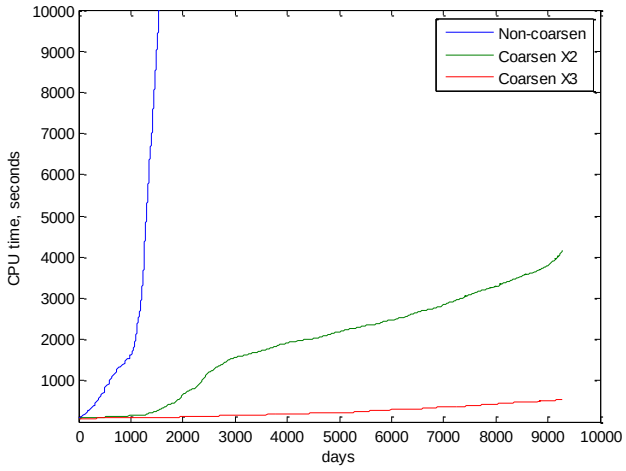

Fig. 2-21 Simulation runtime comparison for different coarsening levels

2.5.3 Global updates in coarse grid

To start with, we focused on matching field wide total liquid (oil and water) production. The initial model responses were very different from the field history in terms of water production. There was almost 100 thousand barrels per day difference in field-wide water production rate. Because of that, the cumulative water production difference amounted to about 150 million barrels. This prompted us to match field total production ahead of any other history data. The regional water production rate differences and misfit distribution map (refer to details below) are shown in Fig. 2-22. We noticed that two regions (HSB, HR) explained the largest differences. The calibration was made using genetic algorithm and pore volume multipliers were applied to those areas, after sensitivity analysis to find appropriate upper and lower bounds. For these sensitivity analysis and updating process, coarsened grid (X3) was used, resulting in large savings in computation time. As shown in Fig. 2-22, the misfits for those two regions have been significantly reduced after the pore volume calibration.

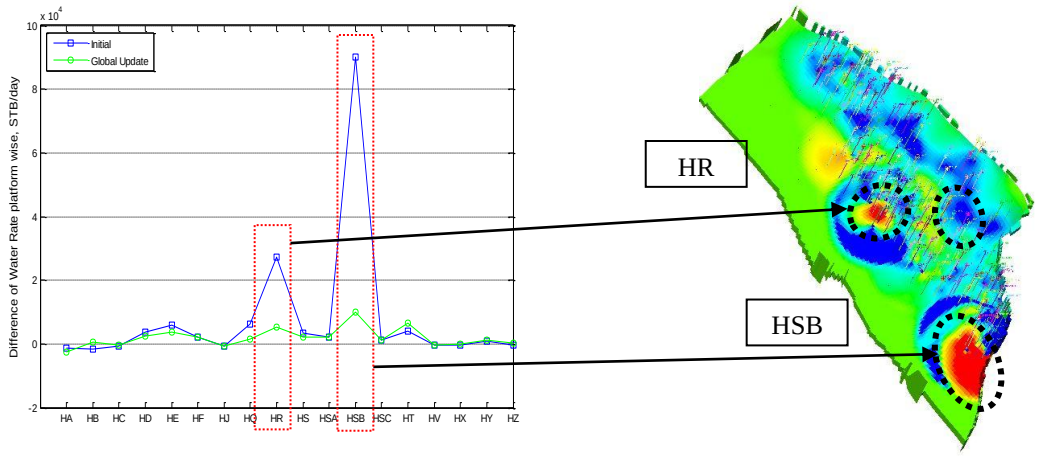

Fig. 2-22 Water production rate difference at time end by region (left) and misfit spatial distribution map (right)

We use optimal interpolation technique (krigging) to generate data misfit spatial distribution map, which is based on regression against observed data values of surrounding data points, weighted according to spatial covariance values. We estimate of a variable at an unmeasured location (specifically, water production difference at this case shown in Fig. 2-22) from observed values (at well locations) at surrounding locations. Then the estimated values are mapped to the cell properties in a certain format (for example, ECLIPSE style (ASCII) properties (*.GRDECL)) to be visualized at commercial package. This map is helpful to use at analyzing error and identifying easily its distribution for large-scale field.

Next, we switched to updating global parameters to match bottom hole pressures and followed the workflow shown in Fig. 2-23. The bottom hole flowing pressure data were given not for all the wells but for some of wells. In this step we again used sensitivity analysis and genetic algorithm for updating models. We observed that calculated reservoir pressure was generally higher than measured (history) pressure throughout the field. As shown in Fig. 2-25, we created 5 regions after considering faults lines and its connectivity.

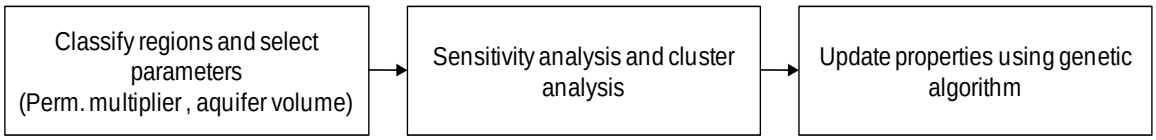

Fig. 2-23 Workflow for global updates matching bottom hole pressure in coarse grid.

We chose regional permeability multipliers and aquifer volume as parameters to match the bottom hole pressure. Sensitivity analysis was performed to find the upper and lower bounds as shown in Fig. 2-24. Although we concentrated on regional pressures, we have shown field-wide average reservoir pressures. The red line in the figure represents average reservoir pressure for the base case. The other lines are for each sensitivity case. The left figure shows the sensitivity of regional permeability multiplier on average reservoir pressure, the right one shows the sensitivity of aquifer volume.

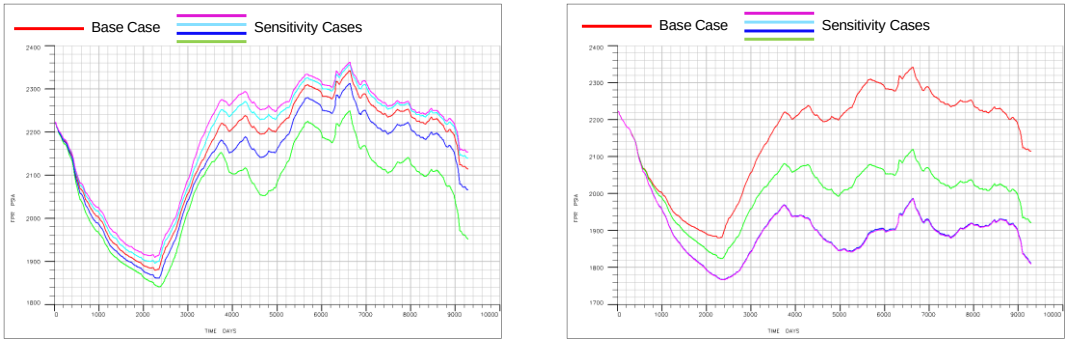

Fig. 2-24 Sensitivity of regional permeability multiplier (left) and aquifer volume (right) to reservoir pressure.

Regional permeability multiplier bounds between 0.5 and 1.5. The aquifer volume sensitivity ranges from 1.25×10^{12} cubic feet to 1.25×10^{8} cubic feet. Genetic algorithm was used for updating these global parameters in this step. One updated model (called GA model 1) is displayed in Fig. 2-25 where we see that updated regional permeability multipliers and aquifer volume were applied.

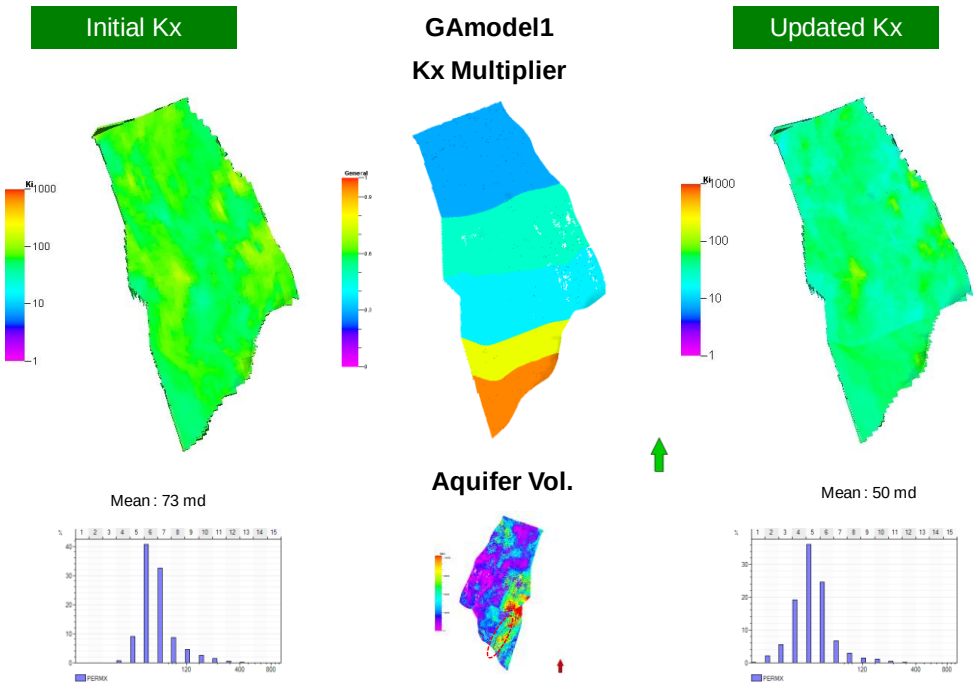

Fig. 2-25 Example of GA model (generated from genetic algorithm)

As shown in Fig. 2-26**,** GA updated models' responses in terms of field reservoir pressure are much lower than initial one, which is now consistent with field observations.

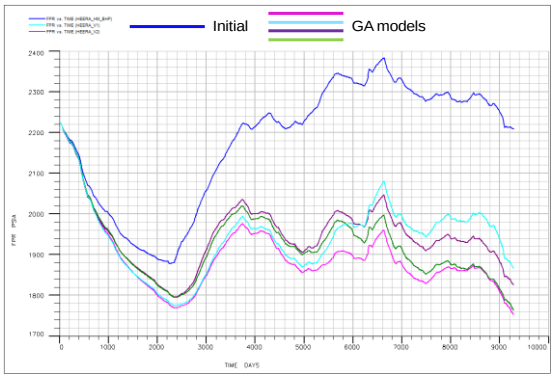

Fig. 2-26 GA models' simulated response compared with initial response

In terms of bottom hole pressures, there was generally about 400 to 800 psi differences for most of wells in initial model as shown in Fig. 2-27. We reduced those misfit and updated models where we see that all selected models' responses are close to the history.

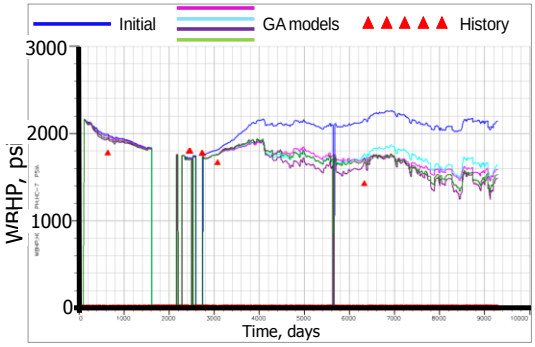

(a) Updated GA models' bottom hole pressure for a well in North Heera

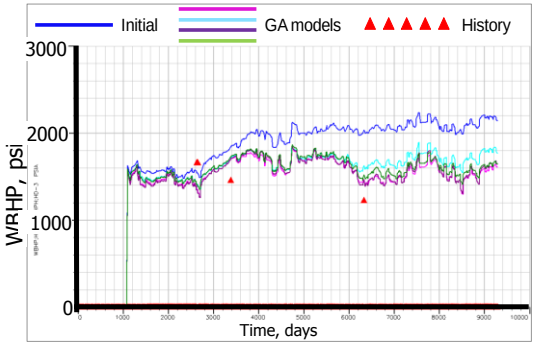

(b) Updated GA models' bottom hole pressure for a well in Middle Heera

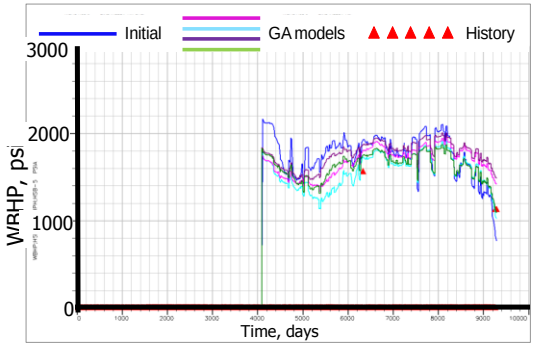

(c) Updated GA models' bottom hole pressure for a well in South Heera

Fig. 2-27 GA models' simulated response compared with initial and observed

2.5.4 Local updates in multiscale framework

As a final step, we did calibration of local parameters (cell permeability) by use of our proposed streamline-assisted multiscale inversion approach. The multiscale inversion starts from coarse scale and refines the grid gradually, and in each grid scale we trace streamline and obtain parameter sensitivity. For this field application, we started with a coarse grid (X3 coarsening) and moved to finer grids (X2 and fine). We calibrated grid cell permeability to match well by well water cut history. Fig. 2-28 shows field water-cut, comparing observed, initial, and updated model. We had quite large differences (about 20% water cut at time end) but now it is reduced to less than 5% difference overall. Not only field water-cut but also individual well water-cut matching have been improved. For example, in Fig. 2-29 we show results for some of key wells. The wells had initially very different water cut and now updated responses are very close to the history.

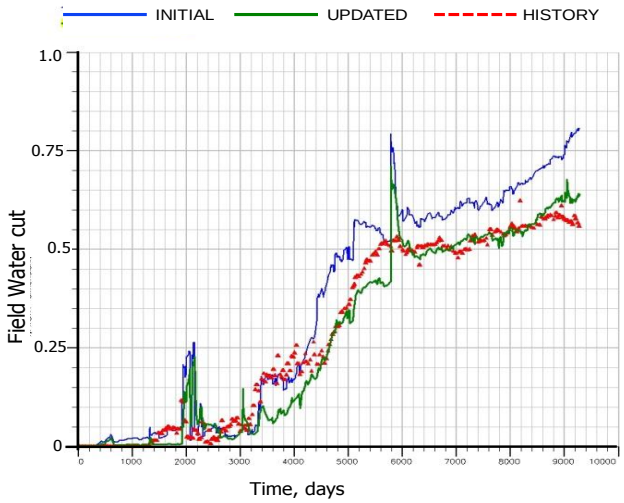

Fig. 2-28 Field water cut by model (initial, updated, history)

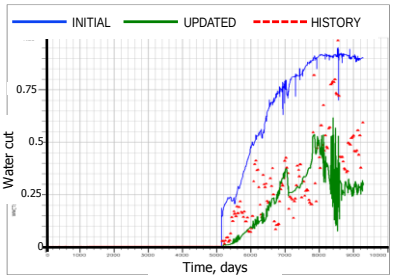

(a) Well P1

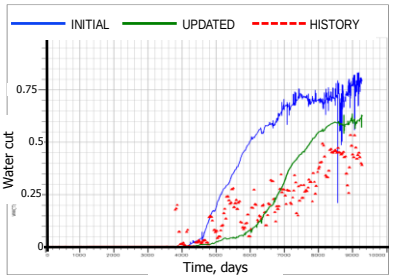

(b) Well P2

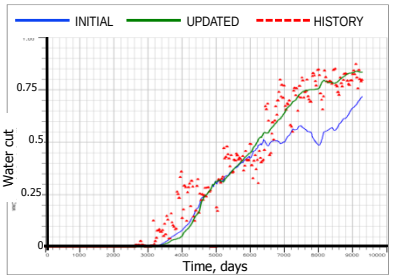

(c) Well P3

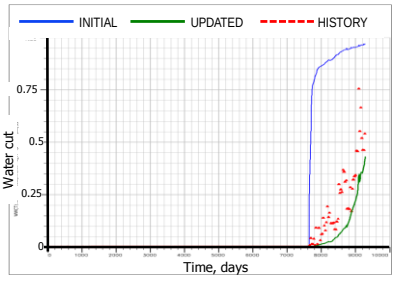

(d) Well P4

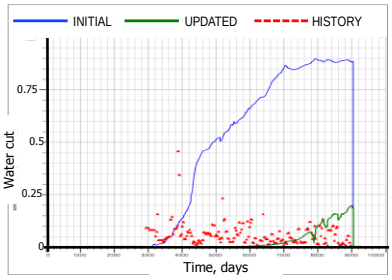

(e) Well P5

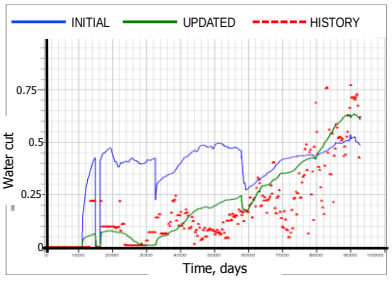

(f) Well P6

Fig. 2-29 Key wells' water cut comparison between models (initial, updated, history)

We revisit regional water production rate difference to compare initial and step-wise updated models' response. As shown in Fig. 2-30, the difference of water production rate by region for global-local updated model (final model, displayed with red line) shows significant improvement compared to global updated model response (displayed with green line). Recall that the field-wise water production was matched and regional

water production rate was balanced quite well from the global update process. After that, we focused on well by well matching in terms of water and oil production rate via a local update. Overall, regional and well-wise water production rates have been further improved while keeping total production rate close to history.

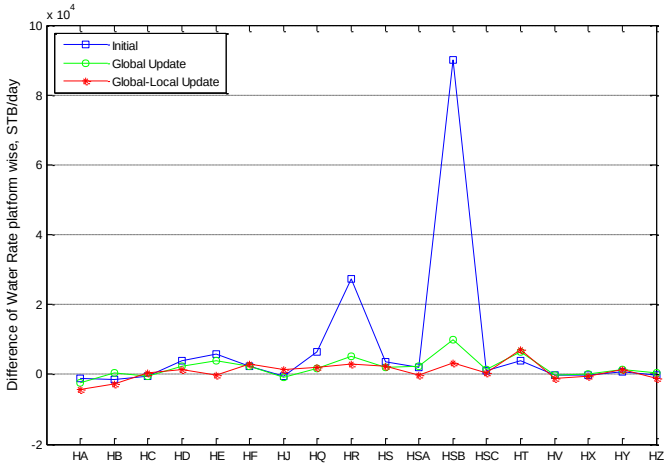

Fig. 2-30 Difference of water production rate by region for models (initial, global-update, global-local update)

The misfit spatial distribution map shown in Fig. 2-31 compares three models (initial, global updated model, global-local updated model) in terms of water production misfit. Because the misfit distribution map has been interpolated by krigging, we can examine its spatial distribution easily. Initial model showed two or three large misfit regions, which were large obstacle for history matching and special attention was given to those. Updated models show that most of the errors not only for those regions but also for whole field were reduced dramatically through global update and the sequential multiscale update.

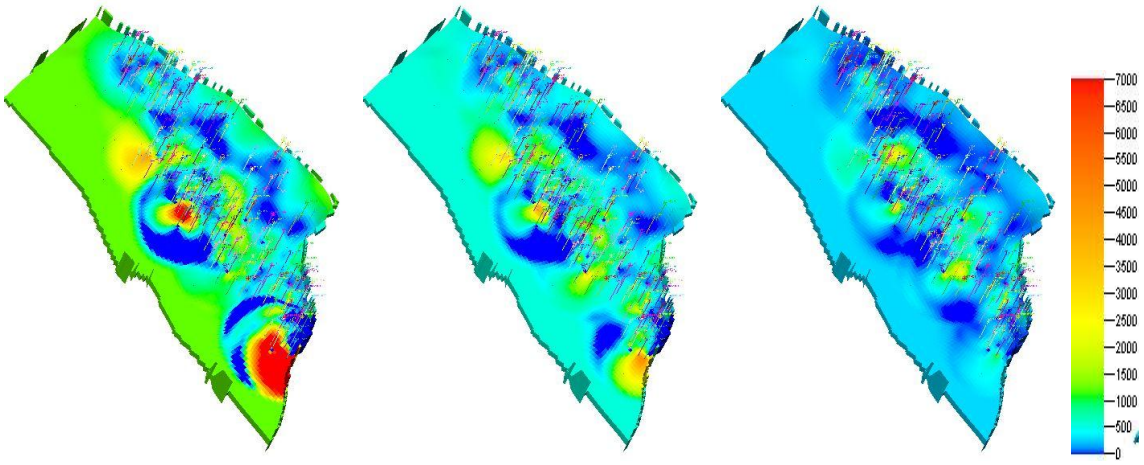

Fig. 2-31 Data misfit (Water production rate difference) spatial distribution map (initial, global-update, global-local update)

During history matching of this large field model, key attention was given to matching of regional and field level pressure (energy) ahead of matching well by well performances to avoid unrealistic updates because of direct small-scale heterogeneity update. Particularly, large reservoir models typically involve large-scale structural and stratigraphic features that should be captured and updated first via global update. From analysis of our updated models, specifically looking at water volume movement patterns, we found that water movement path has been redirected after history matching as shown in Fig. 2-32. The water flux map is generated based on the amount of water in grid cells. We see that initial model was supported with water movement from left side of field (i.e. North Heera) while in the updated model much water movement or flux is observed in the middle region.

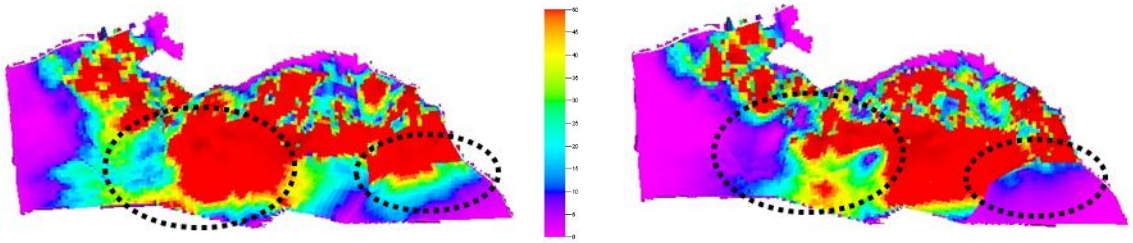

Fig. 2-32 Comparison of models (initial (left), updated (right)) in terms of water flux (shown for one layer)

2.6 Summary and Conclusions

We have presented a hierarchical history matching approach in conjunction with multiscale inversion that follows a sequence of calibrations from global to local parameters, both in coarsened and fine scales. The approach has been tested with 3D benchmark field and an offshore carbonate field that has hundreds of wells with over 25 years of production history. The key findings from this study are:

1. We proposed the inclusion of multiscale approach to the hierarchical global and local history matching procedures (Yin et al. 2010). Its practical feasibility was demonstrated using applications to 3D synthetic model and a large offshore carbonate reservoir model.
2. We found that the use of multiscale approach was successful in history matching a large reservoir model because of desirable multiscale features: computational efficiency, effective iterative minimization, and avoiding local minima.
3. The structured hierarchical history matching with global and local updates worked extremely well. In the global parameter calibration, reservoir energy is matched and its balance between platforms (i.e. regions) is achieved in terms of fluid production and reservoir pressures. In the local parameter calibration, individual well production responses are matched. Because the global reservoir

energy has been calibrated to reasonable level by global updates, the local update using streamline technique found solutions very fast.

4. A stochastic global search approach based on the genetic algorithm combined with a proxy model for the objective function provided effective means to match the global parameters and produce an ensemble of preliminary solutions for the local update.

CHAPTER III

HIERARCHICAL ANALYTICAL APPROACH TO RATE OPTIMIZATION USING FLOOD EFFICIENCY MAPS [*]

In this chapter we provide a simple and easy to use workflow for waterflood rate optimization using streamline-based flood efficiency maps that display the flux and time of flight distribution amongst producing wells. We demonstrate the use of flood efficiency map to optimize the injection/production rates to maximize waterflood sweep efficiency by equalizing the average time of flight (TOF) amongst the producing wells in regional basis. Our optimization approach is extremely efficient because it relies on simple analytic calculations to compute weighting factors for injection and production rates to minimize the TOF variance amongst producing wells. Because the approach does not rely on formal and complex optimization tools, it is particularly well-suited for large-scale field application. Also, the approach can be used with both streamline and finite difference simulators. For finite-difference simulations, the streamlines and time of flight are derived from the flux field generated by the simulator. Multiple examples are presented to support the robustness and efficiency of the proposed waterflood management scheme. These include 2D synthetic examples for validation and a 3D field application.

3.1 Introduction

Streamline technologies have been widely used for reservoir management because of its powerful flow visualization capabilities that allow us to analyze rate allocation, pattern balance and waterflood performance. The connected flux volumes and its relative distribution can be easily obtained in terms of allocation factors from the streamlines. The application of streamlines have been extended to quantitatively analyze and optimize sweep efficiency using the streamline time of flight (TOF) distribution (Alhuthali et al. 2010; Alhuthali et al. 2007). In terms of early application to rate optimization, Grinestaff (1999) used streamline flow visualization to infer inefficiencies in the waterflood and set injection targets. No formal optimization was used here. Well rates were adjusted manually to obtain a more uniform distribution of streamlines amongst the producing wells. Grinestaff and Caffrey (2000) used allocation factors as their primary criterion for optimizing waterflood sweep. Thiele and Batycky (2003) proposed a streamline-based injection efficiency to optimize water injection. The injection efficiency was defined as the ratio of offset oil production to water injection as computed from the streamline-based flux distribution. More recently, Alhuthali et al (2007) presented a rate optimization approach to maximize sweep efficiency through equalizing the waterflood front arrival times at the producing wells. They derived well rate allocation and optimized flood-front management by delaying the water breakthrough at the producing wells. This approach, however, requires calculation of sensitivity of arrival time with respect to production/injection rates and use of constrained optimization methods such as the sequential quadratic programming technique.

In this chapter, we follow-up on the previous work of Alhuthali et al. (2007; 2010) and propose a rapid and easy to use method to optimize production/injection rates. The goal here is to avoid use of complex optimization tools; rather we emphasize the visual and the intuitive appeal of the streamline method. The basic underlying principle here is similar to that of Alhuthali et al (2007; 2010) and relies on two main ideas: (i) equalizing

‘average time of flight’ to all producers (ii) and minimizing the ‘time of flight variance’ within the streamline bundle. To accomplish this, we propose an easy to implement method for rate optimization utilizing streamline-based flood efficiency map. The flood efficiency map shows how the producers/injectors are connected and the relative movement of the flood front towards the producing wells. It consists of two areal maps: a flux distribution map and a time of flight distribution map. Although, the flux distribution maps have been used in the past to visualize flow, the use of TOF distribution map is novel. Using a combination of these two maps, we propose a procedure to optimize flood efficiency without the use of formal optimization tools. The main advantage of the proposed approach is that it is analytic, easy to implement and well-suited for large-scale field applications. Another advantage is its intuitive nature; we can visually examine the flow patterns as the calculations progress.

This chapter is organized into three sections that detail the theory and application of production and injection rate optimization. In the first section, we briefly outline the approaches and illustrate the procedural steps using a synthetic example. Production rate optimization approach is discussed first followed by the injection rate optimization approach. Next, we expand on the background and mathematical formulation underlying the proposed optimization method. Finally, we demonstrate the practical feasibility of our approaches using 3D field applications.

Our proposed method follows a simple and easy to use workflow using streamline-based flood efficiency map. The flood efficiency map, as shown in Fig. 1, is composed of two areal maps: a flux distribution map and a time of flight distribution map. Each of these maps can be generated from readily available streamline properties viz. the flow rate associated with each streamline and the time of flight along the streamlines. The flood efficiency map is a visual and physically intuitive tool for analyzing reservoir flow patterns and we extend its application to rate optimization. Specifically, we define two separate workflows for rate optimization: one is for production rate optimization and the other is for injection rate optimization. Depending upon the needs and the field conditions, one might want to utilize either or both to enhance waterflood efficiency.

3.2 Production Rate Optimization

The production rate optimization consists of two steps: (i) computing weighting factors for the production rates to equalize ‘average TOF’ at producers and (ii) minimizing the TOF variance within the streamline bundle reaching individual producers. First, we utilize the relationship between streamline flow rates and the TOF to compute rate change coefficients. We apply these rate change coefficients for the minimization of the ‘global’ TOF variance in a field- wide or regional basis by equalizing the ‘average TOF’ between producing wells. Second, we calculate weighting factors for ‘local’ update to further minimize the TOF variance by focusing on individual well connections and its bundle of streamlines.

Because the flood efficiency map provides all necessary information including flux and average TOF, the optimization can be carried out in a step-wise manner using a spreadsheet type application. The ease of implementation and the simplified nature of the workflow are the major strengths of our proposed approach. Below, we outline the production rate optimization in a stepwise manner.

3.2.1 Procedure of proposed production rate optimization

- ***Flow simulation and streamline tracing*.** For flow simulation, we can use either a streamline simulator or a finite difference (FD) simulator. If we use a FD simulator, we need to perform streamline tracing using the fluid flux information from the FD simulator.
- ***Streamline-based flood efficiency map construction*.** We aim to display the key information related to flow patterns and reservoir sweep with the flood efficiency map as shown in Fig. 3-1. It includes a flux distribution map and an average TOF distribution map that enable us to optimize waterflood management. The streamlines connecting each injector-producer pair is depicted with a single representative streamline, the fastest streamline. The TOF distribution map displays the ‘average

TOF' between the well pairs. The average TOF is calculated by a simple arithmetic average of time of flight associated with all the streamlines for each connection. The flux distribution map display volumetric flux between connecting wells computed by summing the fluxes carried by the streamlines. The flux distribution map is colored by the total flux connecting the wells while the color in TOF distribution map displays the average TOF. Thus, the flood efficiency map is a compact representation of the reservoir flow pattern and the flood front advancement.

- ***Global update coefficient calculation.*** The average TOF and total fluxes between injector-producer pairs are readily available from the flood efficiency map. Next, rate coefficients for 'global' updates are computed analytically based on the average TOF and flux distribution. This is discussed in detail in the next section. Because these rate coefficients attempts to equalize the average TOF among all connections in a field-wide or regional basis, we denote them as global update coefficients.
- ***Local update weighting factor calculation*.** This weighting factor is targeted to minimize the difference of TOF between individual well pairs in a root mean squared sense. These weighting factors are also derived analytically and incorporated along with the global update coefficients to minimize overall TOF variance. The goal of this step is to fine-tune the production rates in such a way so as to further reduce the variance of TOF in 'local' sense.

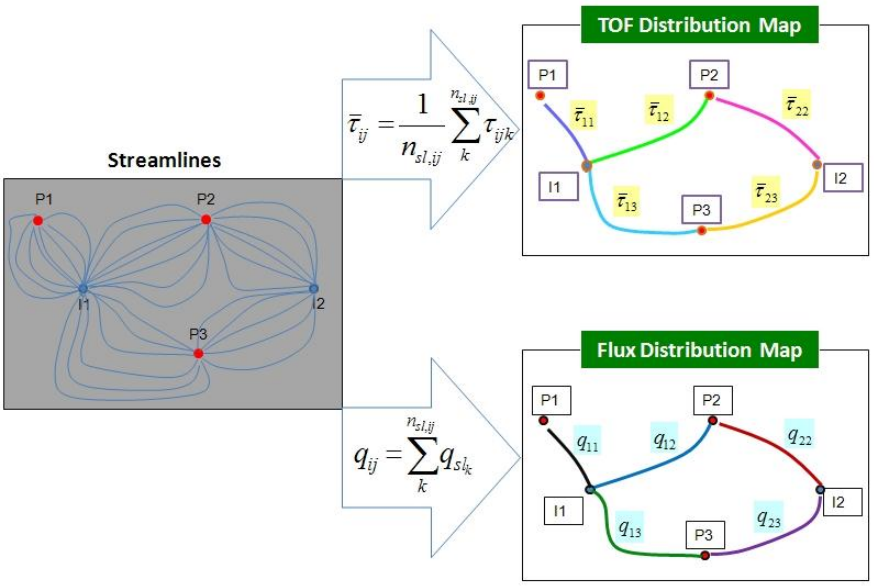

(a) Schematic of flood efficiency map

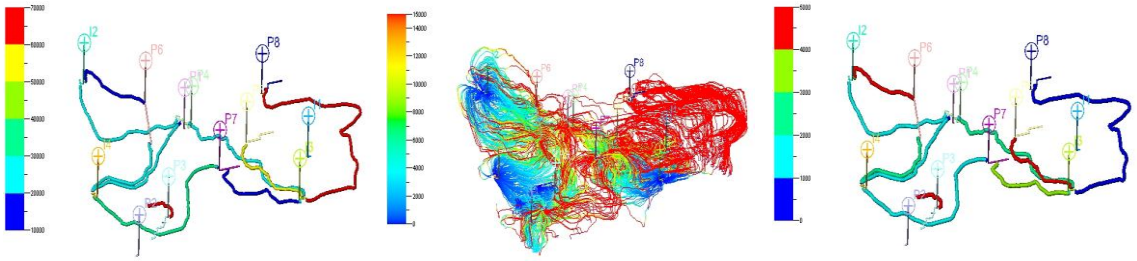

(b) Example : TOF distribution map (left), streamlines (middle), and flux distribution map (right)

Fig. 3-1 Streamline-based flood efficiency map: schematic (a) and example (b)

The overall optimization scheme is depicted in Fig. 3-2. The first figure, Fig. 3-2(a) shows that the optimization process will move the average TOF between well pairs to the global average. Further, the variance of TOF within well pairs will also be minimized as shown in Fig. 3-2(b).

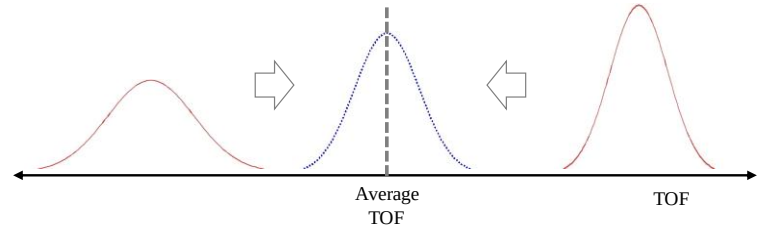

(a) Equalization of average TOF

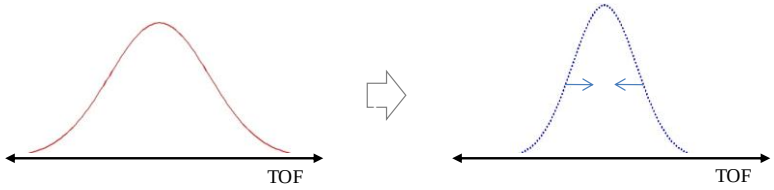

(b) Reduction of TOF variance

Fig. 3-2 Optimization scheme: equalization of average TOF (a) and reduction of TOF variance (b)

The optimization is performed on a time horizon basis as shown in Fig. 3-3. We start with optimizing flow rates for the first time interval and then move to next interval with the optimized rates from the previous time step. We continue this process until the desired time limit.

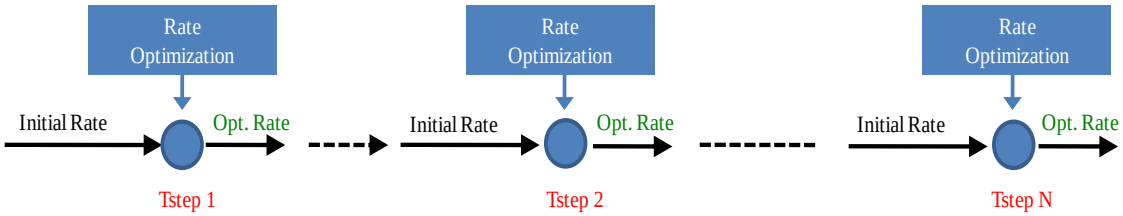

Fig. 3-3 Optimization process at multiple time steps

3.2.2 An illustration of proposed production rate optimization

Before discussing the mathematical background, we will first illustrate the procedure using a synthetic example. We use a two-dimensional two-phase heterogeneous reservoir

model for waterflooding consisting of 4 producers in the corners and 1 injector in the middle. Fig. 3-4 shows the base case for production rate optimization. A high permeability channel connects the producing wells P2 and P4 to the injector I1 as shown in Fig. 3-4(a). The streamlines for the base case are shown in Fig. 3-4(b). For the base case, the production rate is set at 100 RB/day and injection rate at 400 RB/day. This is also reflected in the flux distribution map, Fig. 3-4(c) because of the same color of the four 'representative' streamlines. Fig. 3-4(d) shows that the TOF at each producer is different because of the underlying heterogeneity with the TOF at P2 and P4 being much faster compared to TOF at P1 and P3. The same average TOF distribution is shown in Fig. 3-4(e) with a bar chart. In Fig. 3-4(f) we have focused on individual producers and shown the time of flight distribution of the streamlines reaching each producer. Thus, for optimization we will deal with two kinds of TOF variance: (i) the 'global' variance of average TOF amongst producers as in Fig. 4(e) and (ii) the 'local' variance of TOF at individual producers as in Fig. 3-4(f). From this 2D synthetic example, we will reallocate the production rates to maximize sweep efficiency through minimization of both 'global' and 'local' time of flight variance. The key constraints imposed on this production rate optimization are as follows:

- Injection rate equal to total production rate (voidage balance)
- Maximum allowable production rate per well = 300 RB/day
- Maximum water-cut allowance = 90 %

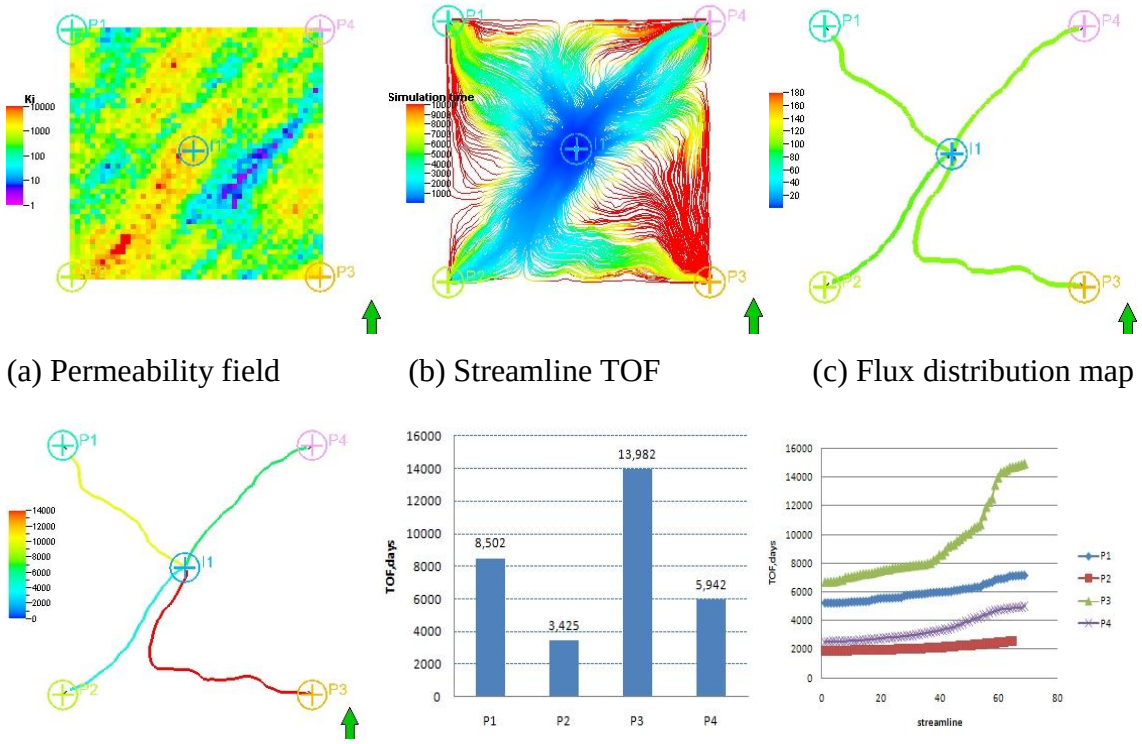

(a) Permeability field (b) Streamline TOF (c) Flux distribution map

(d) TOF distribution map (e) Avg. TOF (f) TOF distribution

Fig. 3-4 Streamline average TOF and flux distribution for base model

Fig. 3-5 shows the results from the optimization. The optimized production rates are shown in Fig. 3-5(b) with different colors indicating different production rate at each producer. While equalizing the TOF based on global and local update coefficients, we end up with increased production rates for P1 and P3 and reduced production rates for P2 and P4. The TOF distribution map after optimization is shown in Fig. 3-5(c) which shows the same color, indicating nearly equal TOF at all producers. On comparing with Fig. 3-4(c) and (d), we can clearly see how the production rates have been redistributed to equalize the TOF. It is also reinforced in Fig. 3-5(d). The 'local' time of flight distribution at individual producers is shown in Fig. 3-5(e). On comparing with Fig. 3-4(f), we can see that the TOF variance has been reduced both amongst the producers (globally) and within the producers (locally).

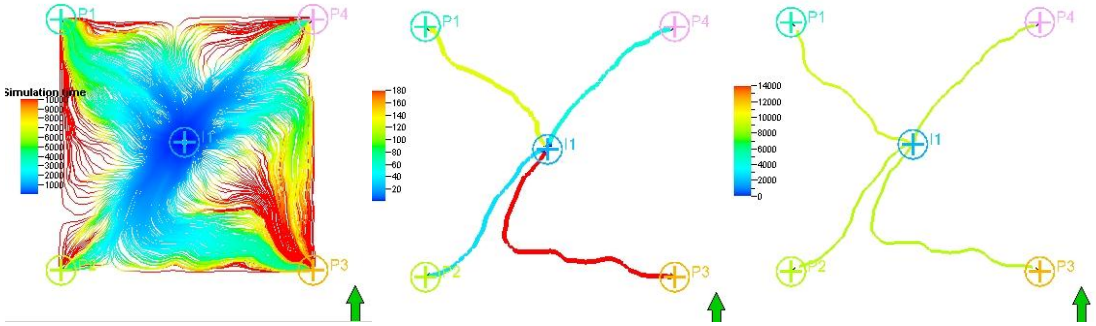

(a) Streamline TOF (b) Flux distribution map (c) TOF distribution map

(d) Avg. TOF (e) TOF distribution

Fig. 3-5 Streamline average TOF and flux distribution for optimization model

Fig. 3-6 shows increased oil production and reduced water production from the optimized model. Recall that we kept the total production rate the same and only reallocated to each producer. Fig. 3-7 shows the water saturation distribution for the base and optimized cases. Around the circled areas, we can clearly see that the optimized model has swept oil much more efficiently compared to the base case.

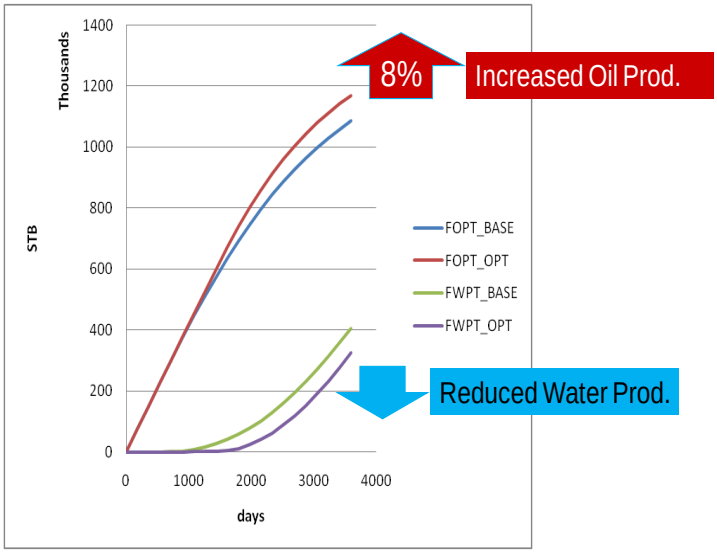

Fig. 3-6 Oil recovery comparison of base and optimized model

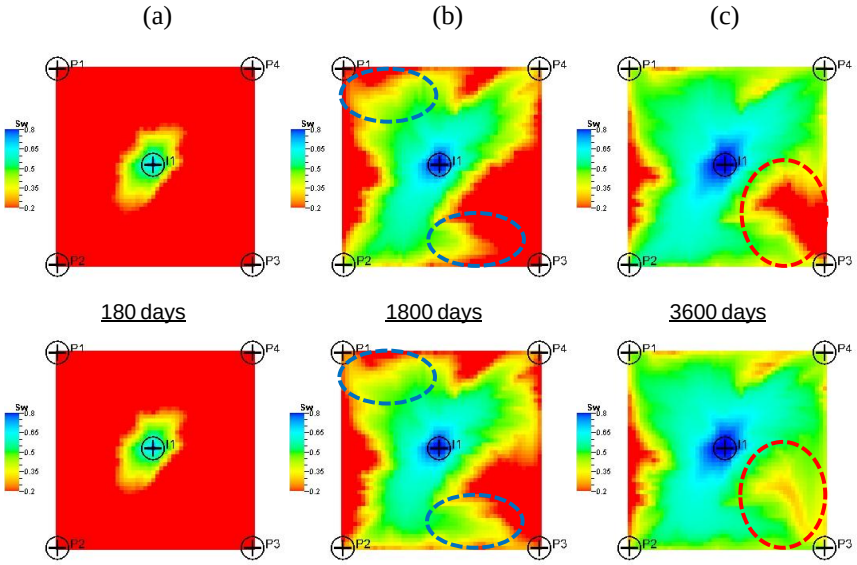

Fig. 3-7 Water saturation map for base (a-c) and for optimized (d-f)

3.3 Injection Rate Optimization

For injection rate optimization, we will first introduce the coefficient of variation which is a normalized measure of dispersion of a distribution. It is a dimensionless quantity defined as the ratio of the standard deviation to the mean. Because we are interested in the TOF distribution, we will define the coefficient of TOF variation (C_v) as follows:

$$C_v = \frac{\sigma_\tau}{\bar{\tau}} \qquad \text{……..……(3.1)}$$

where, σ_τ is the standard deviation of TOF and $\bar{\tau}$ is the mean of TOF.

In accordance with the idea that the variance of TOF affects sweep efficiency, here we define the coefficient of TOF variation as a measure of injection efficiency. We calculate the coefficient of TOF variation for each injector and reallocate the injection rates based on the coefficient of TOF variation. Following is a brief description of the steps.

3.3.1 Procedure of proposed injection rate optimization

- ***Flow simulation and streamline tracing.*** As in production rate optimization, the first step is to trace the streamlines and compute TOF along streamlines. We obtain the streamline information either directly from a streamline simulator or by tracing using fluxes provided by a FD simulator.
- ***Flood efficiency map construction.*** This step follows same procedure as in production rate optimization approach.
- ***Injection rate allocation factor calculation.*** We first calculate the coefficient of TOF variation at all injectors. For each injector, the streamlines leaving the injector and their associated time of flights to producer or producers are used to compute the coefficient of TOF variation. We compute the injection rate reallocation factor (λ_i)

for injection well i based on the weighting factor (ω_i) calculated with the TOF coefficient variations as given in Eq. 3.2 and Eq. 3.3. The reallocation scheme is based on the principle of equalizing injection efficiency for all injectors. Because we want to avoid flow concentration in high permeability regions leading to high variance in TOF, the proposed approach attempts to equalize the coefficient of TOF variation in a field-wide or regional basis.

$$\lambda_i = 1 \pm \omega_i \qquad \text{.....(3.2)}$$

$$\omega_i = \omega_{\max}\left(\frac{C_v^i - C_v^{\min}}{C_v^{\max} - C_v^{\min}}\right) \qquad \text{.....(3.3)}$$

where, C_v^i is the coefficient of TOF variation of well i. $C_v^{\max}$ and $C_v^{\min}$ represents maximum and minimum coefficient of TOF variation in the selected region or field. The weighting factor is adjusted subject to maximum weighting allowance ($\omega_{\max}$). In Eq. 3.2 we need to choose a sign for the weighing factor. This is discussed later in the mathematical formulation section.

3.3.2 An illustration of proposed injection rate optimization

We now illustrate the workflow with a 2D synthetic example. We consider waterflooding in a channelized reservoir with 9 producers and 4 injectors as shown in Fig. 3-8.

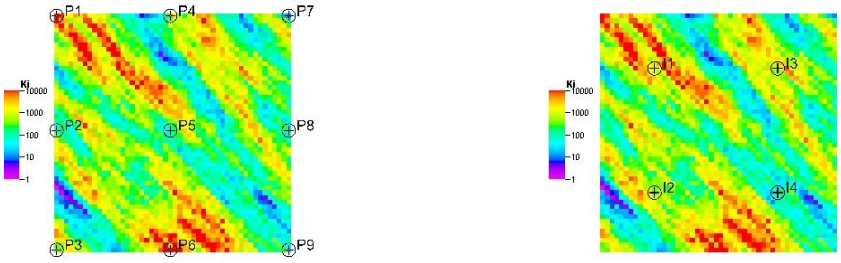

(a) producing wells' location (b) injecting wells' location

Fig. 3-8 Selected 2D heterogeneous model's permeability field with well locations

To illustrate the optimization process we set the base case with each injector injecting water at 200 RB/day and 9 producers producing a total of 800 RB/day. To demonstrate the generality of the approach, production rates were unevenly assigned as shown in Fig. 3-9. We use 6 months optimization time interval for a total of 20 year optimization period. We keep production rates the same and allocate only injection rates. Total injection rate of 800 RB/day is maintained and maximum individual injection rate is capped at 400 RB/day. Fig. 3-9 shows the optimized injection rate for each injection well at each time step. Considering that the initial injection rate at each injector was set at 200 RB/day, the optimization resulted in injectors I2 and I4 injecting more and the other two injectors injecting less.

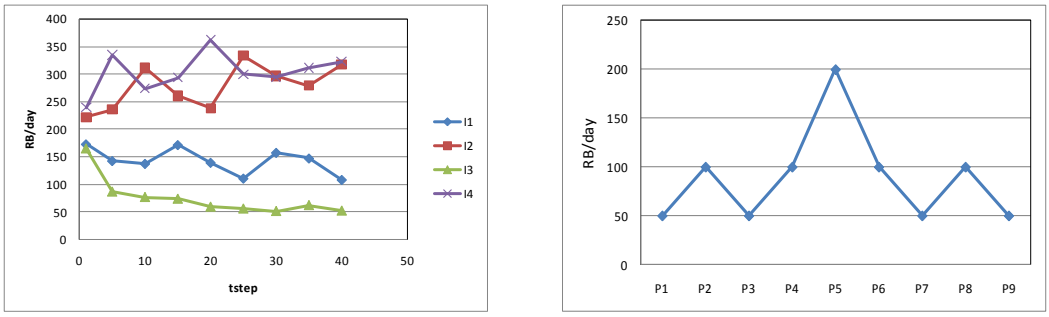

Fig. 3-9 Optimized injection rates for each well and each time step (left) and the production rates (right)

How do these optimized injection rates affect field oil production and sweep efficiency? As we expected, we could reduce the 'global' TOF coefficient of variation in

a field-wide basis as shown in Fig. 3-10(a). Also, in Fig. 3-10(b) and (c) we see that the optimized C_v^i for all wells are converging while the base C_v^i was much more widely distributed, mainly because of one well.

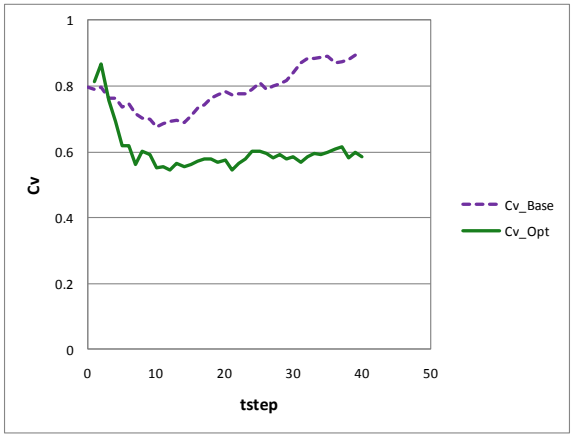

(a) Global coefficient of TOF variation

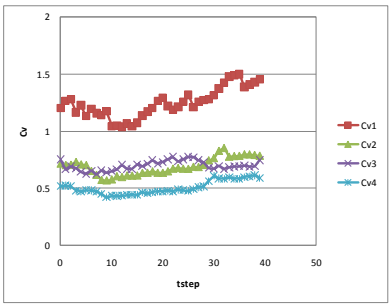

(b) C_v^i : base case

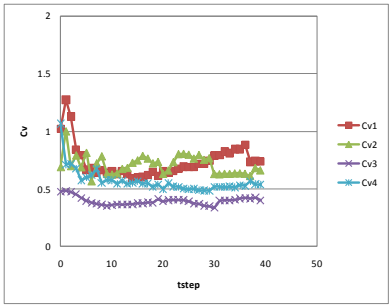

(c) C_v^i : optimized case

Fig. 3-10 TOF coefficient of variation for base and optimized case

Fig. 3-11 shows a comparison between the optimized and the base case in terms of oil saturation distribution at three different times. Clear differences in oil saturation can be found from the middle time step as shown in (d) (e) (f) Fig. 3-11(b) and (e). As we have reduced injection in I1 and I3 and increased injection in I2 and I4 in the optimized model, its impact is reflected on this saturation distribution. Also, we can see significant improvement in sweep at the final step. We

have almost completely swept the reservoir in the optimized model while significant oil saturation still remains between I1 and I3 wells for the base case.

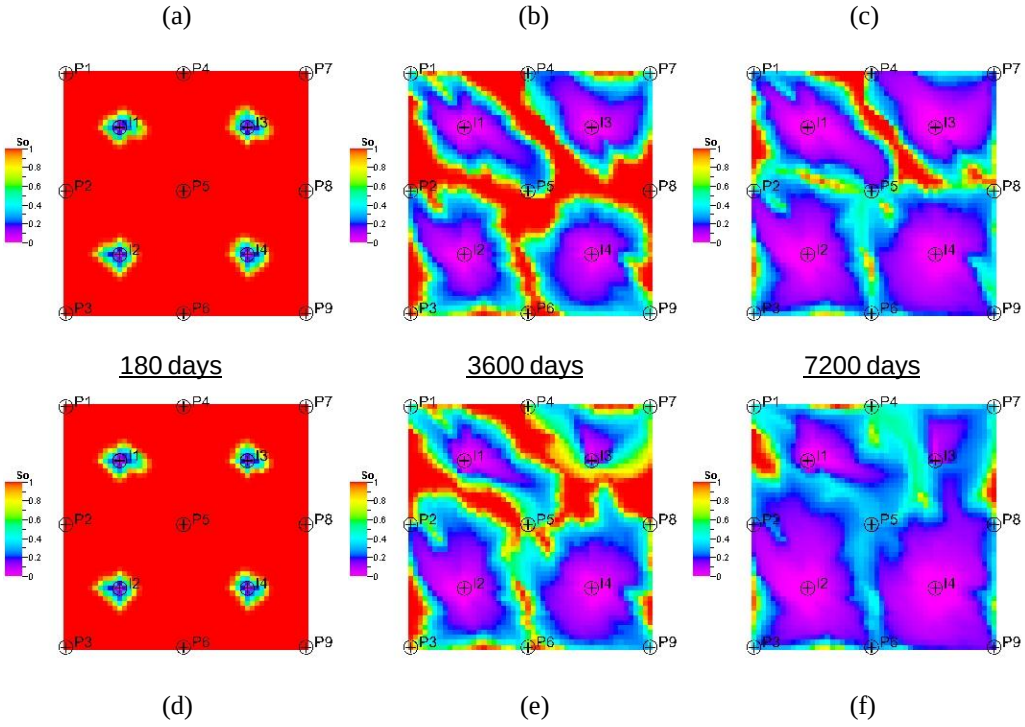

Fig. 3-11 Oil saturation map for base (a-c) and for optimized (d-f)

3.4 Background and Mathematical Formulation

In this section we discuss the mathematical formulation behind the production and injection rate optimization as illustrated in the previous section. We start with the production rate optimization followed by the injection rate optimization. In general, both rate optimizations use TOF variance as the fundamental quantity to reallocate rates. Also, both rate optimizations focus on reducing TOF variance to maximize the sweep efficiency. The specific details vary as discussed below.

As discussed before, for production rate optimization we introduce two-levels of weighting factors viz. global and local update coefficients to equalize average TOF

amongst producers and minimize TOF variance within a producer. The equation for production rate reallocation at well j is given as follows:

$$\Delta q_j = \sum_i \left[\left(\alpha_{ij} \beta_{ij} \right) \cdot q_{ij} \right] \qquad \text{……..……(3.4)}$$

In Eq. 3.4 we see that the change in production rate of well j can be obtained by summing all connected fluxes (q_{ij}) weighted by two update factors (α, β). The calculation of these update factors are discussed below.

3.4.1 Global update coefficient for production rate change

The rate optimization approach by Alhuthali et al (2007; 2010) used analytic sensitivity of the water front arrival time at the producer with respect to well rates. The sensitivities are partial derivatives relating changes in arrival time to small perturbations in production rate and injection rates. The sensitivities can be expressed as follows (Alhuthali, 2007):

$$S_{ij} = \frac{1}{N_{fsl,i}} \sum_{l=1}^{N_{fsl,i}} \frac{\partial \tau_{l,i}}{\partial q_j} \Bigg/ \left[\frac{df_w}{dS_w} \right]_{S_w = S_{wf,l}} \qquad \text{……...…(3.5)}$$

In Eq. 3.5 there is partial derivative $\partial \tau_{l,i} / \partial q_j$ which relates TOF to production rate. Using chain rule, it can be written as follows:

$$\frac{\partial \tau_{l,i}}{\partial q_j} = \frac{\partial \tau_{l,i}}{\partial q_{sl,i}} \frac{\partial q_{sl,i}}{\partial q_j} \qquad \text{……...……(3.6)}$$

By assuming that the streamlines do not shift because of small perturbations in the well rate, we can compute the partial derivative analytically (Alhuthali, 2007):

$$\frac{\partial \tau_{l,i}}{\partial q_{sl,i}} = -\frac{\tau_{l,i}}{q_{sl,i}} \qquad \text{……(3.7)}$$

The expression in Eq. 3.7 indicates that the change in TOF along a streamline connected to producer, i, with respect to the change in total flow rate along the streamline can be obtained as the ratio of the TOF and the flow rate along the streamline. Using the above relation, the production rate change of well, j, can be written as in Eq. 3.8.

$$\Delta q_j = \sum_i \frac{\Delta \bar{\tau}_{ij}}{\bar{\tau}_{ij}} q_{ij} \qquad \text{……...…(3.8)}$$

$$\Delta \bar{\tau}_{ij} = \left(\hat{\tau}_{\mathrm{d}} - \bar{\tau}_{\mathrm{ij}}\right) \qquad \text{……(3.9)}$$

In the above equation $\bar{\tau}_{ij}$ is the average TOF for the streamlines connecting wells i and j and $\Delta\bar{\tau}_{ij}$ represents the difference between the 'desired average TOF' and the current average TOF between wells i and j. The desired average TOF ($\hat{\tau}_{\mathrm{d}}$) is computed as the average TOF of all the streamlines in a field-wide or regional basis, depending upon the scope of optimization. Because there can be multiple connections to a producing well, the production rate change of well j is obtained by summing the product of the average time of flight ratio ($\Delta\bar{\tau}_{ij}/\bar{\tau}_{ij}$) and flow rate for each connection, i. If we define $\Delta\bar{\tau}_{ij}/\bar{\tau}_{ij}$ as the rate change coefficient (α_{ij}), then we have the global update equation as follows:

$$\Delta q_j = \sum_i \alpha_{ij} q_{ij} \qquad \text{……...…(3.10)}$$

3.4.2 Local update weighting factor for production rate change

We augment each rate change coefficient (α_{ij}) with a weighting factor (β_{ij}) so as to further minimize TOF variance within the streamline bundle associated with individual producers. Because the global update coefficient contributes to equalizing average TOF among all connections, in local update we are focusing on the streamline TOF inside each connection. The weighting factor is obtained by minimizing the expected RMS difference of rate change coefficients as given in Eq. 3.11.

$$\min\left[\sqrt{\sum_{k=1}^{m}\sum_{l=1,l\neq k}^{m}\left(\beta_{ij}\alpha_{ijk}-\alpha_{ijl}\right)^2}\right] \qquad \ldots\ldots\ldots\ldots\ldots\ldots\ldots\ldots\ldots\ldots\ldots\ldots\ldots\ldots(3.11)$$

In practice, we will minimize Eq. 3.12 that is equivalent to minimizing Eq. 10 above.

$$\sum_{k=1}^{m}\sum_{l=1,k\neq l}^{m}\left(\beta_{ij}^2\alpha_{ijk}^2-2\beta_{ij}\alpha_{ijk}\alpha_{ijl}+\alpha_{ijl}^2\right) \qquad \ldots\ldots\ldots\ldots\ldots\ldots\ldots\ldots\ldots\ldots\ldots\ldots\ldots\ldots(3.12)$$

Taking derivative with respect to the weighting factor (β_{ij}) and seeking the minimum, we have following expression:

$$2\beta_{ij}\sum_{k=1}^{m}\sum_{l=1,k\neq l}^{m}\left(\alpha_{ijl}^2\right)-2\sum_{k=1}^{m}\sum_{l=1,k\neq l}^{m}\left(\alpha_{ijk}\alpha_{ijl}\right)=0 \qquad \ldots\ldots\ldots\ldots\ldots\ldots\ldots\ldots\ldots\ldots\ldots(3.13)$$

The first and second term in Eq. 3.13 can be written as given in Eq. 3.14 and Eq. 3.15 respectively.

$$2\beta_{ij}(m-1)\sum_{l=1}^{m}\alpha_{ijl}^2 \qquad \ldots\ldots\ldots\ldots\ldots\ldots\ldots\ldots\ldots\ldots\ldots\ldots\ldots\ldots\ldots\ldots\ldots\ldots(3.14)$$

$$2\left[\left(\sum_{l=1}^{m}\alpha_{ijl}\right)^2-\sum_{l=1}^{m}\left(\alpha_{ijl}^2\right)\right] \qquad \text{……..…(3.15)}$$

This leads to the solution for the weighting factor, Eq. 3.16 given as follows:

$$\beta_{ij}=\frac{1}{m-1}\left[\left\{\left(\sum_{l=1}^{m}\alpha_{ijl}\right)^2\Big/\sum_{l=1}^{m}\left(\alpha_{ijl}^2\right)\right\}-1\right] \qquad \text{……(3.16)}$$

3.4.3 Coefficient of TOF variation for injection rate change

We defined the coefficient of TOF variation in Eq. 3.1 where the standard deviation of TOF for injector i is obtained as follows:

$$\sigma_\tau^i=\sqrt{\frac{1}{N_{sl}}\sum_{k=1}^{N_{sl}}\left(\tau_k-\bar{\tau}\right)^2} \qquad \text{……(3.17)}$$

In Eq. 3.17, we include all the streamlines leaving the injector and their corresponding time of flight to producer or producers. The average of TOF ($\bar{\tau}$) is calculated by taking average of all the streamlines associated with injectors in a field-wide or regional basis depending upon the scope of optimization. Now we can define the coefficient of TOF variation of injector i (C_v^i) as follows:

$$C_v^i=\frac{\sigma_\tau^i}{\bar{\tau}} \qquad \text{……..…(3.18)}$$

This coefficient of TOF variation is considered as an injection efficiency factor. The optimized injection rate is obtained based on this efficiency factor using Eq. 3.2 and Eq. 3.3. In Eq. 3.2 we need to choose a sign for the weighing factor. The sign is chosen

based on calculated average TOF. For example, if the average TOF for an injection well is greater than average TOF for the optimization region, we assign a positive sign to compute a reallocation factor greater than 1. This leads to higher injection and reduced time of flight for the injector as desired.

3.5 Production Rate Optimization Application to The Benchmark Brugge Field

In this section we demonstrate the application of our proposed optimization approach with 3D field examples. To start with, we will discuss the application of production rate optimization. For this, we use the data from the SPE benchmark Brugge field (Peters, E. et al. 2009). Next, we discuss the application of injection rate optimization using the data from the Goldsmith field in west Texas.

The Brugge field model was set up as part of an SPE Applied Technology Workshop (ATW) for the purpose of evaluating various production optimization methods. The model properties are based on a North sea brent-type field. The reservoir simulation model has about 60 thousand grid blocks with 9 layers. The field includes 20 vertical producers completed in the top 8 layers and 10 peripheral water injectors completed in all layers. The details about Brugge field can be found in the paper by Peters et al. (2009). Fig. 3-12 shows the permeability field with injection well locations in the left figure and production wells in the right figure.

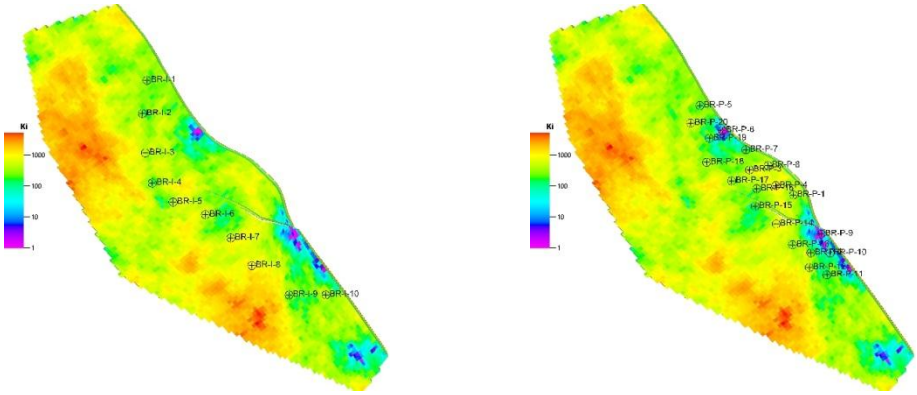

Fig. 3-12 Brugge field permeability distribution and injection wells (left), producing wells (right)

The field history data was provided for history matching purposes (Peters et al, 2009). The closed loop optimization consisted of two steps: updating the model via production data integration using the first 10 years of production history and then, optimizing the production rates for the next 20 years.

In this study, we matched 10 years of production history and then optimized the rates for the next 10 years of production. The optimization time interval used is 6 months. We compared the optimized case with the base case to examine evidence for improved recovery or increased sweep efficiency. The base case involves reactive control whereby the well are produced at prespecified rates and is switched to a minimum rate whenever the water cut reaches 90%. Major considerations and constraints used in this application are as follows:

- Total injection rate equal to total production rate (voidage balance)
- Maximum allowable production rate per well = 3000 RB/day
- Maximum allowable injection rate per well = 4000 RB/day
- Maximum water-cut allowance = 90 % , after that, well is switched to minimum production rate of 10 RB/day

Our optimization workflow include two steps: computation of ‘global’ rate coefficients followed by local update weighting factors as discussed before. Fig. 3-13 shows the production rates for the base case and the optimized case at two different times. Looking at Fig. 13(b), the production rates at the last time step of the optimization period, we see that production rates for wells P-6 through P-11, farthest from the injectors, have increased. On the other hand, the rates for wells P-14 through P-17 have been continuously reduced. Some of the wells are switched to minimum production rate because of water-cut limit. Our optimization approach takes into account changes in well schedules by using the streamline-based flood efficiency map at the time interval of interest. For every single time interval of optimization, we analyze the flow field using the flood efficiency map, identify inefficient producers and suggest new optimized rates.

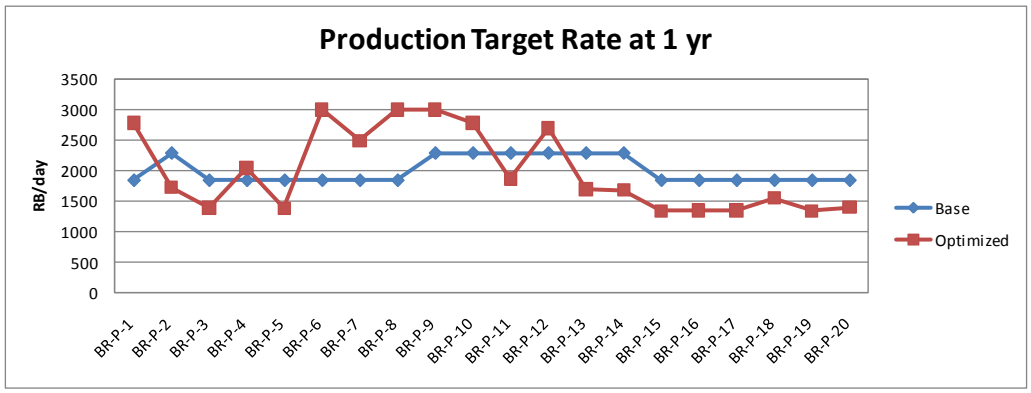

(a) production target rate at 1 year

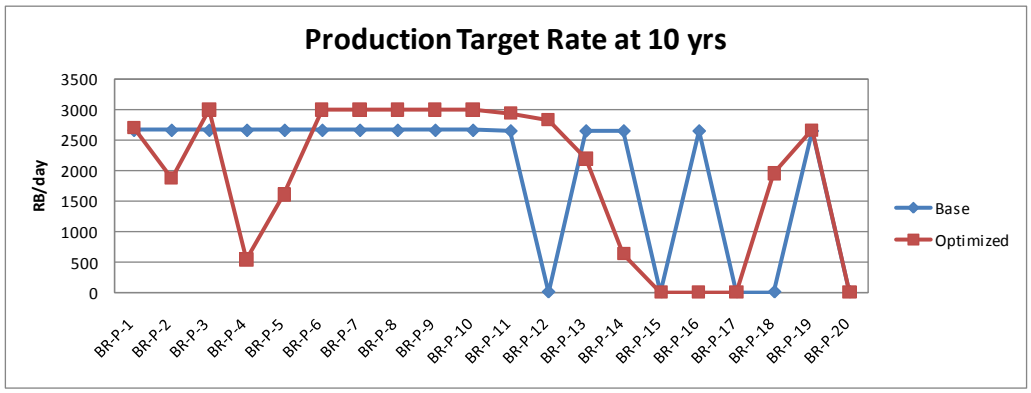

(b) production target rate at 10 year

Fig. 3-13 Production target rate for base (blue) and optimized (red)

Fig. 3-14 compares the optimized case and base case in terms of TOF distributions for each connection at the last time step. The figure clearly shows how TOF variance has been reduced because of optimization. The circled area in the figure shows the TOF for faster streamlines for each connection. The results show the outcome of the optimization in terms of equalizing the average TOF.

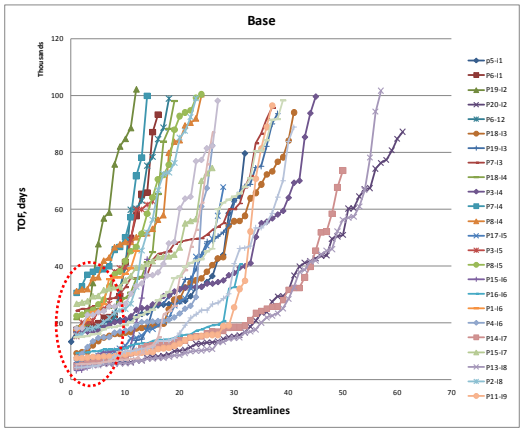

(a) Base case

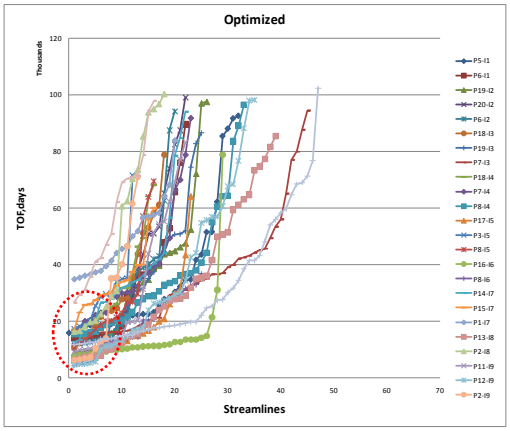

(b) Optimized case

Fig. 3-14 Time of flight for each connection between wells – base (a) and optimized (b)

Fig. 3-15 shows some key regions with the flood efficiency map displaying average TOF. Recall that the streamline in the flood efficiency map shows the fastest streamline path and is colored by the average TOF between the injector-producer pair. Whereas the colors of the connections are very different for the base case, they become very similar after the optimization. This again indicates that the optimization successfully equalized the average TOF to maximize sweep efficiency. The optimization resulted in almost 8% increase in oil production and a similar reduction in water production compared to the base case.

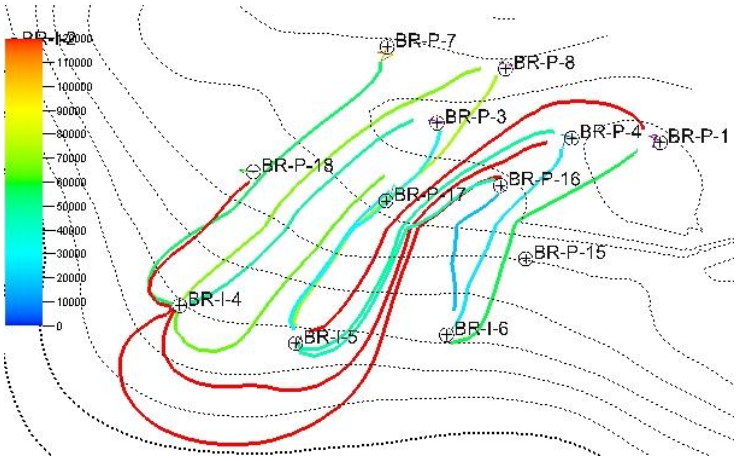

(a) Average TOF flood efficiency map for base case

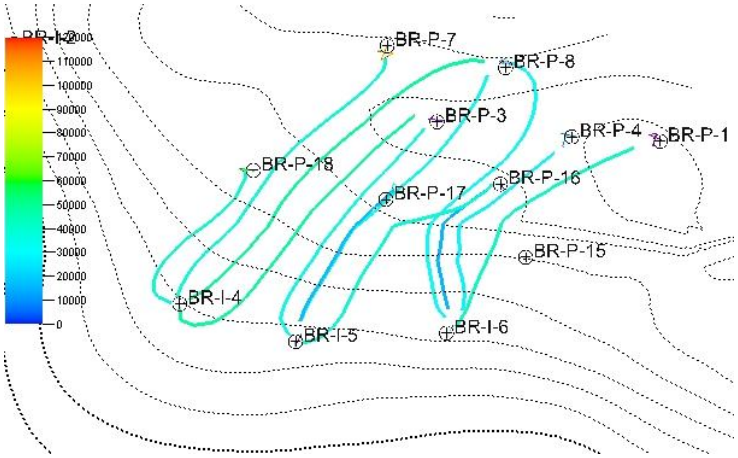

(b) Average TOF flood efficiency map for optimized case

Fig. 3-15 Flood efficiency map showing average TOF of key wells in Brugge: base (top) and optimized (bottom)

Fig. 3-16 shows oil saturation distribution at the end for the base and the optimized case. We marked with circle the regions with large saturation change. We see significantly reduced oil saturation in the optimized case because of improved sweep efficiency.

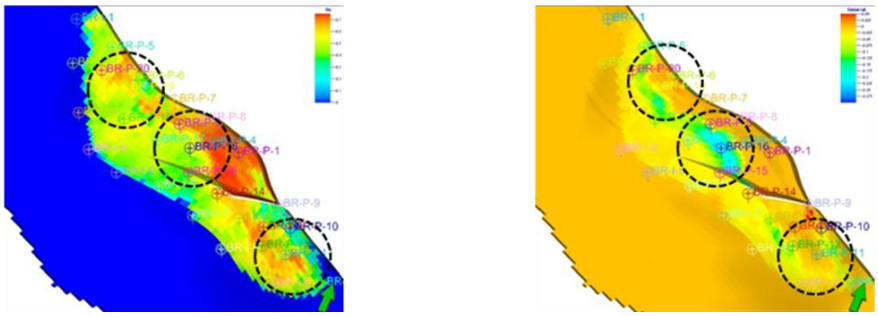

(a) Base

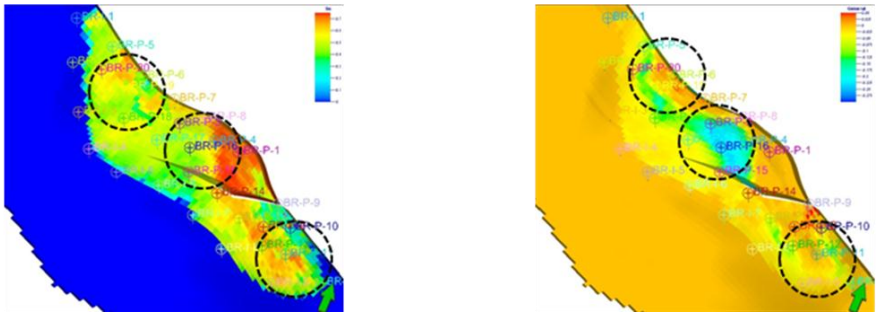

(b) Optimized

Fig. 3-16 Oil saturation (left) at time end and the saturation difference (final Soil – initial Soil, right)

This example involved rate optimization for a mature waterflood using streamline-based flood efficiency map. At the time of optimization, most producing wells already had breakthrough. Instead of controlling the water front arrival time, we improved flood efficiency using simple analytic calculations resulting higher waterflood sweep. The power of the method lies in its simplicity, ease of application and ability to visually analyze and interrogate the results.

3.6 Injection Rate Optimization Application to The GSAU Field

For field applications, very often it is easier to conduct an injection optimization rather than a production optimization because of operational constraints. In this section we

demonstrate the proposed injection rate optimization approach to a CO_2 pilot project area in the Goldsmith San Andrea Unit (GSAU), a dolomite formation located in west Texas. The pilot area has over 50 years of production history before the initiation of the CO_2 pilot project in 1996. Fig. 3-17 shows the pilot project area in the GSAU. In this study we included extra wells located outside the pilot area in order to account for correct boundary conditions. The study area includes 33 producers and 11 injectors with a total of 30,740 grid cells. Fig. 3-18 shows the porosity and permeability distributions along with the producers and injectors location.

Fig. 3-17 Goldsmith field study area: CO_2 pilot area within the box

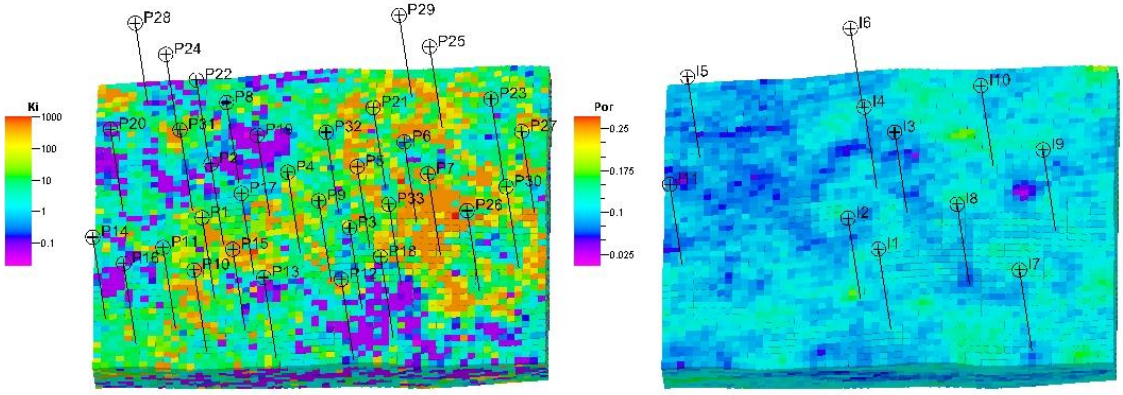

Fig. 3-18 Generated permeability field with producers (left) and porosity field with injectors (right)

For the base case we used the first 21 years of production/injection history. To account for different schedule of production/injection such as changing rates and infill wells, we subdivided the time period into 11 time steps. We kept the same operating conditions except for the injection rates which were changed via optimization.

- Total injection rate are same as history
- Maximum injection bottom-hole pressure: 4500 psi
- Maximum production bottom-hole pressure: 1000 psi
- Water cut limited to 98%

Injection rates were changed based on the injection efficiency factor defined before using the coefficient of TOF variation. For each of the 11 injectors in this field, the rates were updated at each time step. The difference between the optimized and the base injection rates is as shown in Fig. 3-19. The change indicates that the injectors near the boundaries such as I6 and I7 showed significantly increased injection while the wells in the central region such as I2 and I3 showed decreased injection.

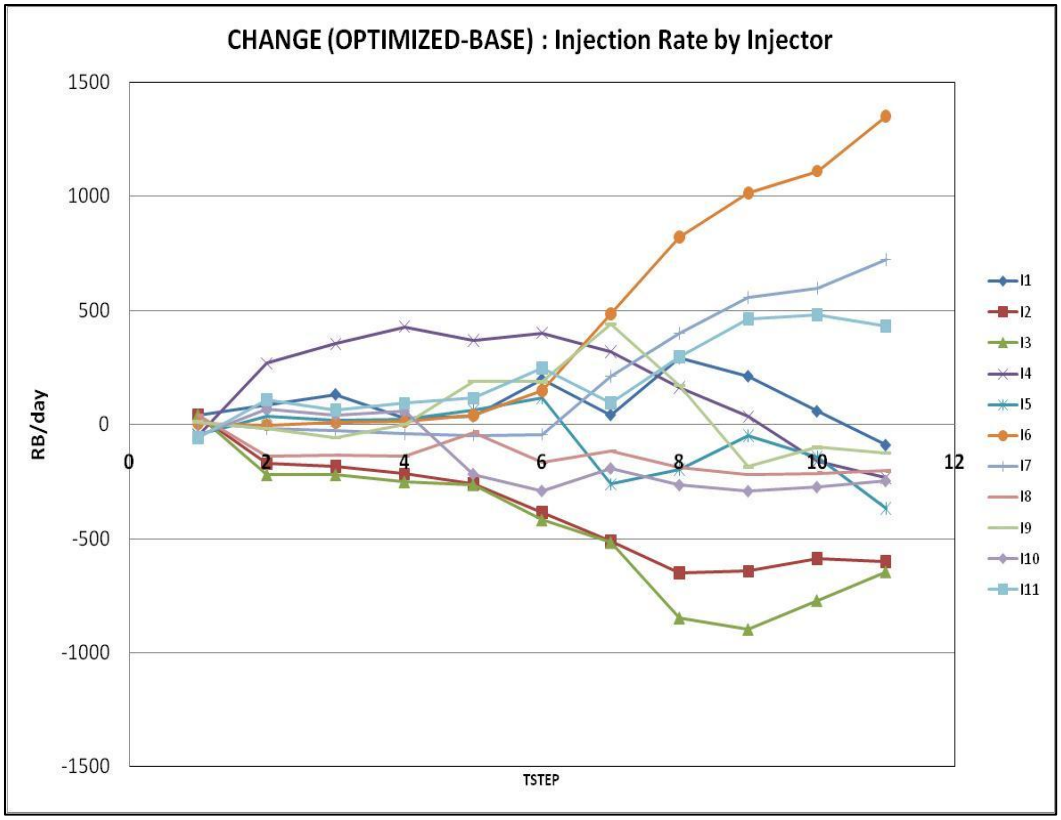

Fig. 3-19 Injection rate change for each injector after optimization

The optimization resulted in increased oil recovery and at the same time reduced water production as shown in Fig. 3-20. The figure in the right shows the wells with an increase or decrease in cumulative oil production of over 100,000 STB. Only one well, P29 seem to be adversely impacted whereas all other wells, in particular well P5 show significant increase in oil production.

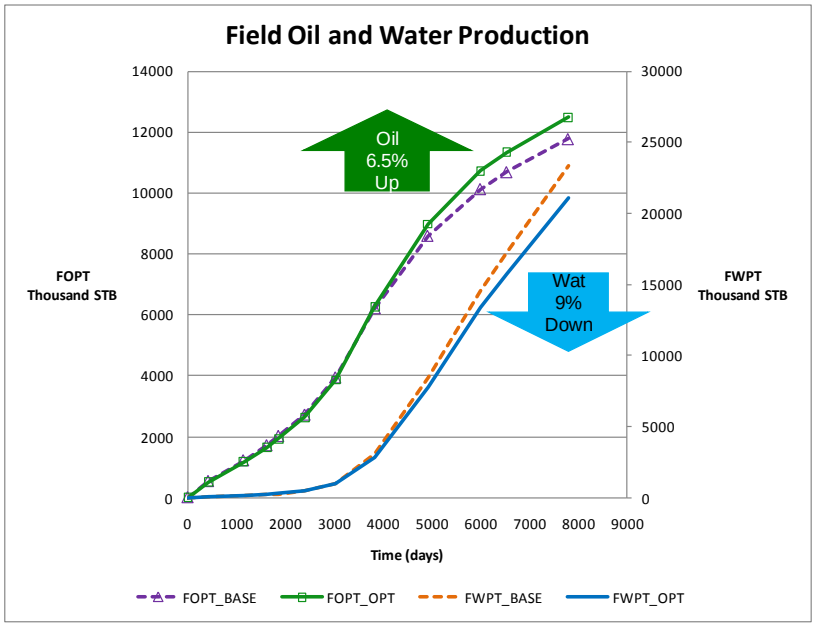

Fig. 3-20 Field oil and water production comparison (left)

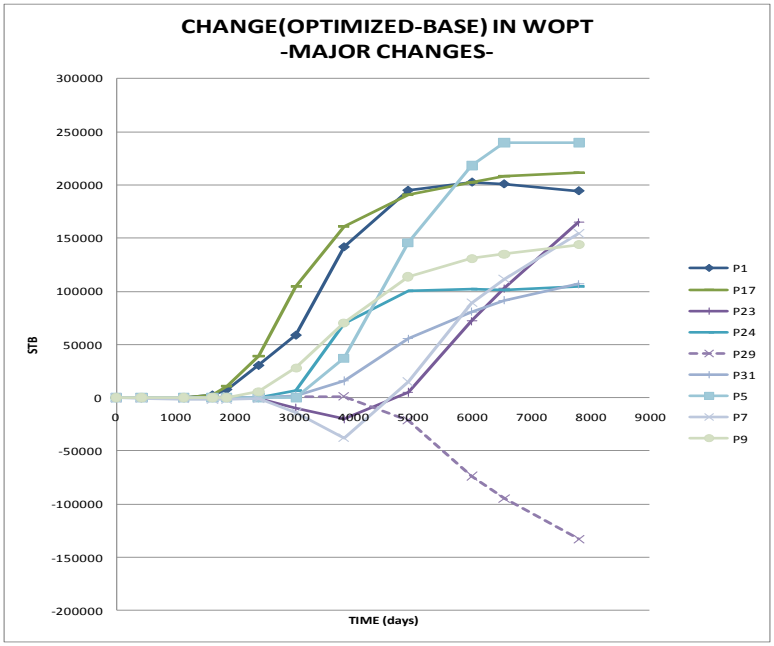

Fig. 3-21 Change in well oil production by well

In Fig. 3-22 we compare the base model and the optimized model in terms of flux connectivity between the wells to gain a more clear understanding of the changes in

injection pattern because of optimization. The streamlines are colored by the amount of flux displayed on the fastest path between each connection. The circled injectors (I6, I7, I11) near the boundaries are injecting at higher rates and showing increased connectivities with surrounding producers. For example, the well I7 in the bottom right supported 4 wells for the base model and after optimization supports 8 producers with higher injection rates. Thus, the areas around the well I7 are much better swept than before. Furthermore, we see that the wells in the central region are also well-connected and the streamlines show good coverage throughout the reservoir in the optimized model.

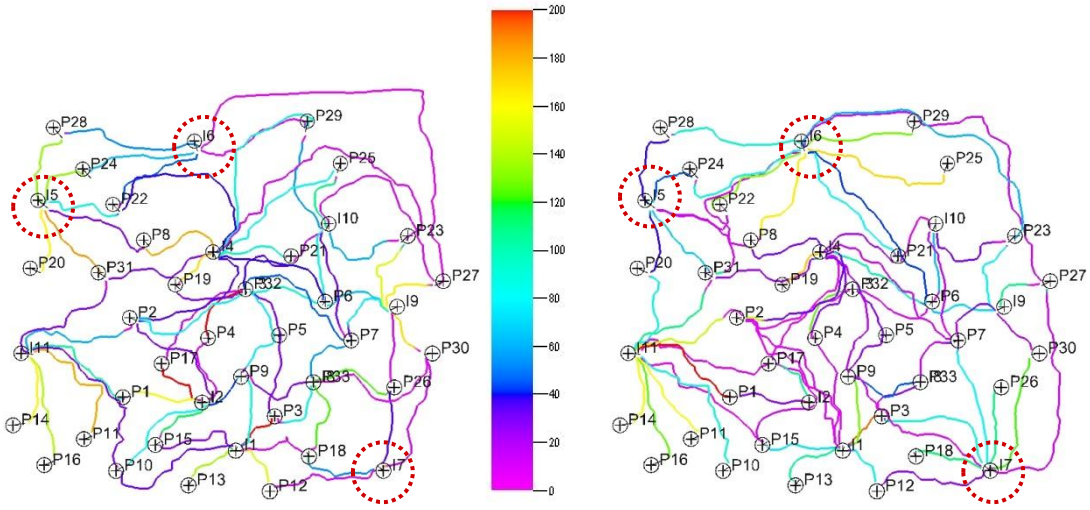

Fig. 3-22 Flood efficiency map showing flux connectivity between wells: base (left) and optimized (right)

Fig. 3-23 compares the optimized and the base case in terms of oil saturation at three different times. The improvement in sweep for the optimized case is obvious here. In particular, the bottom left and the top areas show significant reduction in oil saturation.

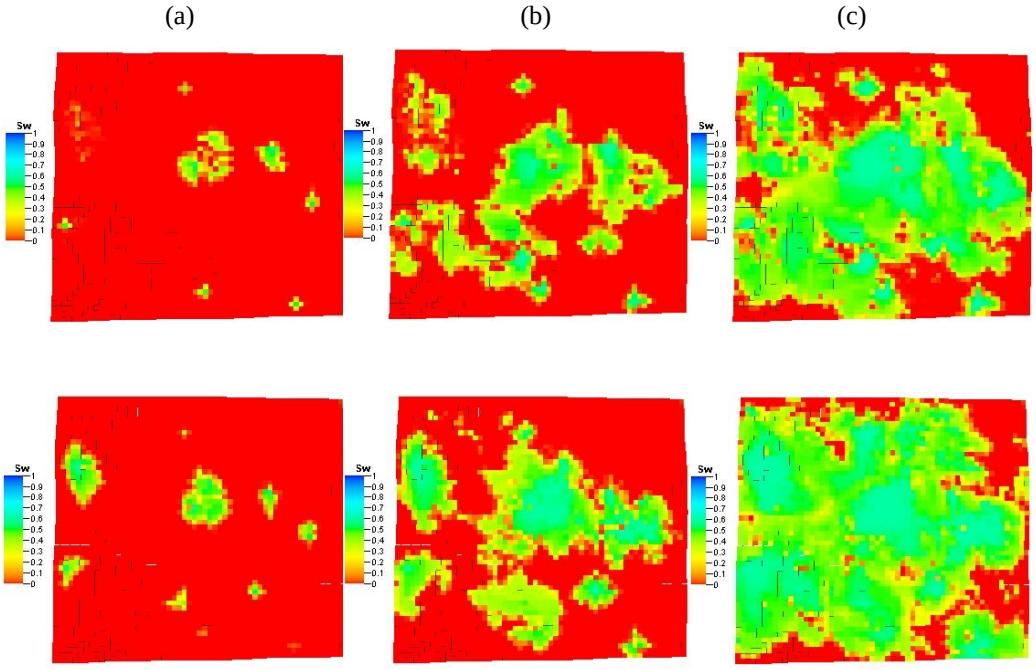

Fig. 3-23 Oil saturation map for base (a~c) and for optimized (d~f)

3.7 Summary and Conclusion

In this chapter, we have presented rapid rate optimization approaches for both injection and production wells utilizing streamline-based flood efficiency maps. The flood efficiency maps are a succinct representation of the flow pattern and flood front progression in the reservoir and can be easily constructed from the streamlines. We outline a systematic and easy to implement method for injection and production rate allocation to maximize sweep efficiency without resorting to formal optimization methods. The major findings in the paper can be summarized below:

1. The flood efficiency map is shown to be an effective tool for reservoir management because it provides valuable information related to reservoir flow patterns and sweep efficiency. Although, the flux distribution maps have been used in the past to visualize flow, the use of TOF distribution map is novel. In

fact, our proposed optimization method mainly relies on the TOF distribution map.

2. Our proposed streamline-based production rate optimization is simple, intuitive and easy to implement. It relies on equalizing the TOF both ‘globally’ (between streamline bundles in terms of average TOF) and ‘locally’ (within streamline bundles) using analytic formulation. The approach is applicable to both new and mature waterflooding as we minimize variance of TOF between injection-production pairs rather than focusing on the water front breakthrough time.
3. A new definition of injection efficiency is proposed in terms of the coefficient of TOF variation. Using this criterion, we propose a systematic approach to injection optimization. Recognizing that in field applications it is more practical to optimize injectors rather than producers, the injection optimization scheme has been proposed as a simple and standalone procedure.
4. The effectiveness of our optimization can be examined by comparing the flood efficiency maps before and after optimization. In particular, the TOF map is a clear indicator of sweep efficiency in terms of the similarity or dissimilarity of the average TOF between the well connections.
5. We have demonstrated the power and utility of our proposed method using a variety of synthetic examples and also field applications.

CHAPTER IV

HIERARCHICAL PARETO-BASED APPROACH TO HISTORY MATCHING UNDER CONFLICTING INFORMATION

In this chapter, we propose to use a Pareto-based multi-objective evolutionary algorithm (MOEA) focusing on finding a set of optimal solutions called Pareto optima. The MOEA makes direct use of a dominance relation for fitness assignments for various objectives, instead of classical fitness score derived based on one-dimensional objective space. The dominance concept can define levels of optimality using multidimensional objective space to sort populations, and classify models into ranks (Pareto fronts). Because it uses a population of models in the search process and optimizes such that the ranks are minimized, the Pareto optimal solutions can provide a measure of uncertainty in predictions. We show how the MOEA identifies optimal solutions by examining the trade-offs between conflicting objectives among multiple plausible solutions; particularly, we demonstrate that it performs better than the weighted-sum approach.

For practical applications, we provide a novel workflow with a Grid Connectivity-based Transformation (GCT) basis coefficients as parameters for calibration using the gradient-free evolutionary optimization algorithm. The parameterization basis is obtained from spectral decomposition of the grid connectivity Laplacian and avoids ad hoc redefinitions of regions while preserving geologic heterogeneity. We demonstrate the power and utility of the proposed workflow using multiple examples. These include 2D synthetic examples for validation and a 3D field application for matching production and seismic data with uncertainty and conflicting information.

4.1 Introduction

The purpose of history matching of reservoir performance is to make reservoir models forecast more accurately and therefore, estimate the range of recovery or provide the

economic assessments of different field development strategies. An ensemble of history-matched models is typically used to predict future reservoir performance and evaluate prediction uncertainty.

Very often, history matching involves the use of multiple objectives, including multiphase production data (water cut and/or GOR), 4D time-lapse seismic data, SFT pressure data, etc.. These objectives can be potentially conflicting because they are from different sources, measurements, and have different levels of uncertainties. For example, the uncertainties in geophysical data are in particular associated with errors in arrival time picking, errors in depth conversion, pre-processing and migration errors, and so on. Those are related to all activities of seismic data including acquisition, processing, and interpretation. Because each data has different potential to observe reservoir characteristics, combining all available data into history matching workflow helps improve the quality of history matching. For example, well-based surveillance (pressure, rates) rarely provides us with much insight on the specific details of the flow paths between wells while seismic surveillance does (Walker and Lane 2007). The spatial information can be observed through time-lapse seismic data. We can thus expect that time-lapse seismic will improve the predictive capability of reservoir models.

Integration of dynamic data typically requires the minimization of a predefined objective function, which consists of a misfit term, typically defined as the difference between observed and simulated data, and appropriate penalty terms. In the recent decade, research on assisted history matching techniques has received a lot of attention in reservoir engineering community and many papers have been published in the literature. There have been a variety of approaches to the minimization of the objective function. These can be classified broadly into three categories: gradient-based methods, sensitivity-based methods, and derivative-free methods. Gradient-based methods typically converge slowly (Gill et al. 1981; McCormick and Tapia 1972) but they have been widely used for automatic history matching; The derivative-free methods such as simulated annealing and genetic algorithms are simple to implement but limited to relatively small number of parameters because of the computational burden (Oliver et al.

2001). Sensitivity-based method uses computed sensitivities that are simply partial derivatives that define the change in production response because of small changes in reservoir parameters. Sensitivity-based methods are attractive because of faster convergence compared to gradient-based methods (Bissell et al. 1992). Specifically, the streamline-based generalized travel time inversion (GTTI) technique has proven to be an efficient means for computing the parameter sensitivities (Cheng et al. 2005; Cheng et al. 2004; Datta-Gupta et al. 2001) because the sensitivities are obtained in a single forward simulation run. The GTTI history matching approach has been successfully applied to several field cases (Cheng et al. 2004; Hohl et al. 2006; Qassab et al. 2003; Rey et al. 2009).

Most of approaches mentioned above typically start with a single initial geological model, usually ends up with a single deterministic history matched model, and thus, does not readily allow for uncertainty analysis. Because reservoir models deals with substantial modeling uncertainties and particularly becomes more complex, uncertainty is required to be quantified by generating alternative simulation models rather than one unique deterministic solution. In this sense stochastic search techniques such as simulated annealing (Galassi et al. 2009; Kirkpatrick et al. 1983; Ouenes et al. 1994),and genetic algorithms (Holland 1992) have been known to be more effective, however these methods require large number of flow simulations, which can be computationally prohibitive, particularly when the parameter space is very large.

Classical history matching techniques typically treat multiple or many objectives optimization problem as single objective optimization problem by aggregating all objectives into a scalar function (weighted-sum) resulting in incomplete exploration of solution space. If those objectives are conflicting to each other, this approach can be problematic. A multiobjective optimization task involving multiple conflicting objectives ideally demands finding a multidimensional Pareto optimal front (Deb and Saxena 2005). Multiobjective optimization evolutionary algorithm (MOEA) is designed to find a representative set of solutions in the Pareto optimal front while most of classical methods aim at finding one preferred solution. As a typical method, Rey et al. (2011)

performed joint integration of seismic and production data using a deterministic approach in which a penalized misfit function that quantifies the production and seismic data misfit is minimized. In the misfit function they have given a weighting factor for each objective depending on the degree of confidence in the data. The solution ends up with one model satisfying the surveillances with a certain level of error unless multiple initial models are used. Similarly, Cheng et al. (2007) also showed joint integration of multiple production data (water cut and GOR) using a travel time inversion.

In this chapter, we focus on multiobjective optimization technique for history matching of reservoir performances. Schulze-Riegert et al. (2007) showed the application of multiobjective optimization technique to history matching of reservoir model using one of MOEA algorithm, Strength Pareto Evolutionary Algorithm (SPEA). It demonstrates that multiple objectives can behave conflictingly because of incomplete parameter space assigned. Han et al. (2010) used non-dominated sorting genetic algorithm (NSGA-II) and compared weighted-sum approach and multiobjective optimization approach using 2D heterogeneous reservoir history matching model. Lately, Hajizadeh et al. (2011) used differential evolution for multiobjective optimization using Pareto ranking (DEMOPR). They used PUNQ model for history matching and coupled the algorithm with Bayesian uncertainty quantification framework to estimate the uncertainty in future recovery. In these applications production data information (water cut, GOR, bottom hole pressure) is only used as objectives but they formulate multiple objective optimization problem by considering either each well as one objective or grouping several wells as an objective.

In this chapter we present multiobjective optimization approach to history matching of reservoir performances where 4D time-lapse seismic data and production data have been used to demonstrate multiple objective problems. First, we show that incorporation of seismic data improves the quality of history matching. Next, we show how the MOEA identifies optimal solutions and how well it performs under conflicting information. We also compare MOEA and typical genetic algorithm based weighted sum approach in terms of finding optimal solutions. For practical applications, we provide a novel

workflow with a Grid Connectivity-based Transformation (GCT) basis coefficients as parameters for calibration using MOEA. We demonstrate the power and utility of the proposed workflow using multiple examples including 2D synthetic examples for validation and a 3D field application for matching production and seismic data with uncertainty and conflicting information.

The organization of this chapter is as follows. First, we discuss the background of multiobjective optimization with mathematical formulation and available methods. Next, we propose a Pareto-based multiobjective optimization method with GCT for history matching of reservoir performances. We illustrate the proposed method with multiple synthetic examples and compare it with the conventional weighted sum approach. Finally, we demonstrate the practical feasibility of our approach through application to a benchmark reservoir, the Brugge field.

4.2 Multiobjective Optimization

In this section we discuss the background of multiobjective optimization, mathematical formulation and the terminology. We introduce two multiobjective optimization techniques; scalarization method and Pareto-based method. We will compare both techniques using a test function set up with conflicting information.

4.2.1 Pareto optimal solutions

Multiobjective optimization problem can be formulated mathematically as follows:

$$\min y = f(x) = \left[f_1(x), f_2(x), ..., f_n(x) \right] \qquad \text{.....(4.1)}$$

It is subject to the following:

$$x = (x_1, x_2, ..., x_m) \in S$$
$$y = (y_1, y_2, ..., y_n) \in O$$

where, *f* is scalar function, n>1, and S is the set of constraints (parameter space).

The space that objective vector belongs is called objective function space denoted as ***O*** as displayed in Fig. 4-1. The performance vector, *f*(x) maps parameter space (***S***) into objective function space (***O***) as shown in the figure below describing two objectives case. Now, consider decision vectors (a, b $\in$ ***S***) and minimization problem; then, *a* is said to dominate *b* (denoted as $a \succ b$) if and only if following condition is met;

$$\forall i \in \{1,2,...,n\}: f_i(a) \leq f_i(b) \ \wedge \ \exists j \in \{1,2,...,n\}: f_j(a) < f_j(b) \qquad \text{.....(4.2)}$$

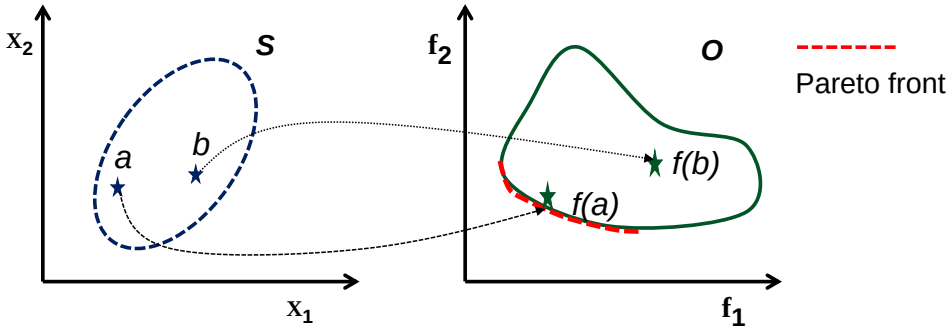

Fig. 4-1 Mapping for multiobjectives from parameter space into objective space

The decision vectors that are non-dominated within the entire search space are defined as Pareto optimal and constitute so called Pareto-optimal set or Pareto-optimal front (Zitzler and Thiele 1999). The solutions on red dotted line in Fig. 4-1 are representing Pareto optimal solutions because an improvement in one objective, f_1, requires degradation in the other objective, f_2. The shape of Pareto front indicates the nature of the trade-off between different objectives.

Two objective sets are called 'conflicting' if the induced weak Pareto dominance relations differ and non-conflicting otherwise (Brockhoff 2009). If we consider conflicting objectives optimization problem, we should observe 'trade-off'. Intuitively speaking, it means that we sacrifice some in the value of one objective to gain some in

the other. Trade-off information can be defined as the change of one objective to the other's change as depicted in following Fig. 4-2. In this study we often use the trade-off ratio and correlation coefficient to describe magnitude of relations between two objectives. For example, conflicting relation between objectives results in negative correlation coefficient.

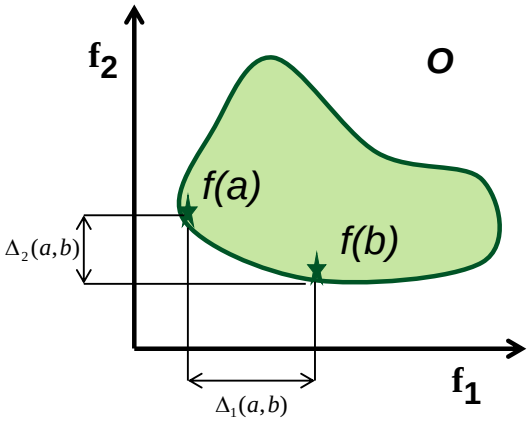

$$T_{ij}(a,b) = \frac{f_i(a) - f_i(b)}{f_j(a) - f_j(b)} = \frac{\Delta_i(a,b)}{\Delta_j(a,b)}$$

Fig. 4-2 Trade-off between objectives

4.2.2 Scalarization (Weighted-sum) approach

The weight-sum aggregation approach appears to be widely used due to its simplicity. The approach involves summing up the weighted objective values (Zitzler et al. 2000). In this study, we illustrate solving multiobjective problems using aggregation-based (single-objective) evolutionary algorithm (hereinafter denoted as GA-SOP). The difference between observed and simulated data is typically described as an objective function (or one of terms in objective function) in most history matching approaches. The weighted-sum of the differences in quadratic form, on which fitness assignment is based, are typically computed as given below.

$$y = \min \sum_{i=1}^{n} \omega_i \cdot \left(f_i^{observed}(x) - f_i^{calculated}(x) \right)^2$$

$$\sum_{i=1}^{n} \omega_i = 1, \omega_i > 0, x \in S \qquad \text{……...……(4.3)}$$

where ω denotes a weighting factor for each objective and n is the number of objectives. The objective values are computed by summing the differences for all the wells and at all measured times in case of history matching problems. In this approach, the determination of the correct weights is one of major difficulties. We do not know which weights are the most appropriate to retrieve a satisfactory solution (Hajizadeh et al. 2011). We do not in general know how to change the weights to consistently change the solution. In general, it is not easy to develop heuristic algorithms that, starting from certain weights, are able to define iteratively weight vectors to reach a certain part of the Pareto front. Besides, it requires possibly huge computation time. In addition, the approach is incapable to cover non-convex Pareto front and thus miss some parts of Pareto solutions resulting in incomplete solutions (Das and Dennis 1997). To achieve efficient points in a non-convex Pareto curve, ε -constraints method was proposed by Chankong and Haimes (1983). The method select one objective out of multiple objectives to be minimized; the remaining objectives are constrained to be less than or equal to given target value. For instance, suppose that we have two objectives where one of objectives (f_2) is chosen to be minimized. The problem is now described with geometric representation shown in Fig. 4-3. The decision maker has to choose appropriate many bounds for the constraints (ε values) to obtain complete Pareto optima. Moreover, this method is not efficient if the number of objectives is large.

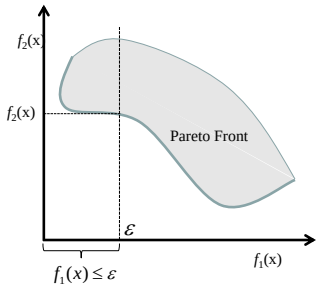

$$y = \min\ f_2(x) \qquad \text{.....} \quad (4.4)$$
$$f_1(x) \le \varepsilon, \quad x \in S$$

Fig. 4-3 Example of the ε-constraints approach showing geometric representation in the non-convex Pareto front in case of two objective optimization problem

4.2.3 Pareto-based multiobjective optimization evolutionary algorithm (MOEA)

Pareto-based techniques unlike aggregation-based technique make direct use of the dominance relation for fitness assignment, where actual Pareto ranks instead of fitness score are used as a measure of success for finding good solutions. Recently Pareto-based techniques are receiving a lot of attention in the area of multiobjective optimization. Some of techniques that have achieved much attention in the evolutionary algorithm (EA) literature include Niched Pareto Genetic Algorithm (Horn and Nafpliotis 1993), Non-dominated Sorting Genetic Algorithm (NSGA-II) (Deb et al. 2002), and Strength Pareto Evolutionary Algorithm (SPGA) (Zitzler and Thiele 1999). In this paper we use particularly NSGA-II algorithm and apply it to multiobjective history matching of reservoir performances. A fast non-dominated sorting procedure is implemented in the NSGA-II. Sorting the individuals of a given population is performed according to the level of non-domination. Typical workflow for NSGA-II is described in the following Fig. 4-4.

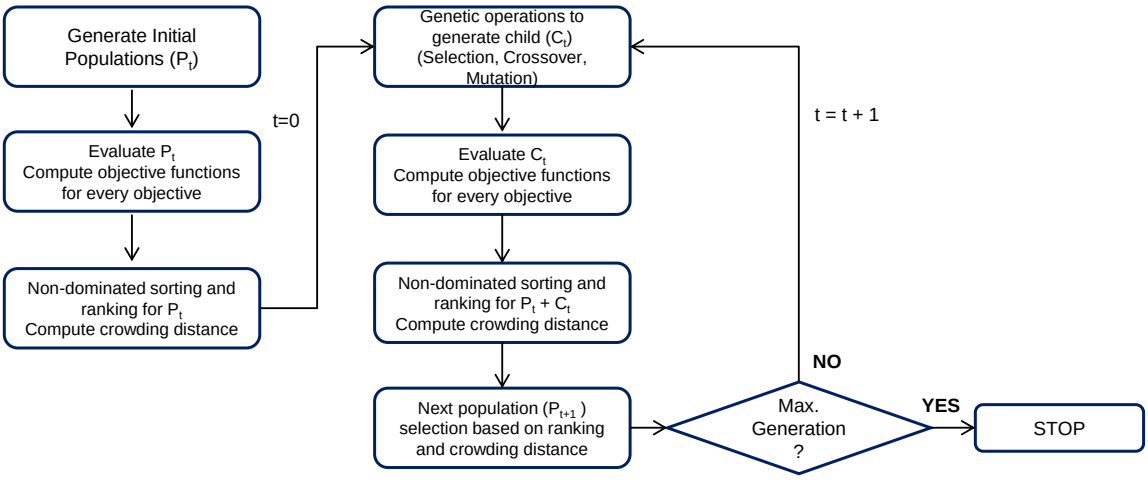

Fig. 4-4 Non-dominated sorting genetic algorithm (NSGA-II) workflow

This workflow is similar to the typical genetic algorithm workflow in that it uses typical genetic operations (crossover, mutation) and chromosome evolutions. The key difference from classical genetic algorithm approach is in the way the selection operator works. The selection process of classical genetic algorithms is based on the evaluation of fitness function for the models. The fitness function (*f(m)*) is typically referred to the objective function in genetic algorithm literature. The selection procedure picks models to be paired for reproduction using the genetic processes of crossover and mutation. The most common selection method in classical genetic algorithm uses the ratio of each model's fitness to the total fitness of all the models to define its probability of selection (Sen et al. 1995) which is shown in Eq. 4.5. Because the fitness function of each model in GA-SOP method is computed based on the summation of objective values, the selection probability ($P_s(m)$) of a model is considerably dependent on the way of weighing objectives.

$$P_s(m) = \frac{f(m)}{\sum_i f_i(m)} \qquad \text{.....(4.5)}$$

In contrast, the selection algorithm in the NSGA-II uses ranking and crowding distance of the models instead of fitness function resulted from weighted sum objectives. We use non-dominated sorting procedure to rank each model. Suppose that we have two objectives to optimize. The models are mapped in the objective space after evaluating each objective as shown in Fig. 4-5. We sort the population based on Pareto dominance concept, employing several fronts of classification for individuals. For solutions of a given population, there may be multiple non-dominated fronts. We first find non-dominated solutions (non-dominated front or Pareto front) that are not dominated by any other model, which is defined as Rank 1. The front number used to replace rank, where smaller front numbers represent higher rank. We assign each front (rank) a unique number and typically represent it by $Front^{k}$, where k ($k > 1$) is the front number. Each model (or individual) is assigned with one front (rank) based on following properties (Fang et al. 2008): (1) A model in $Front^{k+1}$ should be dominated by at least one model in $Front^{k}$; (2) A model in $Front^{k+1}$ may or may not dominate solutions in $Front^{k+2}$. For example, the model 'a' and 'b' are not dominated by any other. They are therefore defined as $Front^{1}$ or Rank 1. The model 'c' is dominated only by one model ('b') in Rank 1. Thus, it is defined as Rank 2. Similarly, the model 'd' is defined as Rank 3 because it is dominated by models in Rank 2. The crowding distance estimating the density of solutions in the objective space is used to preserve the diversity of population, the estimation of crowding distance is described in following Fig. 4-5. It is noted that the diversity and spread of solutions is obtained well because NSGA-II adopts a suitable parameter-less diversity preservation mechanism (Deb et al. 2002).

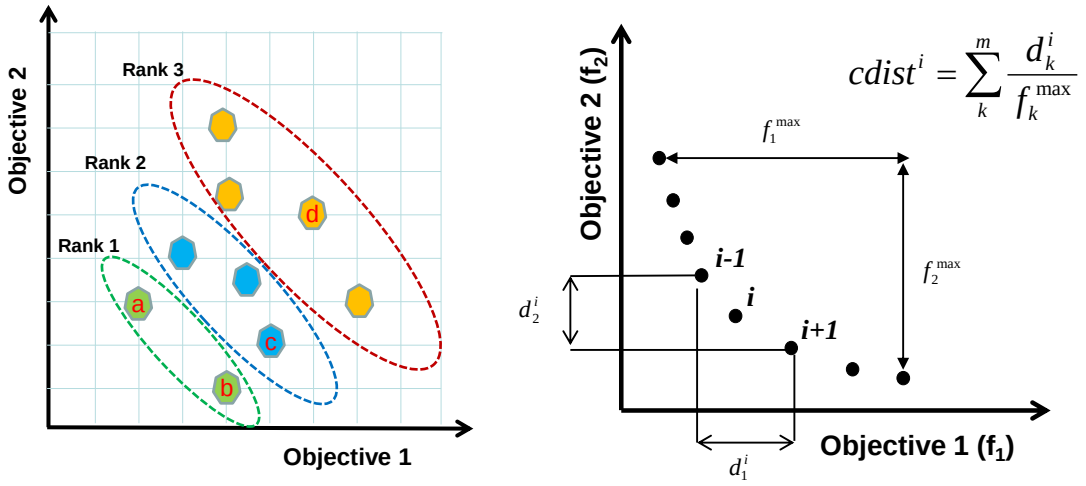

Fig. 4-5 Non-dominated sorting and ranking (left), crowding distance estimation (right)

In the Fig. 4-6 the step-by-step procedure for evolution from generation (t) to next generation (t+1) is illustrated. The genetic operators (crossover, mutation) is applied to the parent population (P_t) at generation (t) to generate offspring population (C_t). Because we typically set same size of children population (N), the combined population (parent and children) becomes twice as large as parent population. Then, non-dominated sorting is performed to perceive the non-dominated fronts (ranks). The idea behind selection is that higher ranked models have higher chances to be selected in the selection process than those in lower ranking. The populations for next generation are obtained from the highest ranked models to the lower ranked models. For example, the models in R_1 is smaller than population size (N), we choose all individuals in R_1 for the next population. The remaining of the next population is chosen sequentially from subsequent ranks. If we cannot accept all solutions in a certain rank anymore because of overflow of population size, the solutions within the rank are sorted in descending order to choose exactly N population members so that those with larger crowding distances are selected into next generation.

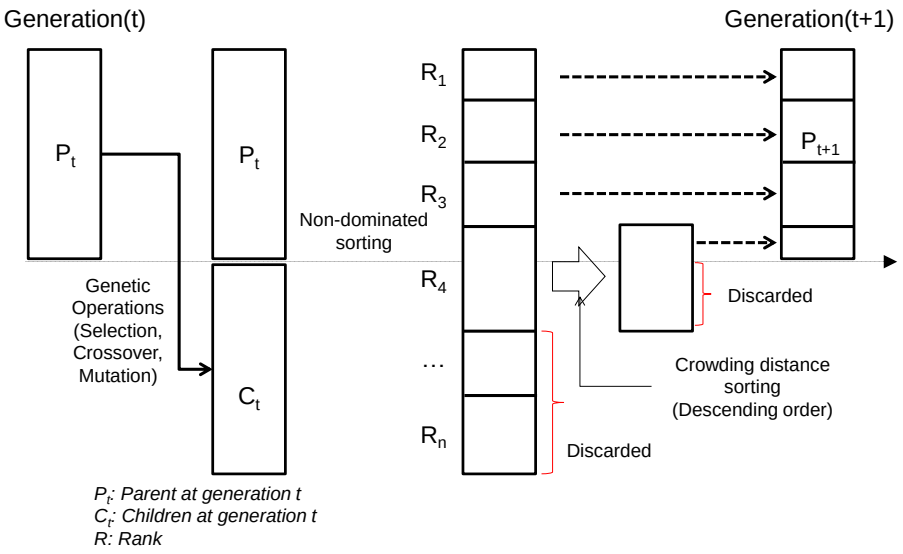

Fig. 4-6 Overview of non-dominated sorting algorithm selection procedure

4.2.4 Comparison of GA-SOP and MOEA approaches with test function

We formulate one test function to compare GA-SOP and MOEA methods under conflictions of conflicting objectives. Fig. 4-7 shows a test function problem where two objectives have completely different minimum. The minimum of objective one (1) is zero at (x_1=0, x_2=0) while the minimum of objective two (2) is zero at (x_1=5, x_2=5). To improve one objective, it requires sacrificing the other. It is so called conflicting objectives. Joining two objectives can turn the two different objective spaces into one global objective space. Equal weighting factor (α=1, β=1) is assigned to each objectives for this example in the Fig. 4-7. It is clearly around a point (x_1=5, x_2=5) that global minimum exists if equal weighting factor is used. We also see that the global optimum or minimum can be changed with weighting factors.

$$f_1(x) = x_1^2 + x_2^2$$

$$f_2(x) = (5x_1 - 25)^2 + (5x_1 - 25)^2 \qquad f(x) = \alpha \cdot f_1(x) + \beta \cdot f_2(x)$$

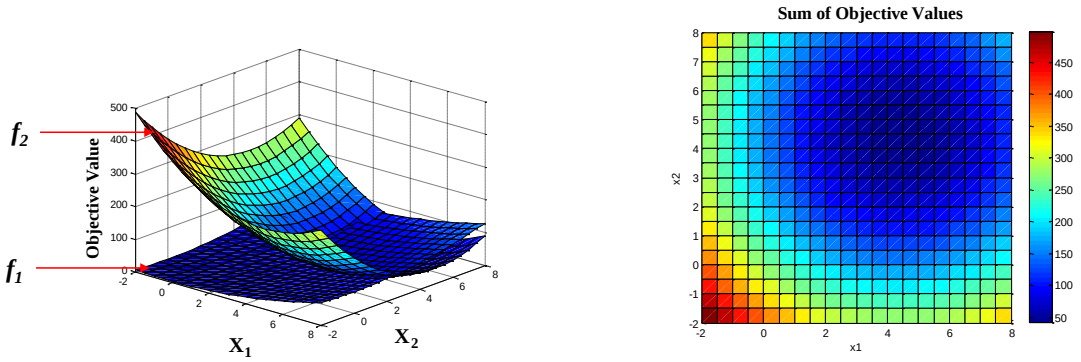

Fig. 4-7 Two objective values in 3D view (left) and sum of objectives in 2D top view (right) when equal weighting factor (α=1, β=1)

Following Fig. 4-8 and the second figure on page 94 show the outcomes from GA-SOP and MOEA runs respectively. For these experiments we have used 50 populations and evolve generations up to 100th. We set the searching space as from -2 and 8 for both parameters. For GA-SOP, equal weighting factor (1) is assigned to objectives. As the results shown in below, the solutions in parameter space show that most of solutions are clustered around a point (x_1=5, x_2=5), which is the global minimum only if equal weighting factor is used. The solutions mapped on objective space show that all final outcomes satisfy the second objective (f_2) much better compared to the first objective (f_1), resulting in incomplete exploration of solution space.

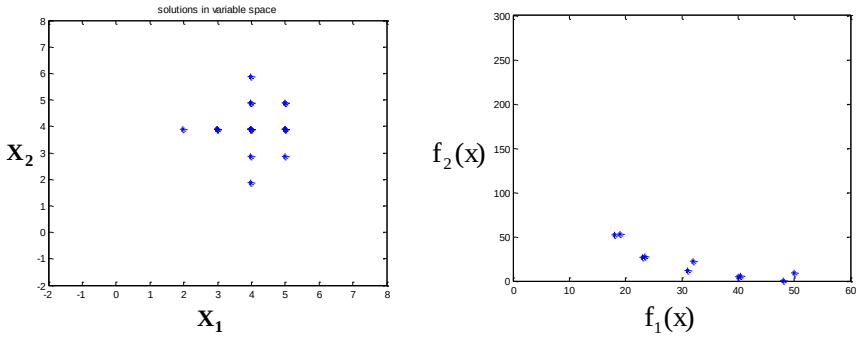

Fig. 4-8 GA-SOP solutions in parameter space (left) and objective space (right) in case of equal weighting factor

The selection probability (Eq. 4.5) based on weighted sum of objective value (fitness) are examined. Fig. 4-9 explains that the most probable selection regions are located around a point (x_1=5, x_2=5) and shows where the models in the region are mapped in the objective space. This answers to why we have as a result of GA-SOP run such solutions (shown in Fig. 4-9) satisfying one objective (f_2).

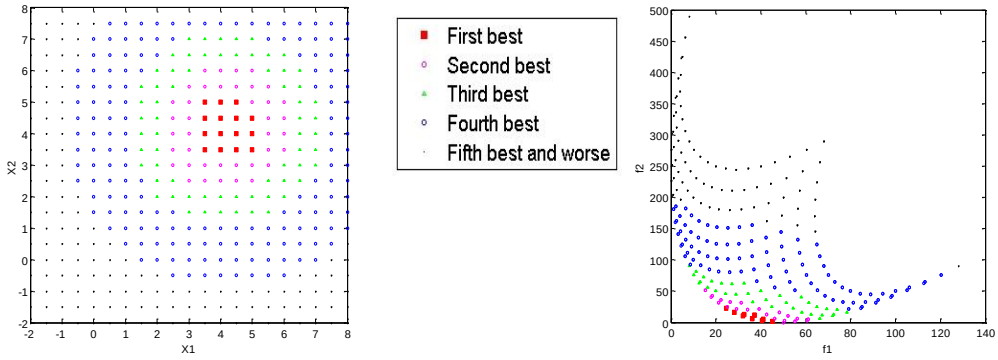

Fig. 4-9 GA-SOP selection probability in parameter space (left) and in objective space (right)

In contrary, the result of MOEA shows in Fig. 4-10 that Pareto-based algorithm searches for complete solutions and discover the trade-off between conflicting objectives. As we notice from the figure below, the solutions in parameter space are not only around points (x_1=0, x_2=0 and x_1=5, x_2=5) which satisfy the first and second objective respectively, but also there are optimal solutions between the points.

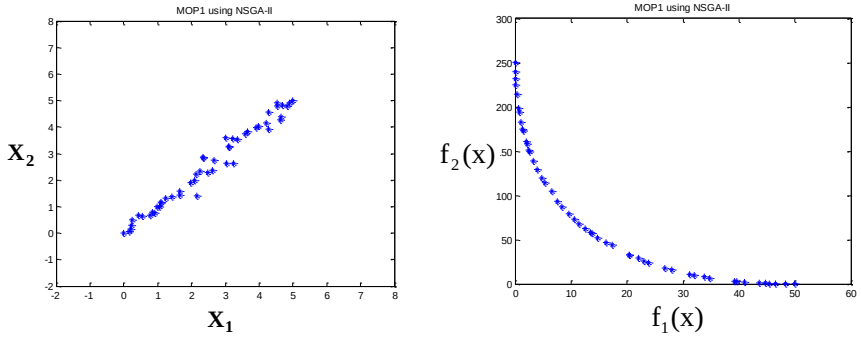

Fig. 4-10 MOEA solutions in parameter space (left) and objective space (right)

Fig. 4-11 shows non-dominated sorting and ranking results. To show these, we ranked all the solutions in objective space and mapped them back to parameter space. There are many fronts (ten or more) formed in this case although just five fronts are shown for simplicity. The MOEA uses a population of solutions in the search process and optimizes such that the ranks are minimized. As the result, we can have the Pareto optimal solutions that are the best ranked models in this case.

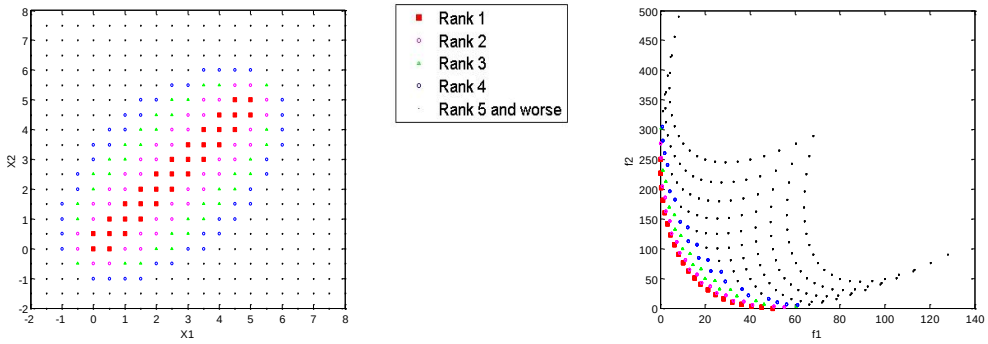

Fig. 4-11 MOEA non-dominated sorting and ranking in parameter space (left) and in objective space (right)

Several more cases with GA-SOP were made to see the effects of weighting factor on the solutions, where different weighting factors are used to construct the objective function. As noticed from figures in the most top two rows in Fig. 4-12, the global minimum point vary with weighting values. Because aggregated approach uses summed objective values for computation of fitness, the solutions in parameter space as result of GA-SOP are mostly located on the point around global minimum points. These experiments conclude that GA-SOP approach is incapable of exploring entire optimal solution space at one run and one set of weighting factor.

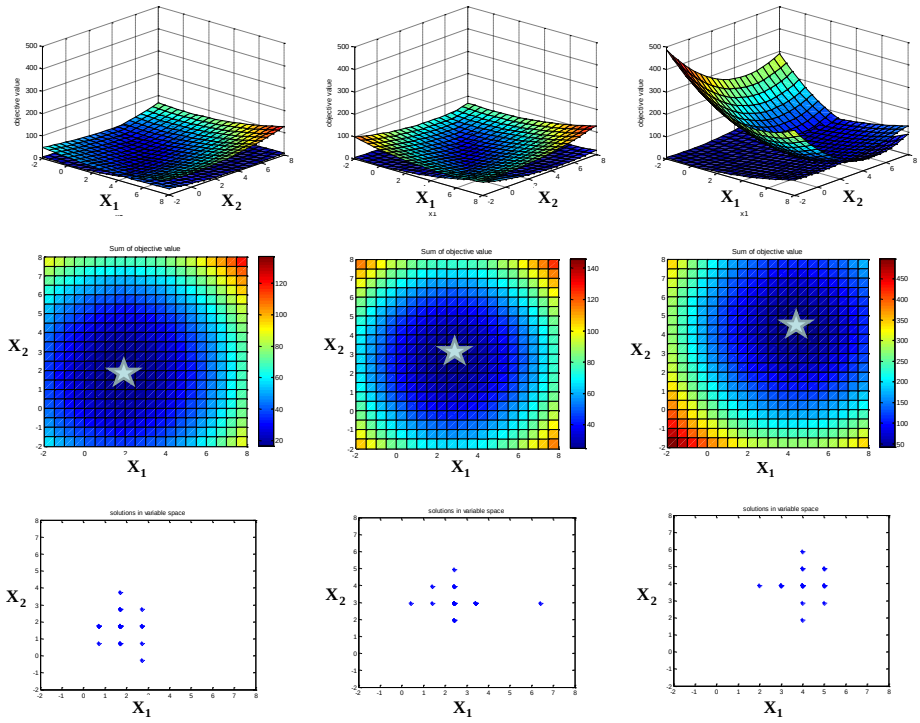

Fig. 4-12 GA-SOP solutions by different weighting factor cases; Case1 (α=1, β=0.1), Case 2 (α=1, β=0.2), Case 3(α=1, β=1) from left

We now examine the objective function behavior by generation for GA-SOP and MOEA run. The Fig. 4-13 shows the GA-SOP convergence behavior that brings more clear sense on how GA-SOP approach sacrifices an objective to improve the other and finds only localized region satisfying a dominating objective in this case. From the figures (population mean, objective f1 behavior), we notice that the first objective (f_1) is sacrificed with improvement of the second objective (f_2), eventually the sum of objectives (f_1+f_2).

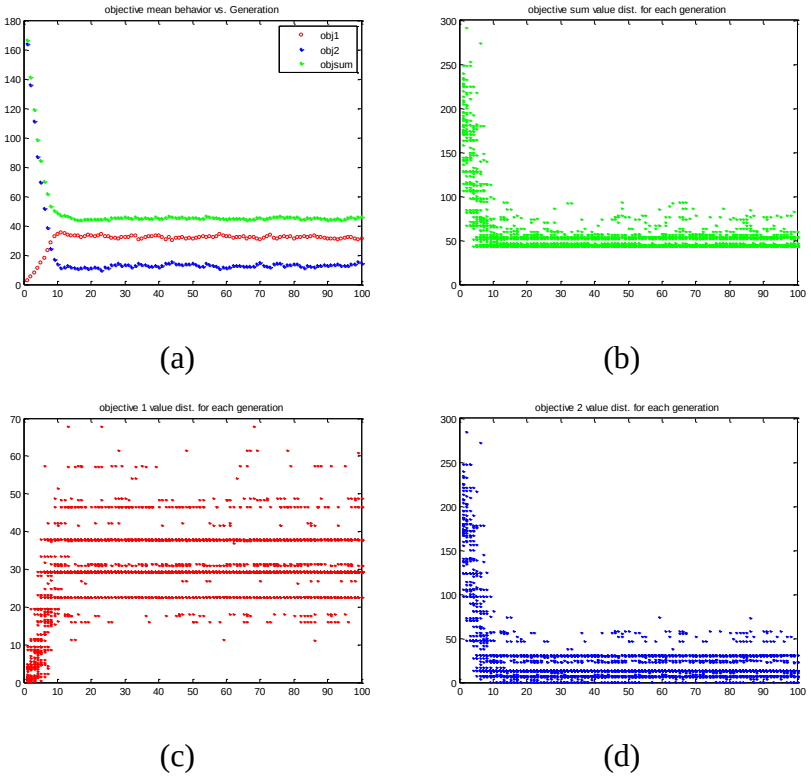

Fig. 4-13 GA-SOP convergence behavior by generation; population mean(a), sum of objectives(b), objective *f1* (c), objective *f2* (d)

MOEA result show that it does not degrade an objective to make the other better as shown in Fig. 4-14. Instead, it discovers complete optimal solutions without sacrifice of any objective. The objective function does not seem to continue to converge after few iterations because of conflict between two objectives.

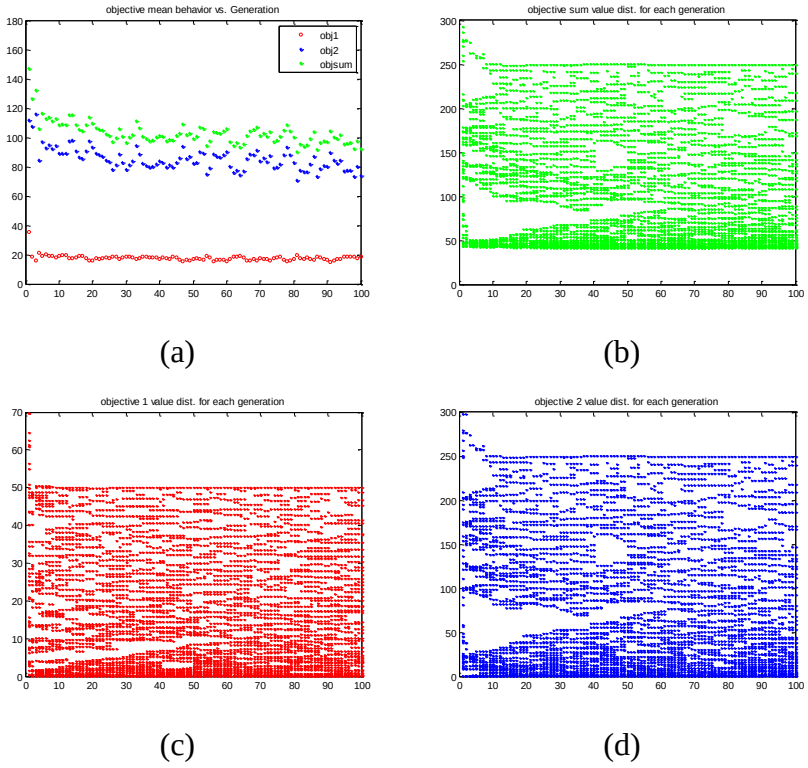

Fig. 4-14 MOEA convergence behavior by generation; population mean(a), sum of objectives(b), objective *f1* (c), objective *f2* (d)

4.3 Developed History Matching Approach Using Pareto-based Multiobjective Evolutionary Algorithm

In this section we propose a Pareto-based multiobjective hierarchical history matching method where a Pareto-based multiobjective evolutionary algorithm with Grid Connectivity-based Transformation (GCT) technique is used for global update, and streamline-based generalized travel time inversion method for local update. We will briefly discuss GCT before explaining details on the workflow.

4.3.1 Pareto-based multiobjective hierarchical history matching

A hierarchical history matching structure proposed in previous paper (Yin et al. 2010), where global parameter calibration is followed by local parameter calibration, is

basically used in this work but Pareto-based multiobjective optimization method replaces classical Genetic algorithm (GA) that they used for global update. Fig. 4-15 shows overview of proposed workflow called Pareto-based multiobjective hierarchical history matching approach. The proposed method comprises a two-step approach: global and local update. In the global calibration, we use MOEA to calibrate large-scale uncertainty or global parameters typically associated with global energy (pressure and pore volume) in the field. The approach considers the trade-off between objectives and detects plausible solutions that tend to satisfy the multiple objectives. As a result of global update, we now have an ensemble of geological models matched to global objectives. Next, we proceed for local update with a set of representative models selected through cluster analysis. In the local calibration, local parameter sensitivities are used to update each selected model using dynamic production responses such as water cut and bottom hole pressure. In particular, streamline-derived sensitivities are used to determine the spatial distribution and magnitude of the local permeability changes in this study. The streamline-based inversion has proven to be an efficient method for computing parameter sensitivity, and has been extensively used for field-scale history matching (Cheng et al. 2005). The proposed workflow combining stochastic and deterministic approach results in a set of diverse history-matched models that can be used for performance predictions and uncertainty analysis.

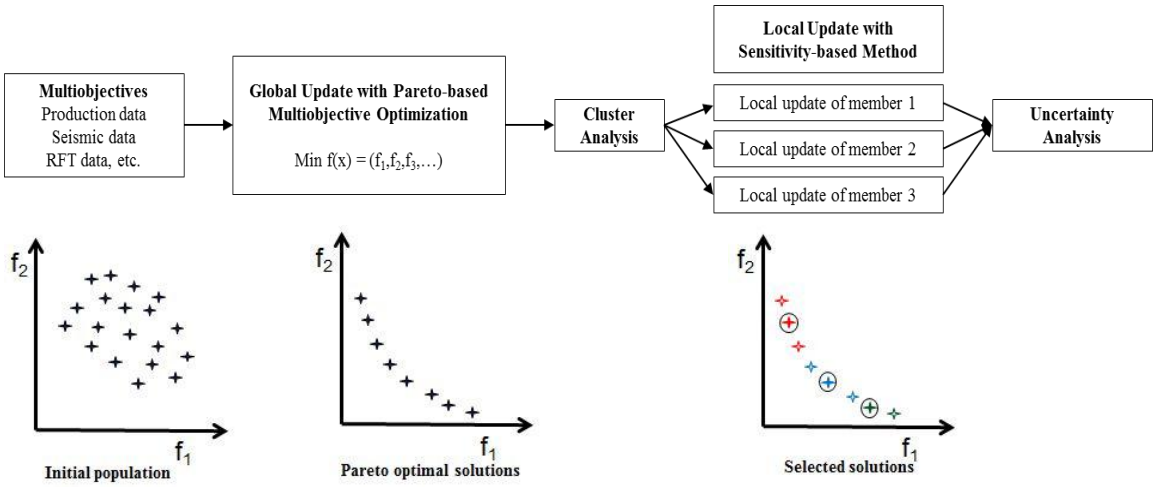

Fig. 4-15 Overview of Pareto-based multiobjective hierarchical history matching

The novel components in the proposed hierarchical workflow (Fig. 4-15) are the Pareto-based multiobjective optimization method and GCT parameterization for global update. The optimization method follows the non-dominated sorting evolutionary algorithm (NSGA-II) (Deb et al. 2002); however, for its application to history matching problem, we use a Grid connectivity-based transformation (GCT) technique (Bhark, E. et al. 2011). The GCT basis coefficients are used as parameters for calibration during the gradient-free updating process. Fig. 4-16 illustrates in detail the Pareto-based multiobjective history matching workflow which is the key part of this paper.

4.3.2 Grid connectivity-based transformation (GCT)

Bhark et el. (2011) presented the development of a general transform basis suitable for structured and unstructured grid geometry. The basis is derived as the eigenvectors of a specific form of the grid Laplacian matrix that captures two-point or immediate-neighbor grid cell connectivity. The parameterization is performed by projecting a property multiplier field onto an orthonormal basis (ϕ) derived from the grid connectivity structure. The linear transform method for parameterization transforms the spatial parameters to and from a transform domain which is efficient for parameter estimation because of fewer parameters. A discrete spatial field is mapped to the transform domain using orthogonal transforms,

$$\mathbf{v} = \Phi^T \mathbf{u} \Leftrightarrow \mathbf{u} = \Phi \mathbf{v} \qquad \text{.....(4.6)}$$

where **u** represents a spatial field and has dimension $N \times 1$, where N is the discretization of the property field. The column vector **v** is M-length spectrum of transform coefficients, or the parameter set in the transform domain, and ϕ is a ($N \times$M) matrix containing M-columns that define the discrete basis functions, each of length N.

For model calibration, a spatial multiplier field has been posed in the multiplicative formulation as follows,

$$\mathbf{u} = \mathbf{u_0} \cdot \Phi \mathbf{v} \qquad \text{.....(4.7)}$$

where u_0 is the prior property field, also called initial model, ϕv defines the multiplier field in the spatial domain and (·) is the element-wise multiplication (scalar product).
For history matching application, a gradient-based BFGS quasi-Newton method was used where the gradient is computed with respect to parameters (transform coefficients, v) in the spectral domain. When the parameters are updated, the heterogeneity at spatial domain is altered corresponding to the modal frequency of each basis function applied in the transform. The details are found in literatures (Bhark, E. et al. 2011; Bhark, E.W. et al. 2011).

4.3.3 Pareto-based multiobjective history matching workflow with GCT

Our proposed workflow designed for multiobjective history matching utilizes Pareto-based multiobjective evolutionary algorithm in conjunction with the GCT technique. We introduce the GCT in the stochastic calibration framework where the basis transform coefficients (**v**) are used as parameters for updating the geologic model using the derivative-free evolutionary algorithm. The parameterization enables to reduce the dimension of parameters, in this case the dimension of transform coefficients (**v**). The reduced parameters require the compact representation for basis (ϕ) to contain only a few basis (ϕ) functions that are able to capture the most relevant spatial information.

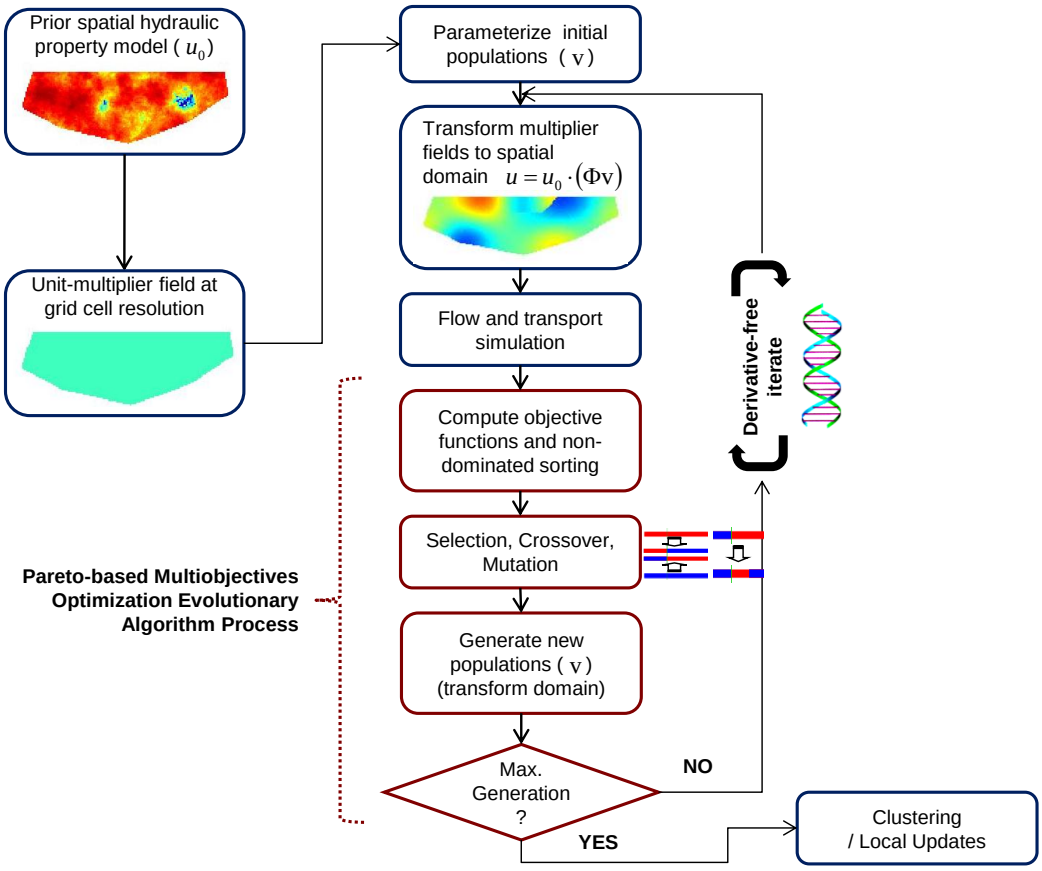

Fig. 4-16 Workflow of Pareto-based multiobjective history matching with GCT

As in typical history matching workflow we start with one initial reservoir model constructed from many different data sources. Multiple models are generated by imposing spatial multiplier fields. For this, we prepare GCT basis from the given grid connectivity information of the reservoir model. In this paper, we use absolute permeability as the estimable property, although other spatially varying properties can be used. First, we parameterize multiplier fields to specify the initial populations and then transform them back to spatial domain. Those are actually obtained with different spectrum of transform coefficients applied to a GCT basis. Next, each model in the population is simulated to obtain the well production responses and saturation distribution that are used for computation of objective function. It is followed by non-

dominated sorting algorithm to sort the models in terms of ranking and crowding distance. We proceed to the selection process where tournament-based method is used. It is followed by typical genetic operations such as crossover and mutation. The generated new chromosomes record information of GCT basis coefficients in spectral domain. They are transformed back to spatial domain for evaluation of the next generation. The derivative-free updating iterations are continued until stopping conditions are reached.

4.4 Synthetic Applications to History Matching of Reservoir Performances

4.4.1 Synthetic application (1): Incorporation of seismic data into multiphase multiobjective history matching

In this section we first illustrate the proposed workflow through an application to the history matching of multiobjectives (production and seismic data). The results show that incorporation of seismic data into history matching can reduce the extent of non-uniqueness of traditional history matching. We use a two-dimensional three-phase heterogeneous reservoir model for waterflooding consisting of 8 producers and 1 injector in the middle as shown in Fig. 4-17. The GCT basis vectors (first ten) for this synthetic example application are shown in Fig. 4-17.

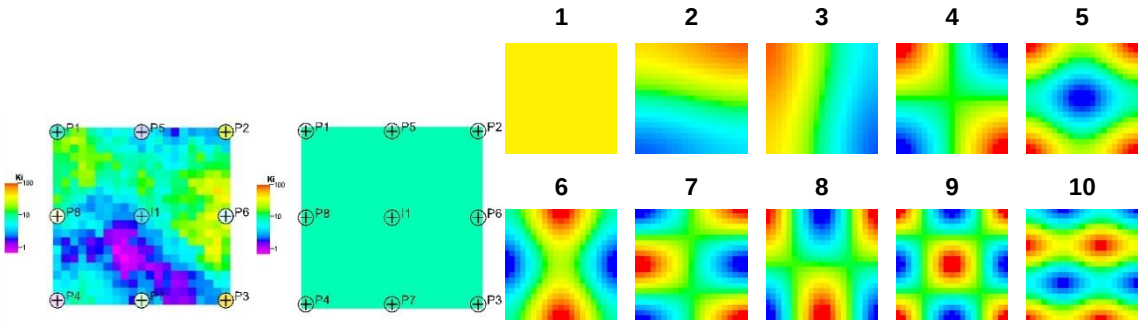

Fig. 4-17 Reference (left), initial (middle), and generated GCT basis vectors (right)

Next, we parameterize the initial parameters with GCT transform coefficients in frequency domain by random sampling of the coefficients and transform them back to spatial domain. Fig. 4-18 shows some of initial multiplier fields that the ten transform coefficients shown in Fig. 4-17 are used to generate. The generated initial populations are simulated to receive flow simulation responses. Next, we compute the objective functions and rank the models based on non-dominated sorting algorithm. It is followed by genetic operations such as selection, crossover, and mutation. Those evolutionary processes are conducted in the frequency domain to create new populations. These updating process using the Pareto-based derivative-free iterations is continued until we reach a specified stopping criteria, defined as the maximum number of iteration, 10 iterations in this case.

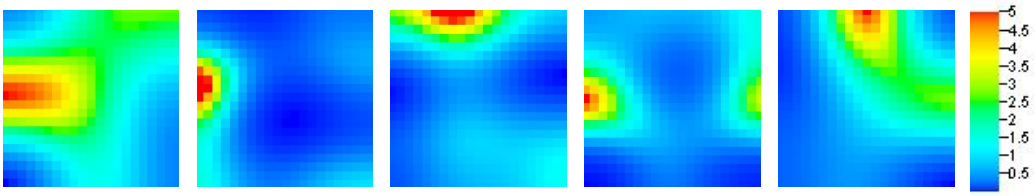

Fig. 4-18 Examples of initial multiplier fields

In this synthetic application, we performs two sets of history matching; (1) production data only and (2) both production and seismic data. The production data include multiphase production responses (water cut and gas-oil ratio). The water saturation changes are used as the seismic derived data. In the first case, we used only production data to calibrate the model. Fig. 4-19 shows the objective function behavior with respect to the number of iteration. The objective functions are averaged value of population in each generation (iteration). We could reduce the data misfits for production data significantly. However, the updated models (Fig. 4-19) show the updated models do not reproduce some of the features in reference model. This is reflected in Fig. 4-20 which shows water saturation displacement changes of updated models do not reproduce seismic derived data as much as the production data. It can be also seen in objective

function shown in Fig. 4-19 that the objective function of seismic data (blue line) shows the objective function of seismic data that doesn't converge well.

Proper specification of data misfit is important because the computed objective affects the searching of the minimum and the offspring selections. For estimating seismic data misfit, many publications including (Roggero et al. 2007) uses typically the quadratic form of data misfit term similar to the first term in following equation. In this study, we have used two elements; one is the direct cell property value difference, which represents absolute errors but it does not include information about continuity and pattern of the fluid displacement. The other is the GCT transform coefficient differences for checking the pattern difference. The objective function we used in this study is shown in equation below.

$$O_{seismic}^{k} = \left[\left(\sum_{i=1}^{ncell} \left(S_{diff,observed}^{i} - S_{diff,updated}^{i} \right)^{2} \right)^{0.5} + \left(\sum_{j=1}^{ncoeff} \left(v_{observed}^{j} - v_{updated}^{j} \right)^{2} \right)^{0.5} \right] / 2 \qquad (4.8)$$

where, $O_{seismic}^{k}$ denotes objective of seismic data for kth model. S_{diff}^{i} denotes cell property value difference for ith cell. v^{j} represents GCT basis transform coefficient corresponding to jth basis vector. As we discussed in the previous section, this coefficient can be obtained by multiplying cell properties to basis function.

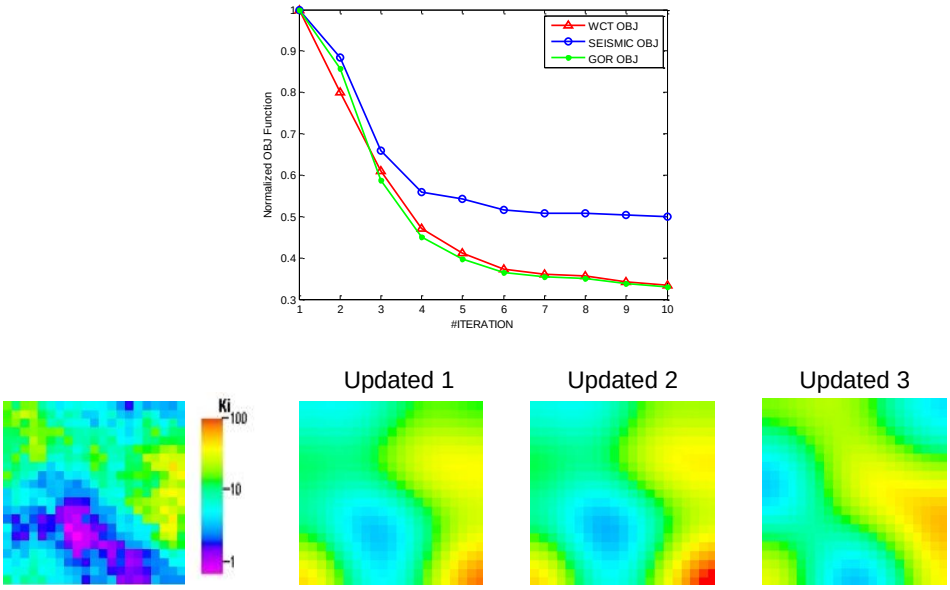

Fig. 4-19 Production data only used: Objective functions (top), reference model (bottom-left) and updated models (bottom-right)

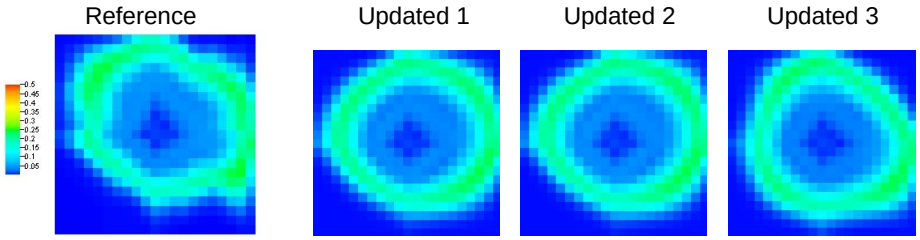

Fig. 4-20 Production data only used: updated seismic water saturation changes from updated models

In addition to production data, we add seismic data (water saturation changes) as the third objective, thus a three (3) objective problem is constituted. The results are shown in Fig. 4-21 and Fig. 4-22. The updated permeability fields and water saturation changes reproduce the reference model quite well. The results are significantly better results compared to the case when only production data is used. All the updated models capture high and low permeability regions in the reference model. We also notice that it improves the objective function of seismic data (shown as blue line).

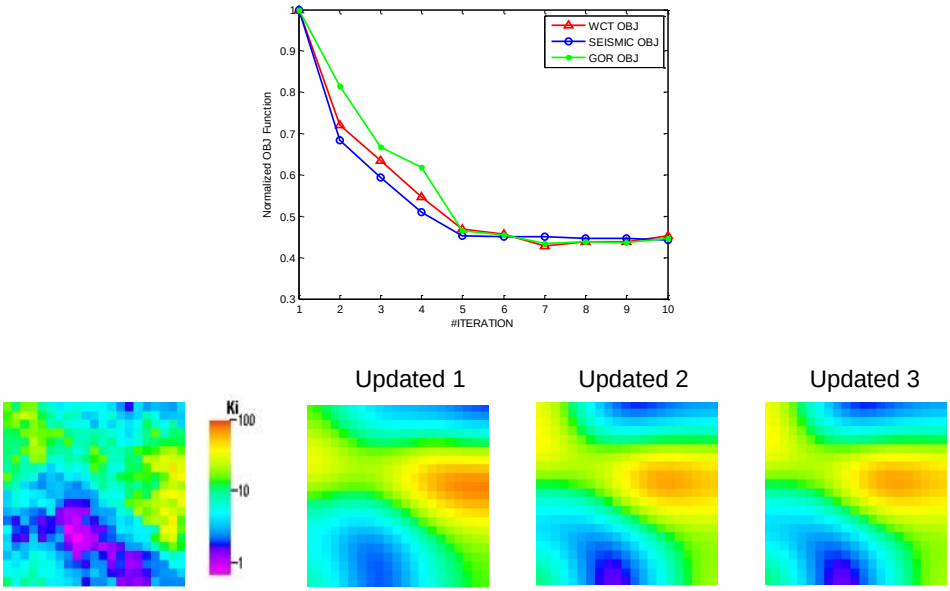

Fig. 4-21 Both production and seismic data used: Objective functions (top), reference model (bottom-left) and updated models (bottom-right)

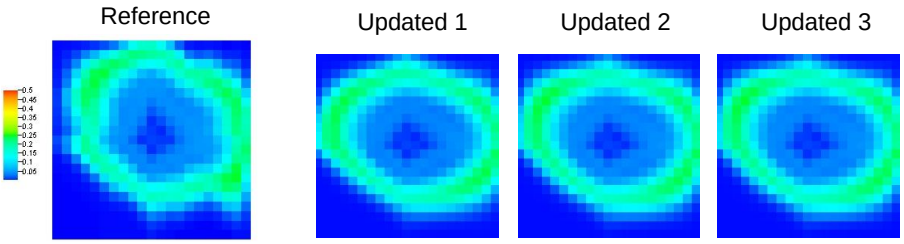

Fig. 4-22 Both production and seismic data used: updated seismic water saturation changes from updated models

We compare updated models of both cases in terms of spectrum frequency of transform coefficients (**v).** Recall that the transform coefficients can be obtained by multiplying grid property model (u) to GCT basis (ϕ). Fig. 4-23 shows two results: (i) transform coefficients for permeability fields and (ii) transform coefficient for seismic water saturation changes. This gives idea about how closely the proposed approach reproduces models. We see that the transform coefficients for updated models are all improved compared to initial model. Particularly, the spectrums of updated model with

addition of seismic data are much close to the spectrums of observed model than the model without seismic data addition This is consistent with the results we have seen above.

Through this application we have demonstrated that the proposed workflow performs well for history matching of multiple objectives. In particular, we showed that the incorporation of seismic data reduced the non-uniqueness and resulted in the improvement of the quality of history matching.

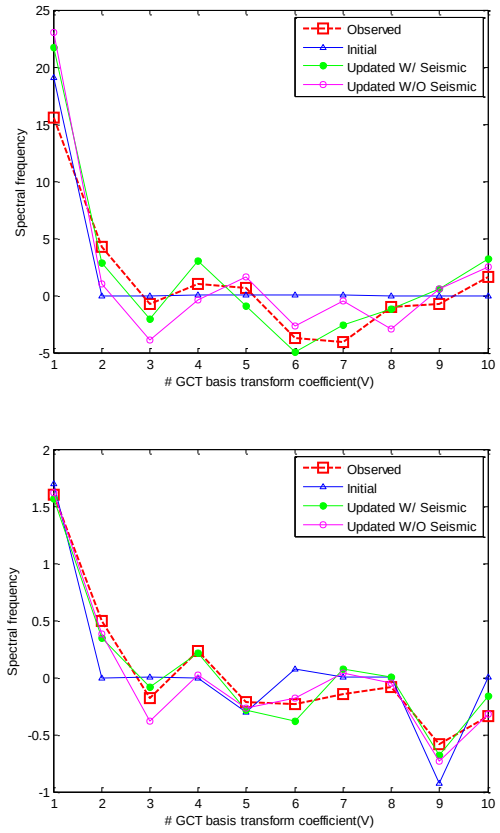

Fig. 4-23 Updated spectrum of transform coefficient: Permeability model (top) and seismic water saturation change (bottom)

4.4.2 Synthetic application (2): Comparison of GA-SOP and MOEA with conflicting information

In this application we focus on comparison between classical approach, aggregation-based (single-objective) method (GA-SOP) and the proposed Pareto-based method (MOEA) with conflicting information. We prepare an intentionally biased 4D time-lapse seismic data set to create conflict between two objectives (production and seismic data). Fig. 4-24 shows reference permeability field, initial permeability field, and true 4D-seismic data and biased seismic data used for this study. The water saturation difference between two measurements is assumed as the 4D seismic data for this illustrative example. This model is two-dimensional heterogeneous model, waterflooding reservoir, and includes 4 producers and 1 injector. We compare the aggregation-based and the Pareto-based approaches in terms of finding optimal solutions.

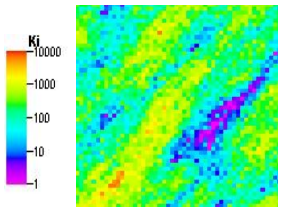

(a)Reference permeability

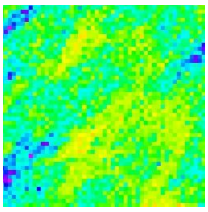

(b)Initial permeability

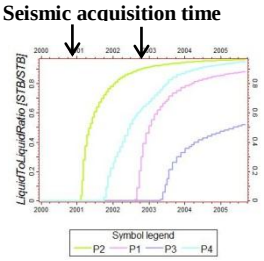

(c)Production data (water-cut)

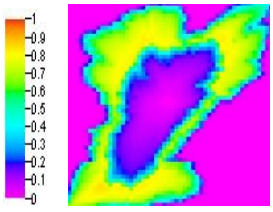

(d)Reference Sw changes

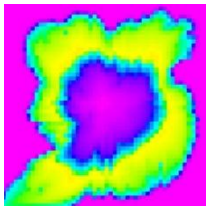

(e)Initial Sw changes

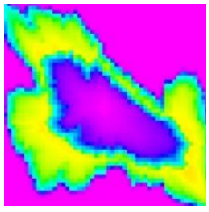

(f)Biased Sw changes (actually used)

Fig. 4-24 Synthetic model (reference and initial), production data, and seismic data used for application (2)

First, we used our proposed method for this conflicting multiobjective history matching. To start with, we parameterize initial permeability multipliers using GCT basis coefficients as illustrated in previous application. From the result of simulations of initial populations, we see strongly negative correlation (-0.72) between two objectives (water cut and water saturation changes) as shown in Fig. 4-25. We find that the confliction between two objectives creates large trade-off because of their inconsistency. To improve either 1st objective (water cut) or 2nd objective (saturation changes) it requires degrading of the other. Because we use strongly biased saturation data, large trade-off is observed.

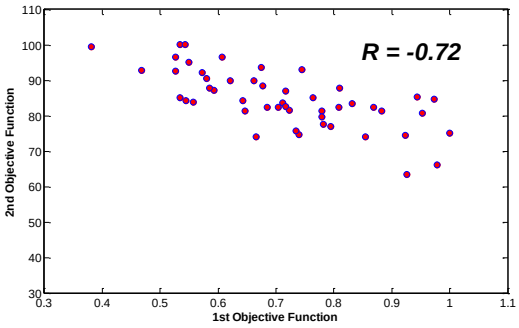

Fig. 4-25 Initial populations in objective domain and correlation between two conflicting objectives

From the results of history matching using the proposed method, in Fig. 4-26 we find relatively large uncertainties on the result in objective space because of the conflicting information. We selected three updated models from final optimal solutions. As shown in Fig. 4-26 those models are far each other in objective domain; one has very optimized misfit for objective one but poor misfit for objective two. Another is opposite with poor result for objective one but good for objective two. The other is in between those. Such results showing large trade-off are clearly revealed on water saturation displacement map. As displayed in Fig. 4-26 one of updated model better reproduces true seismic data, although we input biased water displacement data. It is because production data information tends to correct information about it. The updated model three is the one that

the model is matched very well to seismic biased data. We see that the model tries to displace water toward the direction as the biased water displacement front, although initial geologic heterogeneity prevents shifting the direction of continuity.

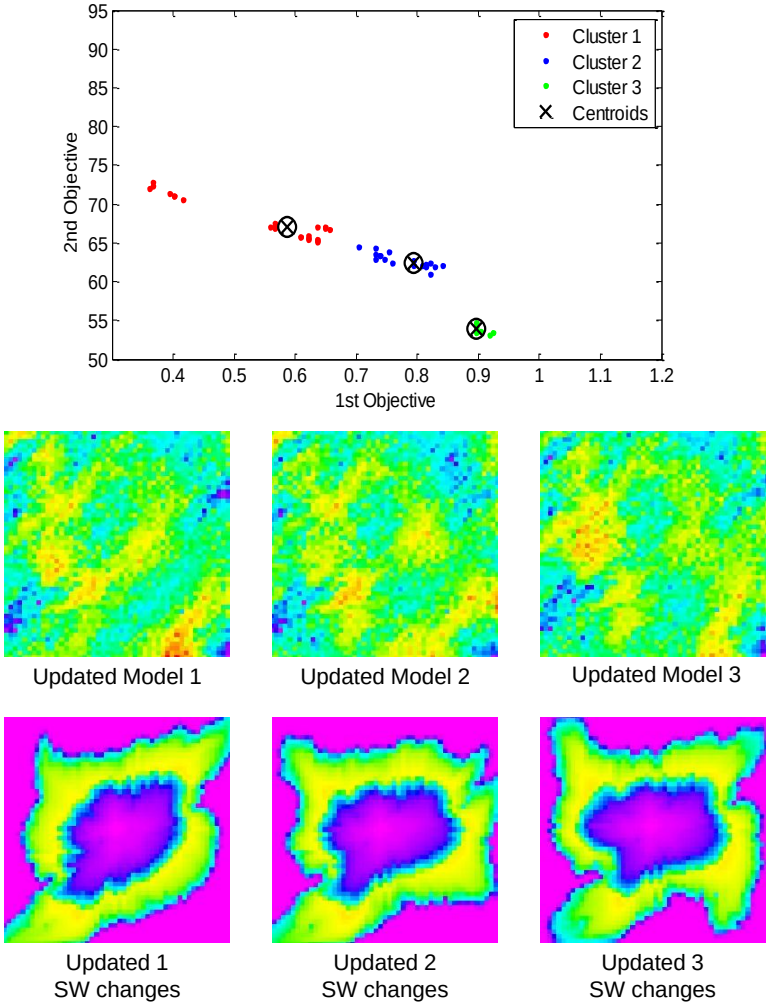

Fig. 4-26 MOEA optimal solutions (top) and three selected models (bottom)

Next, we run aggregation-based genetic algorithm (GA-SOP) with the same test model. For detailed comparison, we made two sets of test runs with different weighting factors assigned to each objective; (1) equal weighting (1:1) and (2) sixty versus one weighing (60:1). Two results are compared with MOEA result in one graph in Fig. 4-27 where we find that MOEA solutions constitutes optimal front while GA-SOP solutions

are clustered in one side or the other side of Pareto front depending on assigned weighting factors.

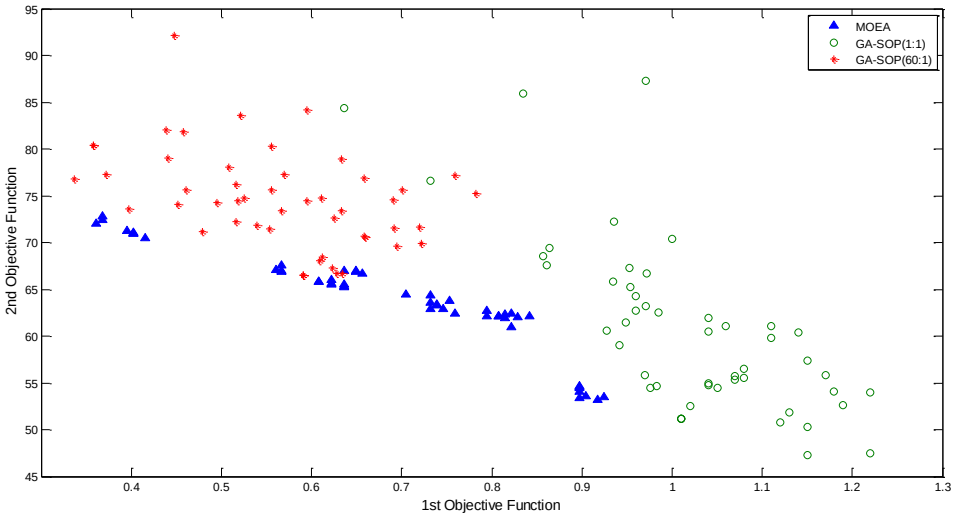

Fig. 4-27 Optimal solutions from MOEA, GA-SOP (equal weighting), and GA-SOP (weighting 60 vs. 1)

In Fig. 4-28 three selected models for each case are displayed. We see significant differences between those results. Three models in the left are obtained when we assign equal weighting factor to objectives (water cut and seismic data) while the other three models in the right are from different weighting factors. We find that equal weighing case resulted in relatively better seismic data matching compared to different weightings. In terms of the quality of production data, different weighting case is better than equal weighting. Such matching quality has been reflected in the updated models.

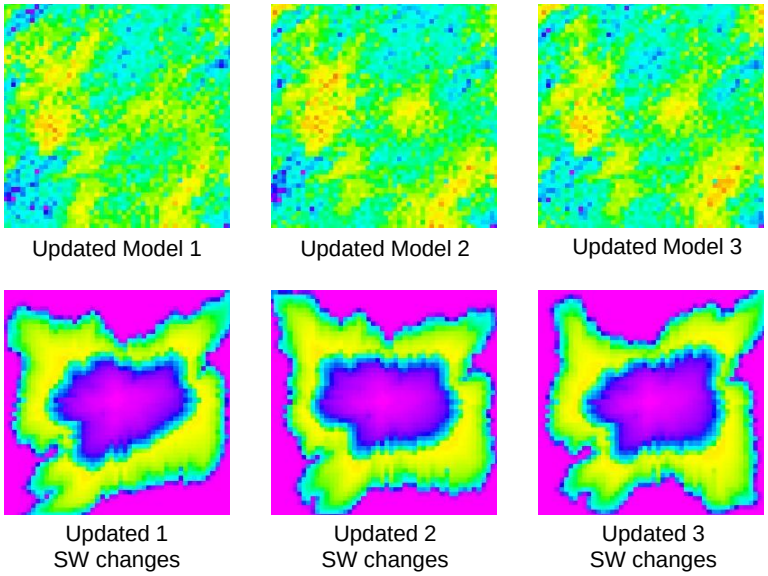

(a) In case of equal weighting

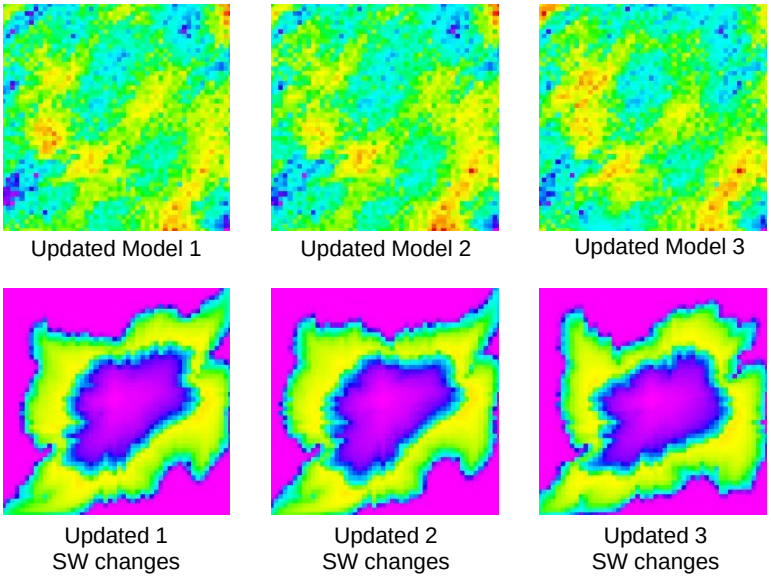

(b) In case of different weighting

Fig. 4-28 GA-SOP selected models; equal weighting (top), weighting 60 vs. 1(bottom)

The results seem to indicate two things. First, GA-SOP approach results in incomplete optimal solutions with different weighting factor giving different solutions. Second, MOEA is able to identify the conflict and discovers more complete optimal solutions at single time run.

4.4.3 Synthetic application (3): Use of optimal coarsened model with coarse GCT basis

Optimal coarsening technique can be incorporated to the proposed workflow. Several publications including (King et al. 2006) have presented the advantages of coarsening, in particular, in case of large reservoir models. The GCT basis for coarsened grid geometry can be obtained as it is done for the fine grid, although it requires construction of coarsened grid internally. Because total number of GCT basis is the same as the number of grid cells, coarsening results in smaller number of GCT basis and further reduction of parameter space. Use of coarsened grid in the global update process where we update large-scale heterogeneity is followed by local update at the fine scale where single cell sized heterogeneity is calibrated at the grid-block level. Not only less simulation time but also less number of parameters usage are the direct outcome from coarsening. In gradient-free method the use of smaller number of parameters and computational efficiencies are key to success because it typically require large number of simulation runs. In that sense the use of coarsened GCT basis can bring significant improvement in the efficiency of the workflow. In the following we show an example application to demonstrate the usefulness of coarsening in the proposed workflow. We used the same synthetic model (NX=50 and NY=50) as in the previous section and performed uniform coarsening (NX=25 and NY=25) so that the number of parameters has been reduced from 2500 to 625. The GCT basis transform coefficient and its spectrum are compared in Fig. 4-29. Besides a reduction of size of parameter space, we observe that coarsened spectrum of transform coefficient shows smaller frequencies in this case, eventually effect on reducing search range of each parameter.

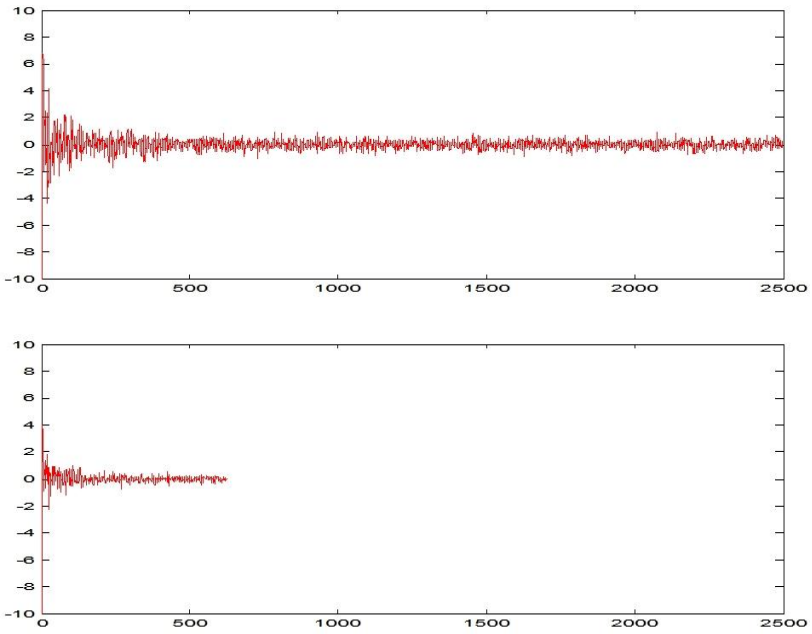

Fig. 4-29 Spectrum of transform coefficient for fine grid (top) and for coarsened grid (bottom)

As in the previous section, we examine the problem of history matching with two objectives (production and seismic water saturation changes) for both coarsened and fine model as shown in Fig. 4-30. From the results of applications of the proposed method, we found that the history matching quality for both are satisfactory, although the details of the changes are different.

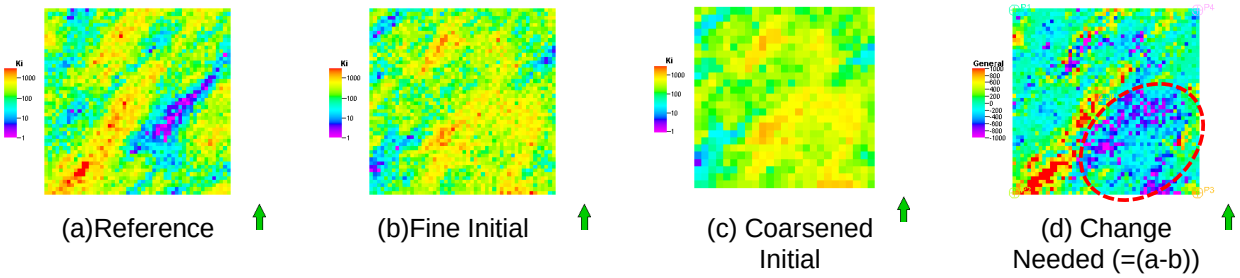

Fig. 4-30 Used models (reference, fine initial, coarsened initial from left to right) and change needed

Fig. 4-31 below compares the results with and without coarsening. The figures in the top row (‘a’ through ‘d’) are about update of fine grid cell using fine-grid GCT basis while figures in the bottom row (‘e’ through ‘h’) are about update of coarsened cell using coarsened-grid GCT. As observed from the updated permeability fields, both approaches capture similar features during the global update.

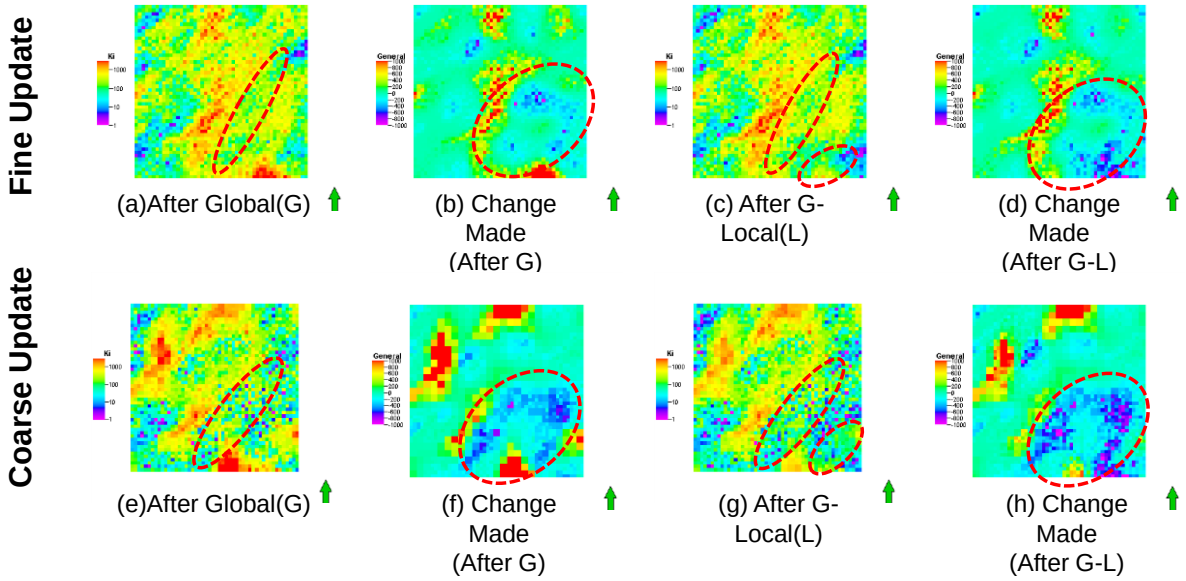

Fig. 4-31 Fine update results (a through d) and coarsened update (e through h); G denotes global update and L denotes local update

After global update, local update with streamline-assisted sensitivity method is used to further improve the matching quality of production data by calibrating local cell permeability. Local update reproduced better the heterogeneity of the reference model, shown in ‘c’ and ‘g’ above. The changes made after global local updates (‘d’ and ‘h’) are compared with change needed (shown in ‘d’ in Fig. 4-30). As we marked key areas with red dotted line, the changed region and the magnitude of changes for both updated models are similar to the change needed shown in Fig. 4-30 ‘d’. Thus, from this example, we demonstrated that coarsened GCT basis does work well in conjunction with the proposed workflow. The use of coarsened GCT brings additional benefits; less

simulation time required (computational efficiency), smaller number of coefficients (reduced parameter space), and smaller searching range for each coefficients (faster convergence).

4.5 Application to Brugge Field

In this section we apply the proposed method of history matching to the Brugge field. We demonstrate its applicability for incorporation of seismic data, its effectiveness for history matching conflicting objectives, and the use of coarsened GCT basis to 3D field reservoir model history matching. The Brugge field model was generated for a benchmark project to test the combined use of waterflooding-optimization and history matching methods in a closed loop workflow as part of an SPE Applied Technology Workshop (ATW). The model properties are designed based on a North sea brent-type field. The model consists of about 60,000 grid cells with 9 layers. The 10 years of production data and inverted time-lapse seismic data were provided, which are used for this study. The detail about Brugge field can be found in the paper by Peters et al. (2009) .

4.5.1 Inverted 4D-seismic data

We used 4D seismic data, specifically pressure and saturation changes across the initial 10 year period of production, as the second and third objective respectively in addition to the production data, the water production rate. The seismic data were generated directly from the reservoir simulation instead of seismic forward modeling and generating synthetic seismic data at Year 0 and Year 10 and inverting those. Also, an upscaled model was used to calculate the pressure and saturation, causing an unintentional bias in the pressure compared to the fine scale truth model (Peters, L. et al. 2009). The bias resulted in a conflict between seismic and production data. Fig. 4-32 below shows 4D

seismic saturation and pressure data where the vertically averaged values over four reservoir zones are provided.

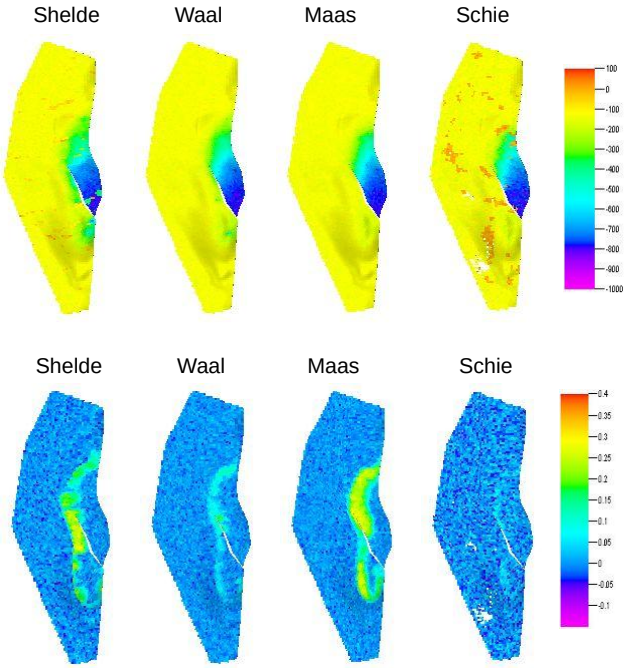

Fig. 4-32 4D seismic data; pressure (top) and water saturation changes (bottom)

4.5.2 Trade-off and corrections between objectives

To start with, conflict between objectives is investigated after initial populations have been generated. One hundred (100) members are sampled, each comprising of twenty (20) GCT basis transformation coefficients. For sampling, Latin hypercube method is used. Sampled variables are applied to simulate production and dynamic results. Those are then used to compare the correlations between objectives, which give idea about how much those are correlated. As discussed in previous section, the correlation does not tell exactly about conflicting information but it is a good way to analyze trade-off pattern and identify confliction between objectives. Fig. 4-33 shows computed correlations between objectives. The figure in the top is obtained using the provided data set (called hereinafter 'base case'). For the 'base case', the correlation between production data (1st

objective) and 4D water saturation data (2nd objective) is 0.41 and the correlation between water and pressure changes (3rd objective) turns out negative 0.09. The correlations indicate low or negative relationship between data. The conflict comes from embedded unintentional bias in the seismic data.

In the literature for many objectives optimization the correlation has been used as a criterion to decide redundant objectives, which are after called 'non-essential' objectives. It is defined that if we drop it from many objectives problem, for example ten (10) objectives problem can be switched to three (3) objectives problem, it does not affect the set of efficient solutions. Although the problem has M objectives, the Pareto optimal front can involve a much lower dimensional interactions. If the objectives are all conflicting, there is an M-dimensional interaction (Deb and Saxena 2005). When such a reduction in the dimensionality is considered, one paper (Agrell 1997) presents the probabilistic method based on correlation and the other (Deb and Saxena 2005) uses correlation together with eigenvalues. However, in this paper the dimensionality reduction is out of main focus although we use the correlation to discuss conflict between objectives.

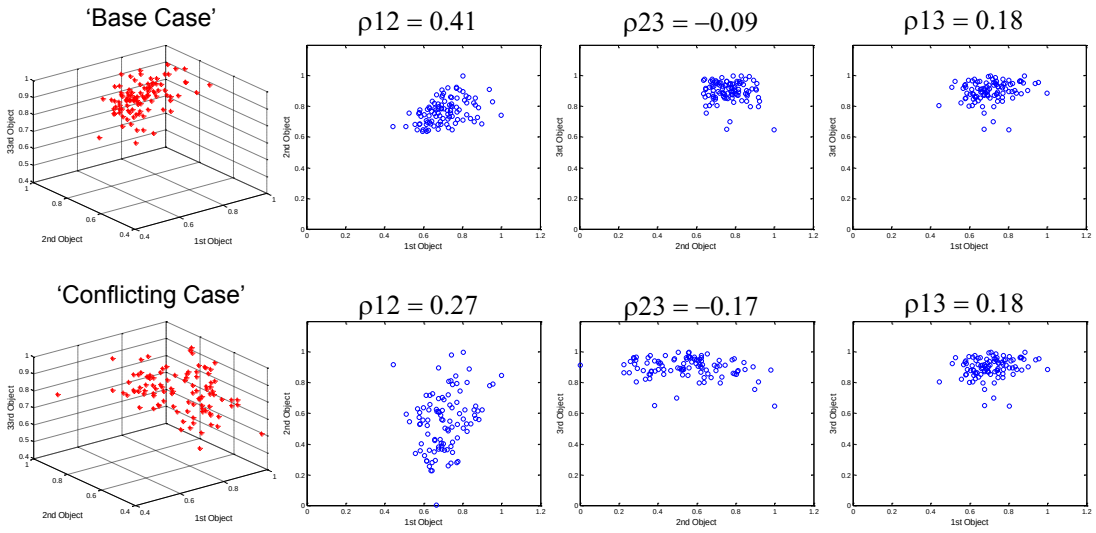

Fig. 4-33 Scatter plot showing correlations between objectives; 'base case' (left) and 'test case' (right)

For comparative study, we set up a ‘conflicting case’ with addition of intentional bias on seismic water saturation changes resulting in more contradictory information for production and pressure data. We used the water saturation changes of initial model for biased data, which is displayed in Fig. 4-34 and compared with actual seismic water saturation data. For two formations (Shelde, Maas), actual seismic water saturation change data, initial model’s data, and corresponding change needed are displayed in the top row. Because we now consider initial saturation change data as our objective data instead of real seismic water saturation change data, the saturation data misfit of initial model is considered zero-data misfit.

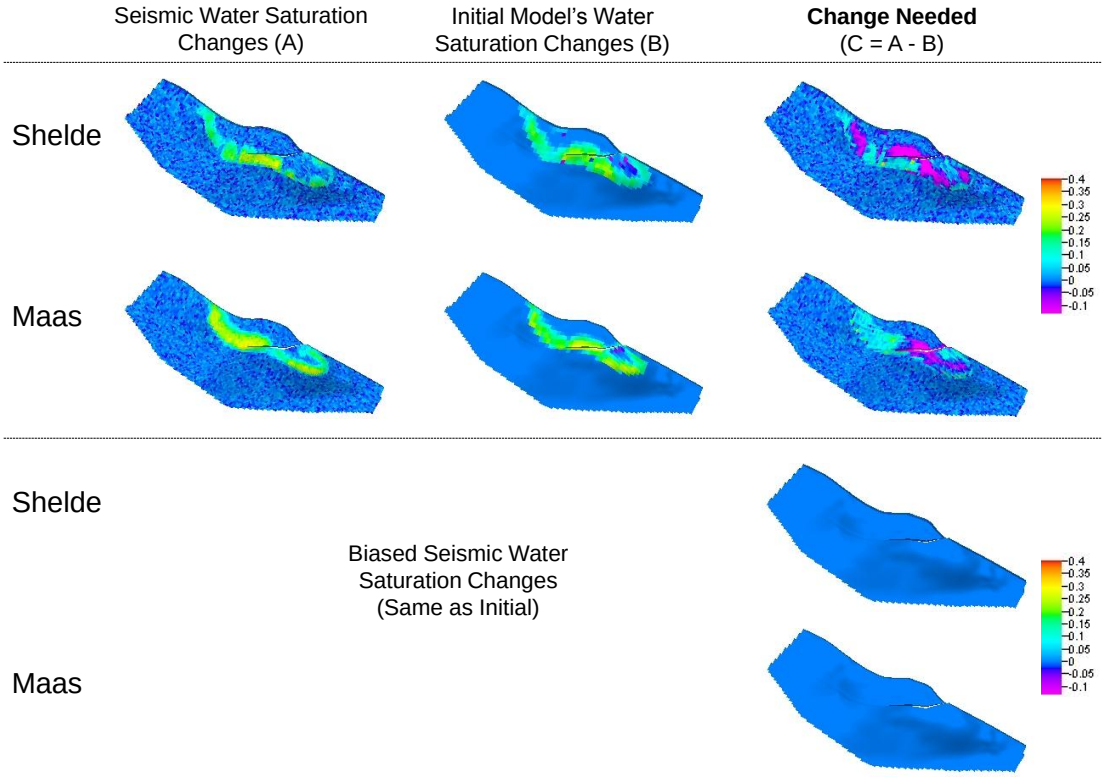

Fig. 4-34 Biased 4D seismic data of water saturation and saturation change needed

The correlation between objectives are computed after addition of bias, which shows that the correlations related to biased water saturation become much negative; correlation between production and saturation (ρ_{12}) is now 0.27 and correlation between

pressure and saturation (ρ_{23}) is negative 0.17 while correction between pressure changes and production data (ρ_{13}) remains the same. In accordance with terms of analyzed correlations, it is noted that the addition of bias on water saturation worsens the relationship between data and results in larger conflict.

4.5.3 Pareto-based multiobjective hierarchical history matching

To start with, we performed grid coarsening by uniformly merging 2 blocks in I, J directions, and optimal layering in K directions resulted in 5 layers from originally 9 layers. The number of total grid cells and active cells of the coarsened model are significantly reduced while preserving major features of heterogeneity of the initial fine-scale model as shown in Fig. 4-35. For example, 44,464 active cells are reduced to 6,343 active cells (approx. 14% compared to the fine model). For global update, while calibrating large-scale features and uncertainty, the use of the coarsened model is a reasonable choice because the coarse-scale simulation saves significant computation cost and we need a lot of simulation runs.

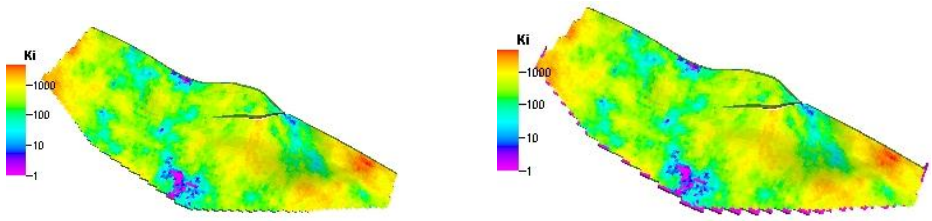

Fig. 4-35 Fine scale permeability model (left) and coarse scale permeability model (right)

We created GCT basis based on the coarsened grid geometry which is compared with the fine GCT basis in Fig. 4-36. The coarsened basis functions can be more consistent with coarse-scale simulation responses than fine-scale basis functions. For this application, twenty (20) coarsened transform basis coefficients are used as parameters to match production data and seismic data.

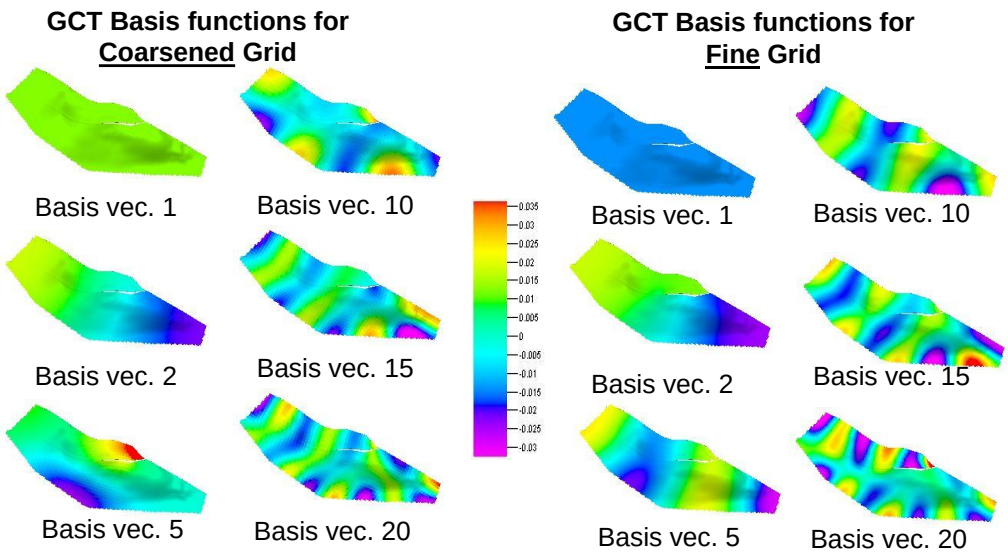

Fig. 4-36 GCT basis functions for coarsened (X2) grid (left) and fine grid (right)

The results are shown in Fig. 4-37 after applying two approaches to same 'conflicting case': 'GA-SOP' and the proposed 'MOEA'. We performed ten (10) iterations for both approaches. As we observed in the previous section, similar behavior has been observed in this case as well; GA-SOP tends to sacrifice one or more objectives to improve total fitness function in the case of conflicting problems. We see that 2nd objective function in GA-SOP method becomes worse with generation while 1st objective is being better satisfied. On the other hand, the proposed MOEA result (in the right column) shows that it reduces the sum of objective functions in few iterations and keeps range of optimal solutions. In particular, we see that the 2nd objective function searches very large space, almost zero to one, and it does not converge to a particular solution. This is exactly showing the beauty of this approach; it does not get to a single compromised solution. Instead, it discovers all possible optimal solutions. Because of that, the solutions may include completely different models: some solutions can be close to real seismic data and others are reproducing biased data more closely. We will show these results in the next section.

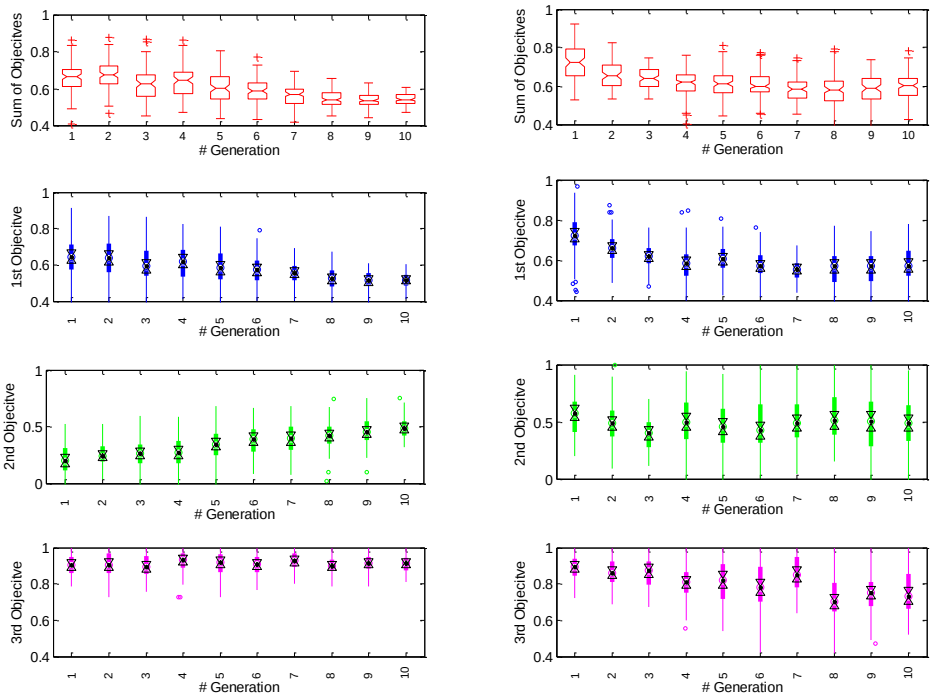

Fig. 4-37 Objective functions by generation: GA-SOP (left) and Proposed MOEA (right)

Our proposed approach reveals uncertainties associated with the conflicting objectives: the large confliction has been reflected on the results with large uncertainties. Large trade-off between objectives is observed particularly in the objective of water saturation changes data. In Fig. 4-38 we observe long-spread Pareto front from scatter plot of optimal solutions both between 1st objective (production data) & 2nd objective (saturation data) and between 2nd & 3rd objectives (pressure data). Improving water saturation data requires large degradation of production and pressure data. The bias in saturation data ended up with constituting such large distributed Pareto optimal solutions. The optimal solutions for the proposed MOEA result are clustered to select representative models for local update. Cluster analysis grouped optimal solutions into predefined number of regions. In this case we picked 3 updated models, marked with centroids shown in Fig. 4-38. The updated model 1 in Cluster 1 matches best to

production data; the updated model 2 in Cluster 2 is the one most closely reproducing biased saturation data (2nd objective), and the updated model 3 in Cluster 3 is reproducing the best pressure changes field (3rd objective). These models are used for local update and uncertainty analysis.

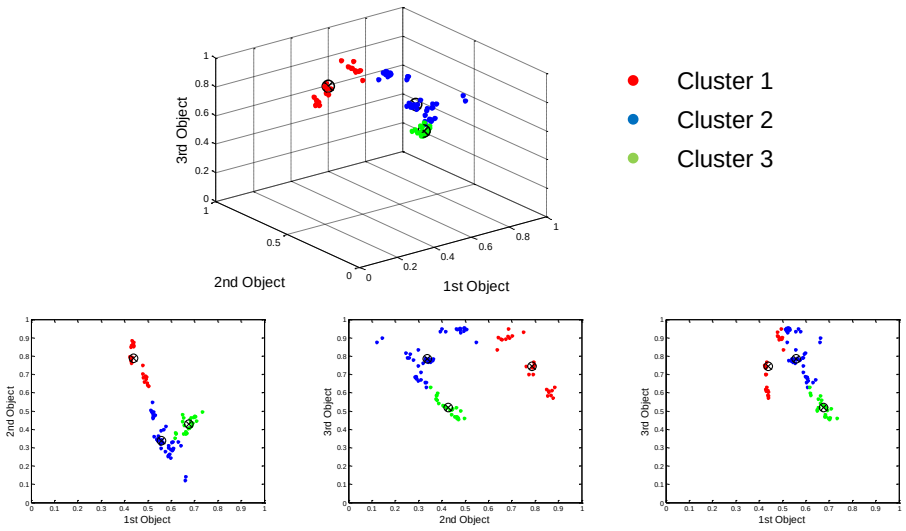

Fig. 4-38 Scatter plot showing optimal solutions for 'conflicting case'; between 1st and 2nd objectives (left), between 2nd and 3rd objectives (middle), between 1st and 3rd objectives (right)

We now review the results from these selected models: water saturation changes distribution, pressure changes distribution, and production data. Fig. 4-39 shows water saturation changes distributions for observed, initial, and updated models. Updated model 1 reproduces actual seismic water saturation data very well even though we have not used it as an objective. However, it is possible because the model is well matched to production data which is more consistent with the true seismic information. Saturation change made in updated model 2 is very similar with change needed based on biased saturation information. Lastly, the updated model 3 is not matching either one very well but it is in between actual seismic data and biased data. We can see here that these

updated models reveal conflict between the data and give clue about the truth by discovering multiple plausible solutions.

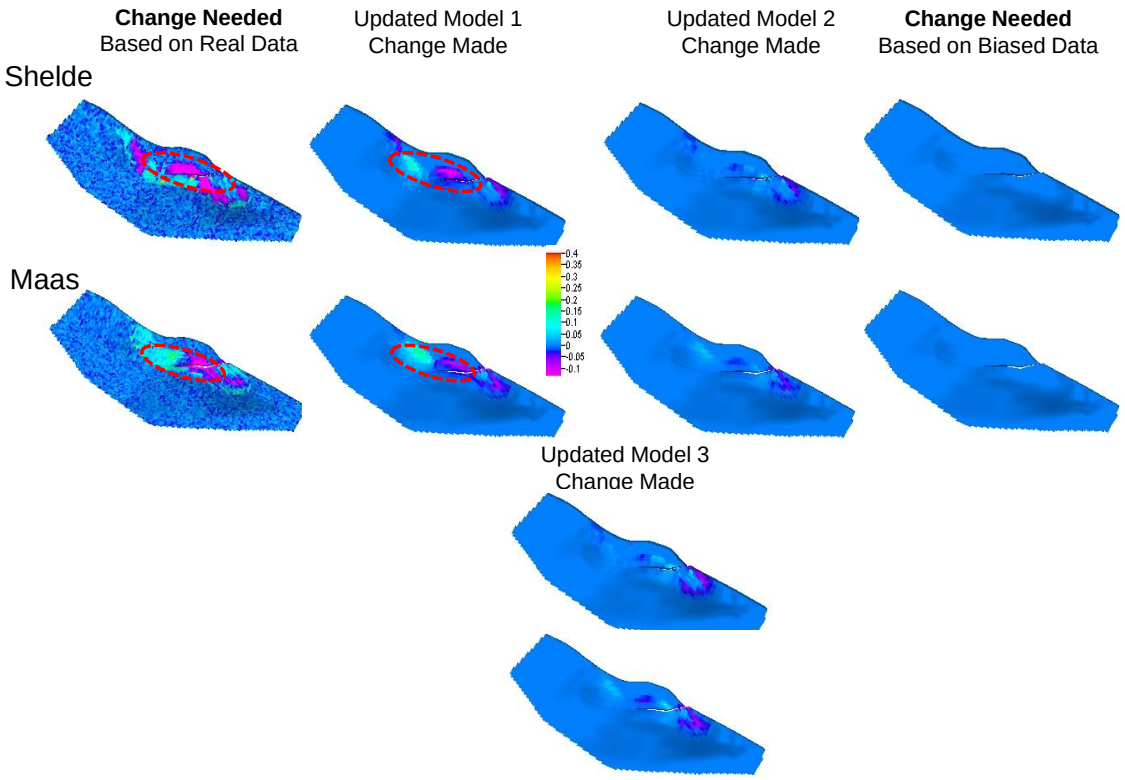

Fig. 4-39 Change needed based on real data (left) and based on biased data (right), updated models' change made (middle)

There was field-wide pressure change differences of about 100 to 200 psi between observed and initial models as noticed in Fig. 4-40. It is apparent that our proposed approach has found many possible optimal solutions associated with pressure changes very well. For example, updated model 3 reproduces observed pressure data very closely while updated model 2 doesn't seem match the data well. Updated model 2 is, as we noted in Fig. 4-39, relatively well-matched to biased saturation data. Thus, we see completely opposite results here at pressure data matching.

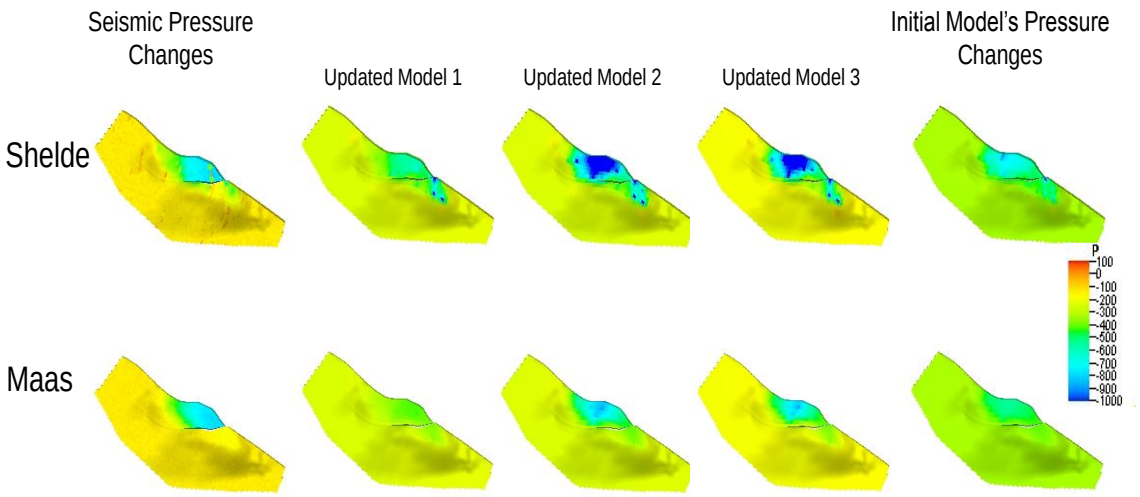

Fig. 4-40 Observed seismic pressure changes (left), updated models' seismic pressure changes (middle), initial model's seismic pressure change (right)

We carry out streamline-based generalized travel time inversion (GTTI) to further improve the production response for each well. We compute sensitivity of production response with respect to local cell property (in this case cell permeability) from the streamlines. The updated permeability field is obtained with minimization of penalized objective functions ensuring that final updated model is not far from the initial or starting model (He et al. 2002). The details on this GTTI method can be found in many publications (Cheng et al. 2006; Yin et al. 2010) .

In Fig. 4-41 we display production data (water production rate) improvement through global and local updates. In multiobjective optimization framework (global update) we improved objective function of production data under uncertainties. The models have been selected from updated ensemble models to further calibrate in local update. The local update with streamline-based GTTI method works very well to improve well by well performances with calibration of small-scale uncertainties (grid cell properties).

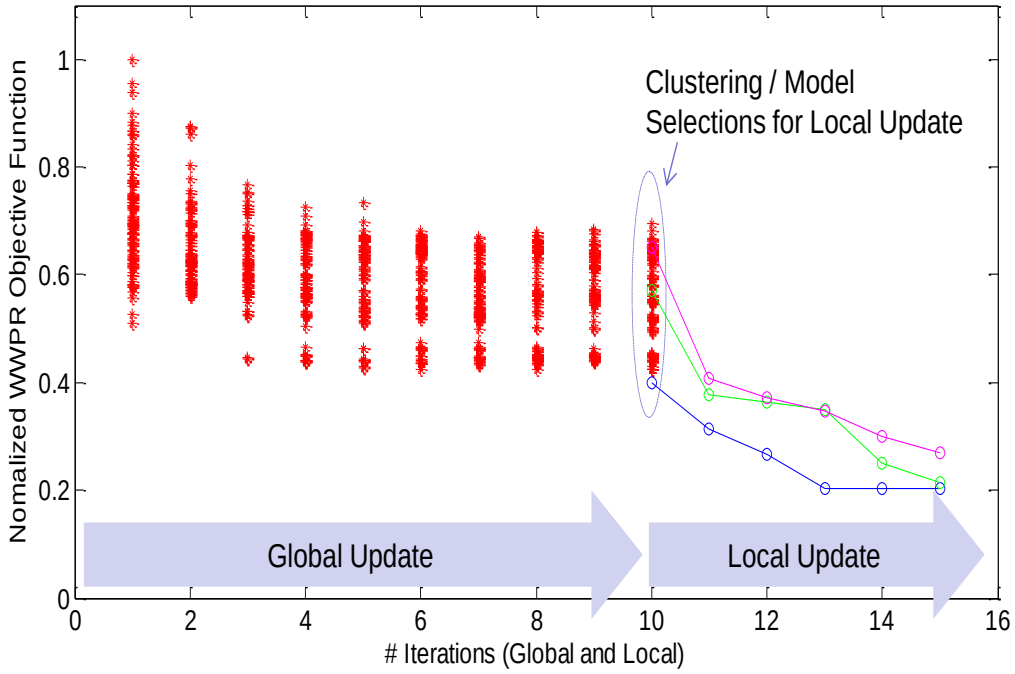

Fig. 4-41 Production data (water production rate) improvement through global and local update

Fig. 4-42 below compares final updated production responses with observed and initial data for all the wells in terms of water production rate. We see dramatic improvement in production data match for most of the wells. Relatively larger uncertainty ranges are observed from the wells (P9, P10, P17) where large bias of water saturation was imposed as displayed in Fig. 4-42. Without post processing for uncertainty, the updated responses of models provide us with a range of uncertainties, one of benefits from this approach.

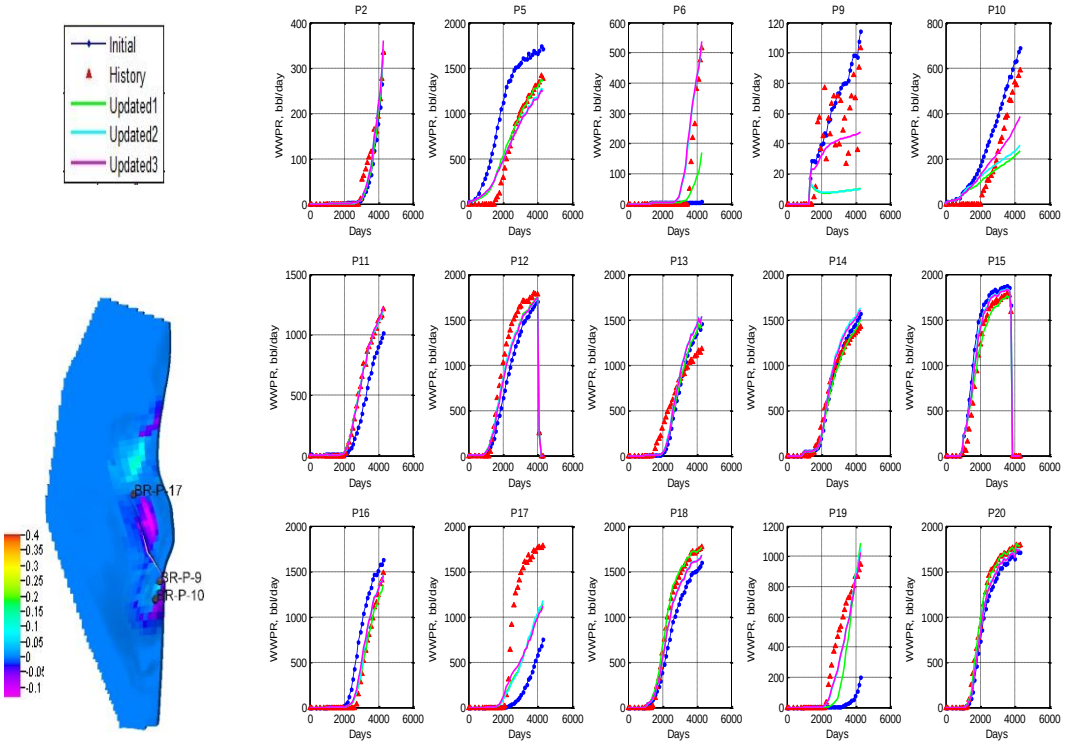

Fig. 4-42 Initial, observed (history), four (3) updated water production rate responses for all producers

Lastly, we predict the range of future production and provide the uncertainty analysis for updated geologic models from two approaches: Pareto-based approach (Proposed MOEA) and weighted-sum approach (GA-SOP). We used 3 representative updated models for each approach to forecast next 10 years production. The results in Fig. 4-43 show cumulative field water production for updated models after global and local updates. The weighted-sum based approach (GA-SOP) result shows very narrow range of prediction outcomes which suggests relatively small uncertainty associated with predictions. These outcomes are not appreciably different from having a single history matched model. In the other hand, proposed approach provides a range in predicted outcomes and therefore some insight into the uncertainty associated with the forecast of future production.

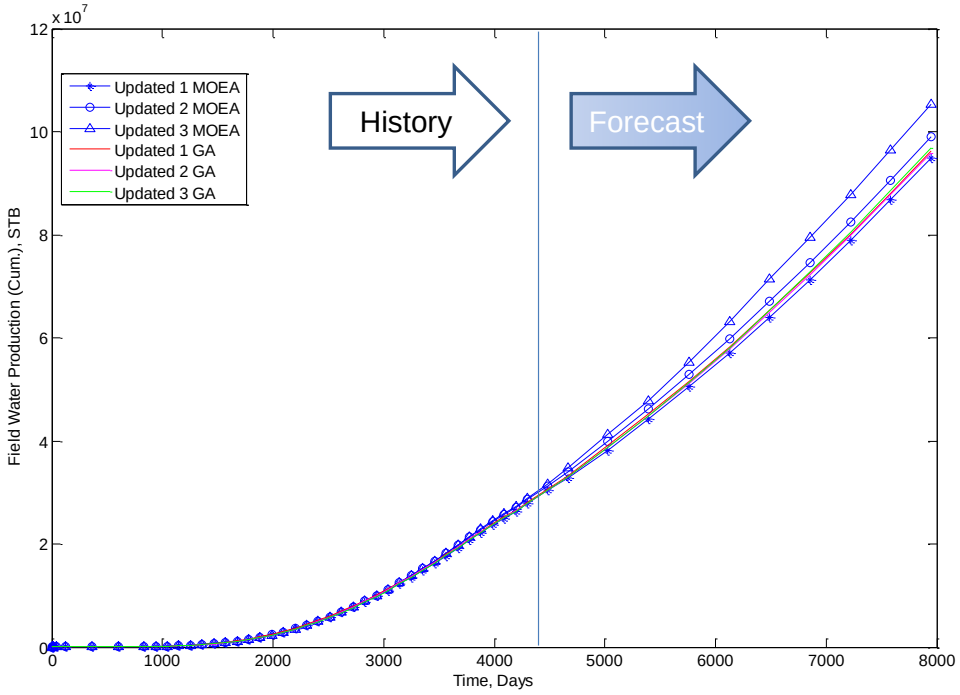

Fig. 4-43 Comparison of updated models in terms of forecast of water production between two approaches (MOEA, GA-SOP)

4.6 Summary and Conclusions

In this paper we have presented a Pareto-based multiobjective hierarchical history matching workflow. History matching very often involves the use of multiple objectives, possibly conflicting with each other, to calibrate reservoir geologic models. We have demonstrated the effectiveness of the proposed method through applications to synthetic models and the benchmark Brugge field. These applications have focused on multiobjective history matching under conflicting information. The major findings in the proposed approach are as follows.

1. The Pareto-based multiobjective evolutionary algorithm (MOEA) seems to outperform the aggregation-based genetic algorithm (GA-SOP) which is

commonly used in history matching applications. The GA-SOP does not account for trade-off between objectives. The MOEA discovers multiple solutions based on the Pareto optimal sets, accounting for the influence of each of the objectives.

2. Combining seismic surveillance data and well-based surveillance data into a system of multiobjective optimization improves the quality of history matching. The seismic water saturation and pressure distribution provide important insight on the shape of flow paths.
3. The proposed workflow forms a hierarchical framework for history matching: the global update is followed by local update. For global update MOEA has replaced classical Genetic algorithm to better account for conflicting multiobjectives. The global match focuses on the calibration of large-scale reservoir heterogeneity. For local update we propose to use streamline-based sensitivity method. Specifically, the Generalized travel time inversion (GTTI) algorithm has proved to be an efficient means to update heterogeneity at grid-cell scale.
4. For practical applications of history matching, GCT technique has been introduced to the Pareto-based multiobjective optimization method. Use of GCT basis coefficients as parameters worked very well for model calibration using gradient-free evolutionary optimization algorithm. In particular, the application of parameterization with GCT basis function resulted in avoiding the ad hoc definition of regional multipliers. For large-scale reservoir and complex reservoir models, the use of coarsened GCT basis is proposed for computational efficiency as well as faster convergence.
5. The proposed Pareto-based multiobjective hierarchical history matching workflow combines the elements of stochastic and deterministic approaches into a workflow. Uncertainty analysis is performed as just one component of the workflow without additional post processing work.

CHAPTER V

CONCLUSIONS AND RECOMMENDATIONS

In this work, we have presented novel history matching and optimization approaches for reservoir management in a mature field. These approaches are aimed at efficiency and effectiveness for applications to large-scale and complex reservoir models because conventional approaches often have difficulties associated with computational inefficiency, loss of geologic realisms, and non-uniqueness.

First, we have presented a hierarchical multiscale approach to history matching (Chapter II), which reduces computational time and improves the quality of history matching. The application to large-scale offshore carbonate reservoir model has demonstrated its suitability and efficiency.

Next, we have proposed a production/injection rate optimization method (Chapter III) which utilizes streamline simulation techniques, particularly, streamline-assisted time of flight and flux distribution maps. We derived simple analytic solutions from the relationship between flow rate and the time of flight to compute rate change coefficients. The proposed method follows a simple and easy to use workflow so that it is efficient for applications to field cases, particularly, mature reservoirs with large numbers of wells.

Lastly, a novel approach to history matching using Pareto-based multiobjective optimization algorithm has been presented in Chapter IV. We have noted that most of history matching and optimization problems in petroleum industry typically have multiple (possibly conflicting) objectives to be satisfied. The proposed approach has outperformed conventional approaches (i.e. Genetic algorithm) using weighted-sum methods, particularly when the objectives are conflicting. The proposed approach provides an efficient workflow where Pareto-based multiobjective evolutionary algorithm incorporates the GCT technique.

5.1 Conclusions

Some specific conclusions can be made from this work. First, the part of dissertation presenting a hierarchical multiscale history matching approach is summarized as follows:

1. We have proposed the inclusion of a multiscale approach to the hierarchical global and local history matching procedures (Yin et al. 2010). Its practical feasibility was demonstrated using applications to 3D synthetic model and a large offshore carbonate reservoir model.
2. We found that the use of multiscale approach was successful in history matching a large reservoir model because of desirable multiscale features: computational efficiency, effective iterative minimization, and avoiding local minima.
3. The structured hierarchical history matching with global and local updates worked very well. In the global parameter calibration, reservoir energy is matched and its balance between platforms (i.e. regions) is achieved in terms of fluid production and reservoir pressures. In the local parameter calibration, individual well production responses are matched. Because the global reservoir energy has been calibrated to reasonable level by global updates, the local update using streamline technique found solutions very fast.
4. A stochastic global search approach based on the genetic algorithm combined with a proxy model for the objective function provided effective means to match the global parameters and produce an ensemble of preliminary solutions for the local update.

Next, some conclusions are about the proposed novel rate optimization approach summarized in the following:

1. The flood efficiency map is shown to be an effective tool for reservoir management because it provides valuable information related to reservoir flow patterns and sweep efficiency. Although, the flux distribution maps have been

used in the past to visualize flow, the use of TOF distribution map is novel. In fact, our proposed optimization method mainly relies on the TOF distribution map.

2. Our proposed streamline-based production rate optimization is simple, intuitive and easy to implement. It relies on equalizing the TOF both 'globally' (between streamline bundles in terms of average TOF) and 'locally' (within streamline bundles) using analytic formulation. The approach is applicable to both new and mature waterflooding as we minimize variance of TOF between injection-production pairs rather than focusing on the water front breakthrough time.
3. A new definition of injection efficiency is proposed in terms of the coefficient of TOF variation. Using this criterion, we propose a systematic approach to injection optimization. Recognizing that in field applications it is more practical to optimize injectors rather than producers, the injection optimization scheme has been proposed as a simple and standalone procedure.
4. The effectiveness of our optimization can be examined by comparing the flood efficiency maps before and after optimization. In particular, the TOF map is a clear indicator of sweep efficiency in terms of the similarity or dissimilarity of the average TOF between the well connections.

Finally, some conclusions from the hierarchical Pareto-based multiobjective history matching work are as follows:

1. The Pareto-based multiobjective evolutionary algorithm (MOEA) seems to outperform the aggregation-based genetic algorithm (GA-SOP) which is commonly used in history matching applications. The GA-SOP does not account for trade-off between objectives. The MOEA discovers multiple solutions based on the Pareto optimal sets, accounting for the influence of each of the objectives.
2. Combining seismic surveillance data and well-based surveillance data into a system of multiobjective optimization improves the quality of history matching: seismic water saturation and pressure distribution provide better insight on the

shape of flow paths while production data concentrates on the fractional flow of fluids.

3. The proposed workflow forms a hierarchical framework for history matching: the global update is followed by local update. For global update MOEA has replaced classical Genetic algorithm to better account for conflicting multiobjectives. The global match focuses on the calibration of large-scale reservoir heterogeneity. For local update we propose to use streamline-based sensitivity method. Specifically, the Generalized travel time inversion (GTTI) algorithm has proved to be an efficient means to update heterogeneity at grid-cell scale.
4. For practical applications of history matching, GCT parameterization technique has been introduced to the Pareto-based multiobjective optimization method. Use of GCT basis coefficients as parameters worked very well for model calibration using gradient-free evolutionary optimization algorithm. In particular, the application of parameterization with GCT basis function resulted in avoiding the ad hoc definition of regional multipliers. For large-scale reservoir and complex reservoir models, the use of coarsened GCT basis is proposed for computational efficiency as well as faster convergence.
5. The proposed Pareto-based multiobjective hierarchical history matching workflow combines the elements of stochastic and deterministic approaches into a workflow. Uncertainty analysis is performed as just one component of the workflow without additional post processing work.

5.2 Recommendations and Future Work

The proposed multiscale streamline-assisted inversion method has proven to be an efficient means for history matching large-scale field models. The effectiveness of proposed method can be further verified with applicability to flexible-domain consisting of various grid-scales in a field. For example, we can think of a simulation model where different scales of grid coarsening and refinement are used in a model and it can include

irregular grid system with local grid refinements and partially areal and vertical coarsening. Because reservoir model becomes more complex and diverges to unstructured grid system, one may take opportunity to extend the applicability of proposed streamline-based multiscale inversion method to those increasing levels of complexity in reservoir models.

In chapter IV, we have shown applications to history matching of time-lapse seismic and production data using Pareto-based evolutionary algorithm with GCT. Through the applications, we have demonstrated that incorporation of seismic data can decrease uncertainty in the reservoir model and increase the reliability of the production forecasts because of seismic data features; information about the change in the reservoir dynamic properties and high density spatial information. The seismic data resolution is typically different from the resolution of simulation model. Upscaling and downscaling properties (static, dynamic) are one of active research areas associated with joint seismic and production data inversion. Uniform coarsened GCT basis, implicitly corresponding to the grid resolution, has been successfully tested. We can extend its applicability to construct the grid-connectivity matrix for the model including the different levels of coarsening and/or refinement partially or locally. Because the resolution of the heterogeneity description varies with grid cell size, the basis vectors would implicitly correspond to the specific grid resolution if GCT was constructed for the grid. This capability leads to the merging of multi-scale and multi-resolution approaches. GCT basis consistent with data resolution would improve performance of minimization during history matching of seismic data.

Lastly, we have proposed a novel multiobjective hierarchical history matching approach that has been successfully applied to history matching of both synthetic and the Brugge model. Current Pareto-based evolutionary algorithms being used for multiobjective optimization typically work best to the problems having smaller number of objectives (about five or so) for the task of finding a well-representative set of optimal solutions. These algorithms have difficulties on handling larger number of objectives associated with stagnation of search process, increased dimensionality of Pareto-optimal

front, and relatively high computational cost. Because most of history matching problems involve typically a large number of (ten or more) objectives to be satisfied, one may make special efforts for solving those large objective history matching and optimization problems.

REFERENCES

Aanonsen, S.I., SPE, Centre for Integrated Petroleum Research, University of Bergen. 2008. Efficient History Matching Using a Multiscale Technique. *SPE Reservoir Evaluation & Engineering* **11** (5): pp. 154-164. DOI: 10.2118/92758-PA

Agrell, P.J. 1997. On Redundancy in Mcdm. *European Journal of Operational Research* **98** (3): 571-586.

Alhuthali, A.H., Datta-Gupta, A., Yuen, B. et al. 2008. Optimal Rate Control under Geologic Uncertainty. Paper SPE 113628 presented at the SPE/DOE Improved Oil Recovery Symposium, Tulsa, 19-23 April.

Alhuthali, A.H., Datta-Gupta, A., Yuen, B. et al. 2010. Field Applications of Waterflood Optimization Via Optimal Rate Control with Smart Wells. *SPE Reservoir Evaluation & Engineering* **13** (3): 406-422.

Alhuthali, A.H., Oyerinde, D., and Datta-Gupta, A. 2007. Optimal Waterflood Management Using Rate Control. *SPE Reservoir Evaluation & Engineering* **10** (5): 539-551.

Bhark, E., Rey, A., Datta-Gupta, A. et al. 2011. Multiscale Parameterization and History Matching in Structured and Unstructured Grid Geometries. Paper SPE 141764 presented at the SPE Reservoir Simulation Symposium, Woodland, Texas, 21-23 February.

Bhark, E.W., Jafarpour, B., and Datta-Gupta, A. 2011. A Generalized Grid Connectivity-Based Parameterization for Subsurface Flow Model Calibration. *Water Resources Research* **47**: 32. DOI: 10.1029/2010WR009982

Bissell, R., Killough, J.E., and Sharma, Y. 1992. Reservoir History Matching Using the Method of Gradients on a Workstation. Paper SPE 24265 presented at the European Petroleum Computer Conference, Stavanger, Norway, 24-27 May. DOI: 10.2118/24265-MS.

Bittencourt, A.C. and Horne, R.N. 1997. Reservoir Development and Design Optimization. Paper SPE 38895 presented at the SPE Annual Technical Conference and Exhibition, San Antonio, Texas, USA, 5-8 October. DOI: 10.2118/38895-MS.

Brockhoff, D. 2009. Many-Objective Optimization and Hypervolume Based Search. Doctor of Science, University of Dortmund.

Chankong, V. and Haimes, Y.Y. 1983. *Multiobjective Decision Making Theory and Methodology*. New York: Elsevier Science. Original edition. ISBN.

Cheng, H., Datta-Gupta, A., and He, Z. 2005. A Comparison of Travel-Time and Amplitude Matching for Field-Scale Production-Data Integration: Sensitivity, Nonlinearity, and Practical Implications. *SPE Journal* **10** (1): 75-90. DOI: 10.2118/84570-PA

Cheng, H., Dehghani, K., and Billiter, T. 2008. A Structured Approach for Probabilistic-Assisted History Matching Using Evolutionary Algorithms: Tengiz Field Applications. Paper SPE 116212 presented at the SPE Annual Technical Conference and Exhibition, Denver, Colorado, USA, 21-24 September. DOI: 10.2118/116212-MS.

Cheng, H., Osako, I., Datta-Gupta, A. et al. 2006. A Rigorous Compressible Streamline Formulation for Two- and Three-Phase Black-Oil Simulation. *SPE Journal* **11** (4): 407-417. DOI: 10.2118/96866-PA

Cheng, H., Oyerinde, D., Datta-Gupta, A. et al. 2007. Compressible Streamlines and Three-Phase History Matching. *SPE Journal* **12** (4): 475-485. DOI: 10.2118/99465-PA

Cheng, H., Wen, X.-H., Milliken, W.J. et al. 2004. Field Experiences with Assisted and Automatic History Matching Using Streamline Models. Paper SPE 89857 presented at the SPE Annual Technical Conference and Exhibition, Houston, Texas, USA, 26-29 September. DOI: 10.2118/89857-MS.

Das, I. and Dennis, J.E. 1997. A Closer Look at Drawbacks of Minimizing Weighted Sums of Objectives for Pareto Set Generation in Multicriteria Optimization Problems. *Structural Optimization* **14** (1): 63-69. DOI: 10.1007/BF01197559

Datta-Gupta, A., Kulkarni, K.N., Yoon, S. et al. 2001. Streamlines, Ray Tracing and Production Tomography: Generalization to Compressible Flow. *Petroleum Geoscience* **7** (1): S75-S86.

Deb, K., Pratap, A., Agarwal, S. et al. 2002. A Fast and Elitist Multiobjective Genetic Algorithm: Nsga-Ii. *IEEE Transactions on Evolutionary Computation* **6** (2): 182-197.

Deb, K. and Saxena, D.K. 2005. *On Finding Pareto-Optimal Solutions through Dimensionality Reduction for Certain Large-Dimensional Multi-Objective Optimization Problems*. Number 2005011, Indian Institute of Technology, Kanpur, PIN 208016, India (November 2011).

Fang, H., Wang, Q., Tu, Y.-C. et al. 2008. An Efficient Non-Dominated Sorting Method for Evolutionary Algorithms. *Evolutionary Computation* **16** (3): 355-384.

Floris, F.J.T., Bush, M.D., Cuypers, M. et al. 2001. Methods for Quantifying the Uncertainty of Production Forecasts: A Comparative Study. *Petroleum Geoscience* **7** (S): S87-S96. DOI: 10.1144/petgeo.7.S.S87

Galassi, M., Davies, J., Theiler, J. et al. 2009. *Gnu Scientific Library Reference Manual - Third Edition (V1.12)*: Network Theory Ltd. Original edition. ISBN 0954612078.

Gill, P.E., Murray, W., and Wright, M.H. 1981. *Practical Optimization*: New York: Academic Press. Original edition. ISBN 0122839528.

Grinestaff, G.H. 1999. Waterflood Pattern Allocations: Quantifying the Injector to Producer Relationship with Streamline Simulation. Paper SPE 54616 presented at the SPE Western Regional Meeting, Anchorage,Alaska, 26-28 May.

Grinestaff, G.H. and Caffrey, D.J. 2000. Waterflood Management: A Case Study of the Northwest Fault Block Area of Prudhoe Bay, Alaska, Using Streamline Simulation and Traditional Waterflood Analysis. Paper SPE 63152-MS presented at the SPE Annual Technical Conference and Exhibition, Dallas, Texas.

Hajizadeh, Y., Christie, M., and Demyanov, V. 2011. Towards Multiobjective History Matching: Faster Convergence and Uncertainty Quantification. Paper SPE 141111 presented at the SPE Reservoir Simulation Symposium Woodland, Texas, 11-14 March.

Han, Y.M., Park, C., and Kang, J.M. 2010. Estimation of Future Production Performance Based on Multi-Objective History Matching in a Waterflooding Project. Paper SPE 130500 presented at the SPE EUROPE/EAGE Annual Conference and Exhibition Barcelona, Spain, 14-17 June.

He, Z., Yoon, S., and Datta-Gupta, A. 2002. Streamline-Based Production Data Integration with Gravity and Changing Field Conditions. *SPE Journal* **7** (4): 423-436. DOI: 10.2118/81208-PA

Hohl, D., Jimenez, E., and Datta-Gupta, A. 2006. Field Experiences with History Matching an Offshore Turbiditic Reservoir Using Inverse Modeling. Paper SPE 101983 presented at the SPE Annual Technical Conference and Exhibition, San Antonio, Texas, USA, 24-27 September. DOI: 10.2118/101983-MS.

Holland, J.H. 1992. Genetic Algorithms. *Scientific American* **267** (1): 44-50.

Horn, J. and Nafpliotis, N. 1993. *Multiobjective Optimization Using the Niched Pareto Genetic Algorithm*. Illinois Genetic Algorithms Laboratory

Kim, J.-U., Datta-Gupta, A., Jimenez, E.A. et al. 2010. A Dual Scale Approach to Production Data Integration into High Resolution Geologic Models. *Journal of Petroleum Science and Engineering* **71**: 147-159. DOI: 10.1016/j.petrol.2010.01.006

King, M.J., Burn, K.S., Wang, P. et al. 2006. Optimal Coarsening of 3d Reservoir Models for Flow Simulation. *SPE Reservoir Evaluation & Engineering* **9** (4): 317-334.

Kirkpatrick, S., Gelatt, C.D., and Vecchi, M.P. 1983. Optimization by Simulated Annealing. *Science* **220** (4598): 671-680.

Li, R., Reynolds, A.C., and Oliver, D.S. 2003. History Matching of Three-Phase Flow Production Data. *SPE Journal* **8** (4): 328-340. DOI: 10.2118/87336-PA

Ma, X., Al-Harbi, M., Datta-Gupta, A. et al. 2008. An Efficient Two-Stage Sampling Method for Uncertainty Quantification in History Matching Geological Models. *SPE Journal* **13** (1): 77-87. DOI: 10.2118/102476-PA

Mamonov, A., Couet, B., Bailey, W.J. et al. 2007. Optimal Gridding: A Fast Proxy for Large Reservoir Simulations. Paper SPE 111378 presented at the SPE/EAGE Reservoir Characterization and Simulation Conference, Abu Dhabi, UAE, 28-31 October. DOI: 10.2118/111378-MS.

McCormick, G.P. and Tapia, R.A. 1972. The Gradient Projection Method under Mild Differentiability Conditions. *SIAM Journal on Control* **10** (1): 93-98. DOI: 10.1137/0310009

Mitra, N.K. and Kumar, A. 2008. Managing Mature Indian Offshore Fields - a Case History. Paper 117950 presented at the Abu Dhabi International Petroleum Exhibition and Conference, Abu Dhabi, UAE, 3-6 November. DOI: 10.2118/117950-MS.

Oliver, D.S., Reynolds, A.C., Bi, Z. et al. 2001. Integration of Production Data into Reservoir Models. *Petroleum Geoscience* **7** (S): S65-S73. DOI: 10.1144/petgeo.7.S.S65

Ouenes, A., Bhagavan, S., Bunge, P.H. et al. 1994. Application of Simulated Annealing and Other Global Optimization Methods to Reservoir Description: Myths and Realities. Paper SPE 28415 presented at the SPE Annual Technical Conference and Exhibition, New Orleans, Louisiana, 25-28 September. DOI: 10.2118/28415-MS.

Pan, Y. and Horne, R.N. 1998. Improved Methods for Multivariate Optimization of Field Development Scheduling and Well Placement Design. Paper SPE 49055 presented at the SPE Annual Technical Conference and Exhibition, New Orleans, Louisiana, USA, 27-30 September. DOI: 10.2118/49055-MS.

Park, H.-Y. and Datta-Gupta, A. 2011. Reservoir Management Using Streamline-Based Flood Efficiency Maps and Application to Rate Optimization. Paper SPE SPE-144580-MS presented at the SPE Western North American Region Meeting, Anchorage, Alaska, USA, 7-11 May 2011. DOI: 10.2118/144580-ms.

Peters, E., Arts, R.J., Brouwer, G.K. et al. 2009. Results of the Brugge Benchmark Study for Flooding Optimization and History Matching. Paper SPE 119094 presented at the SPE Reservoir Simlation Symposium, Woodlands,TX, 2-4 February.

Peters, L., Arts, R., Brouwer, G. et al. 2009. Results of the Brugge Benchmark Study for Flooding Optimisation and History Matching. Paper 119094-MS presented at the SPE Reservoir Simulation Symposium, The Woodlands, Texas, USA, 2-4 February. DOI: 10.2118/119094-MS.

Qassab, H., Pavlas, M.K.R., Afaleg, N. et al. 2003. Streamline-Based Production Data Integration under Realistic Field Conditions: Experience in a Giant Middle-Eastern Reservoir. Paper SPE 84079 presented at the SPE Annual Technical Conference and Exhibition, Denver, Colorado, 5-8 October.

Rey, A., Ballin, P.R., Vitalis, C.F. et al. 2009. Assisted History Matching in an Offshore Turbidite Reservoir with Active Reservoir Management. Paper SPE 124950 presented at the SPE Annual Technical Conference and Exhibition, New Orleans, Louisiana, USA, 4-7 October. DOI: 10.2118/124950-MS.

Rey, A., Bhark, E., Datta-Gupta, A. et al. 2011. Streamline-Based Rapid Integration of Time-Lapse and Production Data into High-Resolution Geologic Models. Paper SPE 139519 presented at the SPE Annual Technical Conference and Exhibition, Denver, Colorado, 30 October to 2 November.

Roggero, F., D.Y.Ding, Berthet, P. et al. 2007. Matching of Production History and 4d Seismic Data - Application to the Girassol Field, Offshore Angola. Paper SPE 109929 presented at the SPE Annual Technical Conference and Exhibition Anaheim, California.

Romero, C.E. and Carter, J.N. 2001. Using Genetic Algorithms for Reservoir Characterisation. *Journal of Petroleum Science and Engineering* **31** (2-4): 113-123. DOI: 10.1016/S0920-4105(01)00124-3

Sambridge, M. and Mosegaard, K. 2002. Monte Carlo Methods in Geophysical Inverse Problems. *Reviews of Geophysics* **40** (3): 1009. DOI: 10.1029/2000rg000089

Satyajit Taware, S., Texas A&M University; Torsten Friedel, SPE, Schlumberger; Akhil Datta-Gupta, SPE, Texas A&M University. 2011. A Practical Approach for Assisted History Matching Using Grid Coarsening and Streamline-Based Inversion: Experiences in a Giant Carbonate Reservoir. Paper presented at the SPE Reservoir Simulation Symposium, 21-23 February 2011, The Woodlands, Texas, USA. DOI: 10.2118/141606-MS.

Schulze-Riegert, R., Krosche, M., Fahimuddin, A. et al. 2007. Multiobjective Optimization with Application to Model Validation and Uncertainty Quantification. Paper SPE 105313 presented at the SPE Middle East Oil & Gas Show and Conference, Bahrain.

Schulze-Riegert, R.W., Axmann, J.K., Haase, O. et al. 2002. Evolutionary Algorithms Applied to History Matching of Complex Reservoirs. *SPE Reservoir Evaluation & Engineering* **5** (2): 163-173. DOI: 10.2118/77301-PA

Sen, M.K., Datta-Gupta, A., Stoffa, P.L. et al. 1995. Stochastic Reservoir Modeling Using Simulated Annealing and Genetic Algorithms. *SPE Formation Evaluation* **10** (1): 49-56. DOI: 10.2118/24754-PA

Taware, S., Park, H.-Y., Datta-Gupta, A. et al. 2012. Well Placement Optimization in a Mature Carbonate Waterflood Using Streamline-Based Quality Maps. Paper SPE 155055 presented at the SPE Oil and Gas India Conference and Exhibition, Mumbai, India, 28-30 March.

Thiele, M.R. and Batycky, R.P. 2003. Water Injection Optimization Using a Streamline-Based Workflow. Paper SPE 84080 presented at the SPE Annual Technical Conference Exhibition, Denver,Colorado, 5-8 October.

Vasco, D.W., Yoon, S., and Datta-Gupta, A. 1999. Integrating Dynamic Data into High-Resolution Reservoir Models Using Streamline-Based Analytic Sensitivity Coefficients. *SPE Journal* **4** (4): 389-399. DOI: 10.2118/59253-PA

Walker, G.J. and Lane, H.S. 2007. Assessing the Accuracy of History-Match Predictions and the Impact of Time-Lapse Seismic Data: A Case Study for the Harding Reservoir. Paper Society of Petroleum Engineers 106019 presented at the SPE Reservoir Simulation Symposium, Houston, Texas, 26-28 February.

Williams, G.J.J., Mansfield, M., MacDonald, D.G. et al. 2004. Top-Down Reservoir Modelling. Paper SPE 89974 presented at the SPE Annual Technical Conference and Exhibition, Houston, Texas, USA, 26-29 September.

Yeten, B., Durlofsky, L.J., and Aziz, K. 2002. Optimization of Nonconventional Well Type, Location and Trajectory. Paper SPE 77565 presented at the SPE Annual Technical Conference and Exhibition, San Antonio, Texas, USA, 29 September-2 October 2002. DOI: 10.2118/77565-MS.

Yin, J., Park, H., Datta-Gupta, A. et al. 2010. A Hierarchical Streamline-Assisted History Matching Approach with Global and Local Parameter Updates. Paper SPE 132642 presented at the SPE Western Regional Meeting, Anaheim, California, USA, 27-29 May. DOI: 10.2118/132642-MS.

Yoon, S., Malallah, A.H., Datta-Gupta, A. et al. 2001. A Multiscale Approach to Production-Data Integration Using Streamline Models. *SPE Journal* **6** (2): 182-192. DOI: 10.2118/71313-PA

Zitzler, E., Deb, K., and Thiele, L. 2000. Comparison of Multiobjective Evolutionary Algorithm: Empirical Results. *Evolutionary Computation* **8** (2): 173-195.

Zitzler, E. and Thiele, L. 1999. Multiobjective Evolutionary Algorithms: A Comparative Case Study and the Strength Pareto Approach. *IEEE Transactions on Evolutionary Computation* **3** (3).

APPENDIX

USER MANUAL OF MULTI-PURPOSE SOFTWARE FOR STREAMLINE TRACING, HISTORY MATCHING, RESERVOIR MANAGEMENT & DEVELOPEMNT

A.1 Introduction

In this manual, we will introduce the overview, objectives, and key features of DESTINY that has been developed for multi-purposes; streamline tracing, history matching, and reservoir management & development. It is followed by procedure of how to set the interface file and finally examples of streamline tracing, history matching and reservoir management. There are basically two different ways to run DESTINY, which include use of applications i)Standalone launcher and ii) Petrel plug-in. In this manual, the use of standalone launcher has been discussed.

A.2 Overview of DESTINY

Fig. A. 1 shows DESTINY working environment. As shown here, DESTINY interfaces with different simulators and run under window and Linux system. It generates standard files enabling visualization at commercial packages such as Petrel.

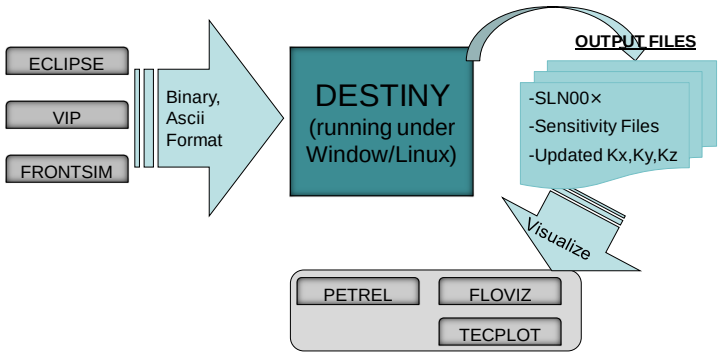

Fig. A. 1 Overview of DESTINY working environment

Note that the description in this manual is based on only ECLIPSE100 developed by Schlumberger for the simplicity of documentation although DESTINY has been interfaced to several commercial and in-house simulators such as VIP, ECLIIPSE300 (black oil mode) etc.

A.3 Objectives

The main objectives of DESTINY are to trace streamline even in complex corner point and faulted (non-neighbor connection) geometry as well as the sensitivity coefficient computation of generalized travel time inversion (He et al., 2002; Cheng et al., 2005; Oyerinde et al., 2007). In addition, DESTINY provides reservoir management tool such as drainage and swept volume calculation. Besides, it has ability to do rate optimization either for injection rate or for production rate based on simple analytic approach (Park and Datta-Gupta 2011). Following summarizes main features in DESTINY:

- Streamline Tracing and Visualization in corner point geometry and faulted cells from finite difference velocity field
- Streamline-based assisted History Matching for calibration of high resolution geologic models to production data
- Reservoir Management/Optimization for analyzing and optimizing drainage/swept volumes, well connectivity using flood efficiency maps
- Reservoir Development for optimal infill well placement

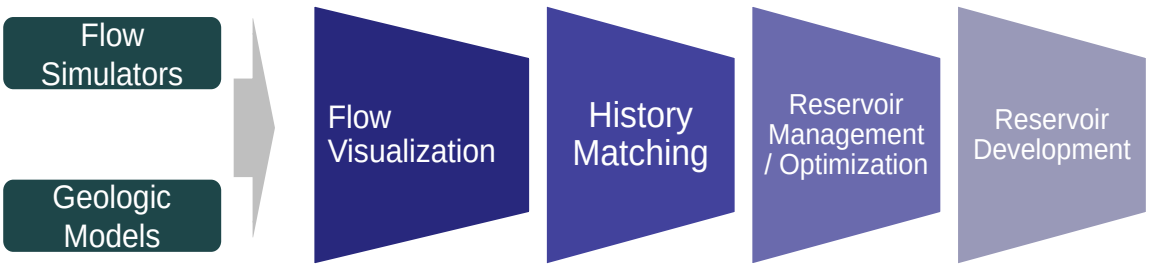

Fig. A. 2 DESTINY main features

A.4 Streamline applications using DESTINY

Streamlines provide several benefits for reservoir characterization and management. The streamline trajectories and time of flight are useful for visualizing reservoir flow dynamics. Using streamlines, we can easily identify the drainage volumes and swept volumes associated with producers and injectors, respectively. This provides us with a natural way to identify potential infill producer and injector locations during waterflooding. Streamlines can also be used to identify and visualize the connectivity and communication among wells or between wells and the aquifer. This allows us to identify the source of and also allocate fluid volumes associated with individual producers and injectors. This information can be utilized for pattern balancing and flood optimization.

A powerful application of streamlines is in waterflood management and optimization. The streamline time of flight provides us with a dynamic picture of the flood front evolution. By adjusting the injection and production rates at the wells, we can manage the movement of the flood front to maximize waterflood sweep efficiency. This gives us an efficient approach to optimal waterflood management through rate control.

A commonly held misconception about the application of streamlines is that the technology is limited to incompressible flow and requires injectors and producers. In reality, the streamlines are simply a representation of the velocity field and streamlines exist whenever there is an underlying velocity field. This allows us to take advantage of the streamline technology in conjunction with finite difference simulation. For example, we can apply streamlines to compute and visualize the drainage volumes in tight gas reservoirs using the flux field generated from the finite difference simulation. The drainage volumes of existing wells can then be used to optimize infill locations based on undrained parts of the reservoir.

Streamlines are particularly useful for history matching. Streamlines can be used to identify and target changes during history matching. In particular, streamlines can be used to efficiently compute the sensitivity of the production response to reservoir

parameters such as porosity and permeability. These sensitivities can then be used to facilitate manual history matching or can be used in conjunction with inversion algorithms to suggest updates to the geologic models. Reconciling high-resolution geologic models to production history is a very time-consuming aspect in reservoir modeling. Current practice still involves a tedious and manual history-matching process that is highly subjective and often employs ad-hoc property multipliers that can lead to loss of geologic realism. Streamline can aid during history matching in terms of (i) efficiency in workflow, (ii) obtaining geologic insight (iii) understanding reservoir dynamics and, (iv) preserving geologic realism.

A.4.1 Workflow of DESTINY (History matching workflow)

Fig. A. 3 shows the general process of DESTINY. First, it runs the forward simulator and reads the output of the simulator. The forward simulator can be either a finite difference or a streamline simulator. The current options for simulators include ECLIPSE, VIP and FRONTSIM. For finite difference simulators, DESTINY utilizes the flux field to compute streamlines and time of flight. This information can then be used to visualize swept volumes and drainage volumes of existing wells during waterflooding and also for gas reservoirs to locate potential locations for infill producers or injectors. The flux associated with streamlines can also be used to optimize injection and production rates of the wells to maximize flood performance. DESTINY is particularly useful for streamline-assisted history matching. Using DESTINY, we can visualize the sensitivities of production data with respect to reservoir properties. These sensitivities depict the region of the geologic model impacting the production data. Guided by these sensitivities, we can either manually update the geologic model to match the production data or use inverse modeling techniques for suggested updates to the model.

Fig. A. 3 Overview of workflow for inversion

Fig. A. 4 shows the overall work flow of streamline tracing and production history matching.

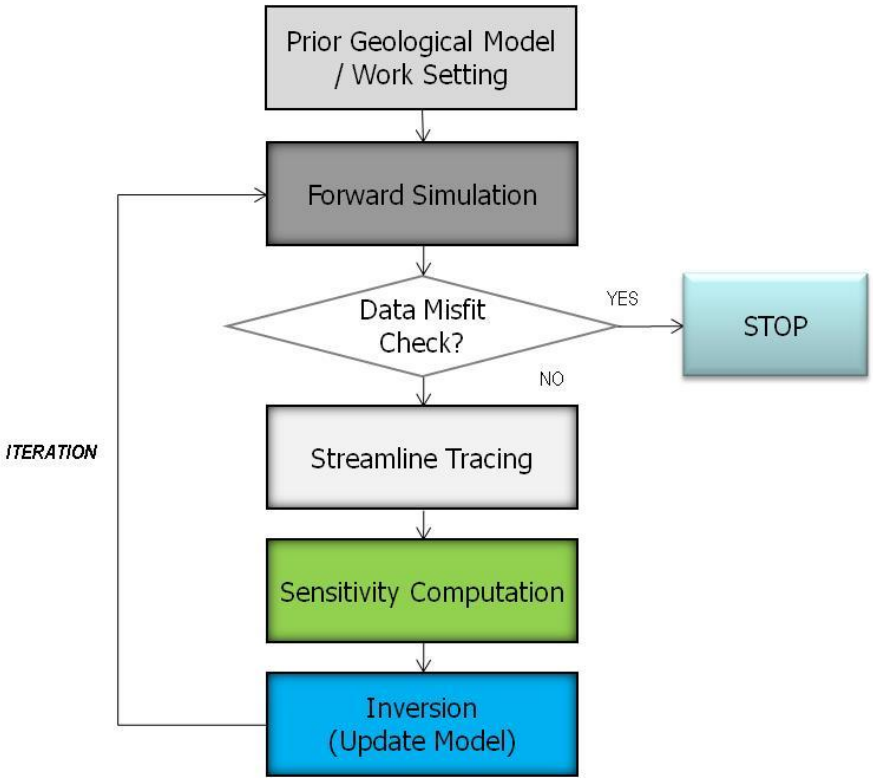

Fig. A. 4 Inversion workflow in DESTINY

The use of commercial simulators in DESTINY provides a great deal of flexibility in terms of grid geometry, well conditions and process simulations. However, because of the multiple options offered by commercial simulators and the resulting variations in setting up the simulation deck, instead of scanning the input deck made by the users,

DESTINY scans output files from simulator to obtain the necessary data to trace streamlines and compute time of flight. It enables users to fully utilize flexibility for describing the flow simulation model and leads to robust streamline tracing without failure because of the fixed simulation output file format.

A.5 Modules in DESTINY

DESTINY contains three (3) different modules (tracing, inversion, reservoir management) as shown in Fig. A. 5.

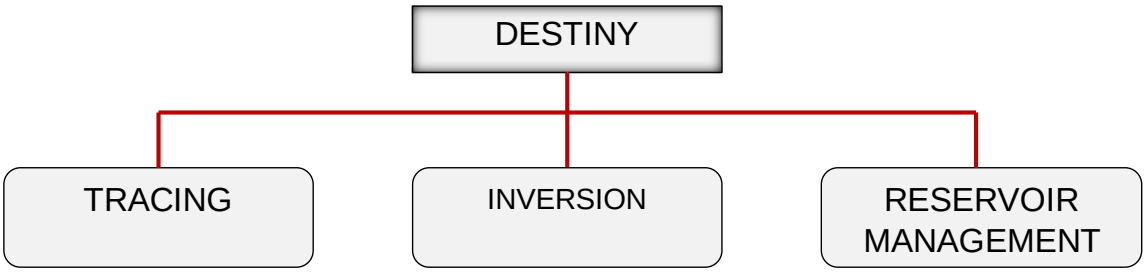

Fig. A. 5 Modules available in DESTINY

Tracing module is core module in the sense that the others are assisted by tracing module. For example, inversion module and reservoir management module calls tracing module to get assistance in terms of streamlines. These separated modules are intended to keep powerful of capacity in DESTINY and also be flexible to update each module for developers. However, users do not recognize if it is based on separated modules.

A.5.1 Tracing module

Tracing module contains very specialized tracing abilities in addition to typical streamlines tracing as shown below in Fig. A. 6.

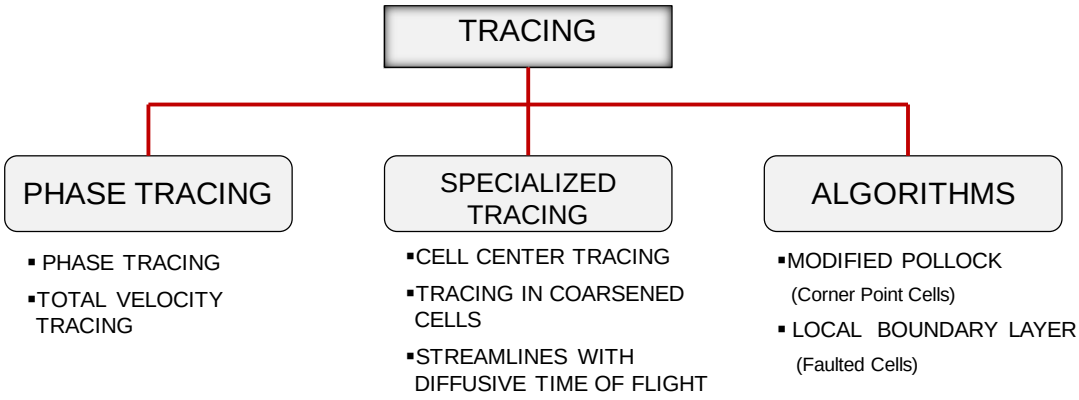

Fig. A. 6 Key features in DESTINY tracing module

First, following gives phase tracing example. It compares phase tracing with total velocity tracing. Water and oil phase tracing can capture mobile water and oil movement.

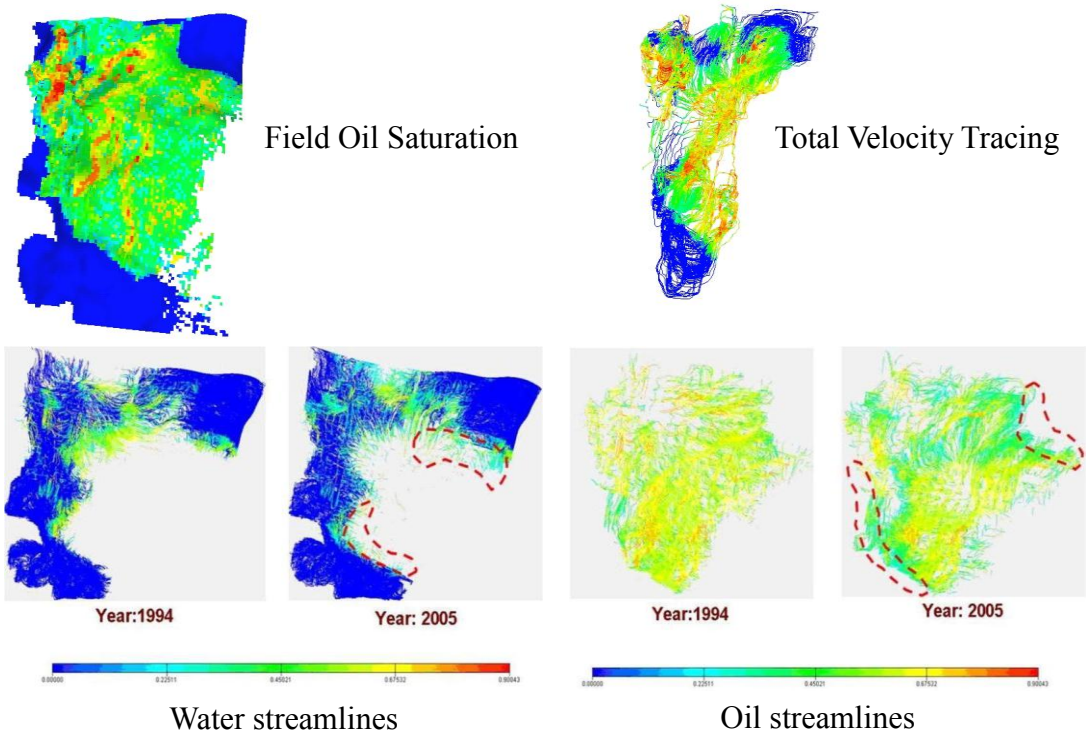

Fig. A. 7 Examples of phase streamlines

Second, following shows example of cell centers tracing. We trace from every cell center to either toward producers or toward injectors. It gives very high resolution of reservoir flow analysis.

- Cell center tracing depicts high resolution flow visualization
- Streamline time of flight ‘to producer’ and ‘to injector’ focuses on drainage or sweep patterns

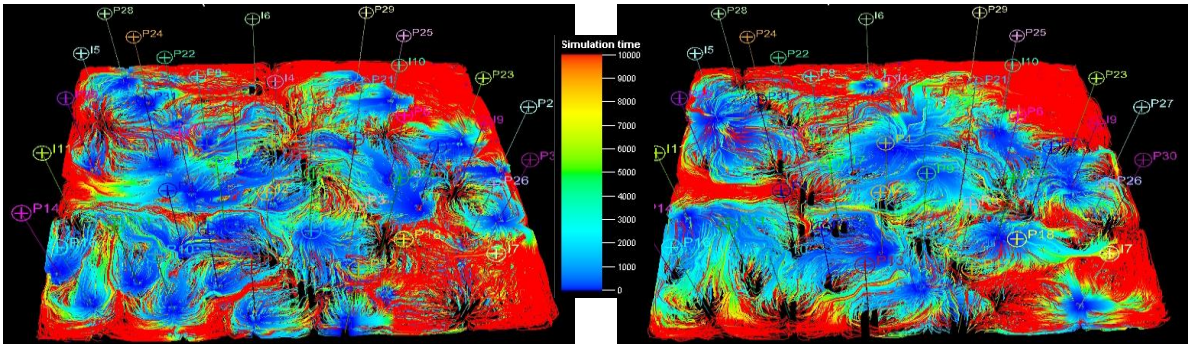

Cell centers to producers Cell centers to injectors

Fig. A. 8 Examples of streamlines traced from cell centers

Third, DESTINY can trace streamlines in coarsened geometry. Following shows the examples of coarsened streamlines in different scales of coarsening. Top three figures show permeability fields at different scale of coarsening. Bottom ones show streamlines traced on the coarsened geometry.

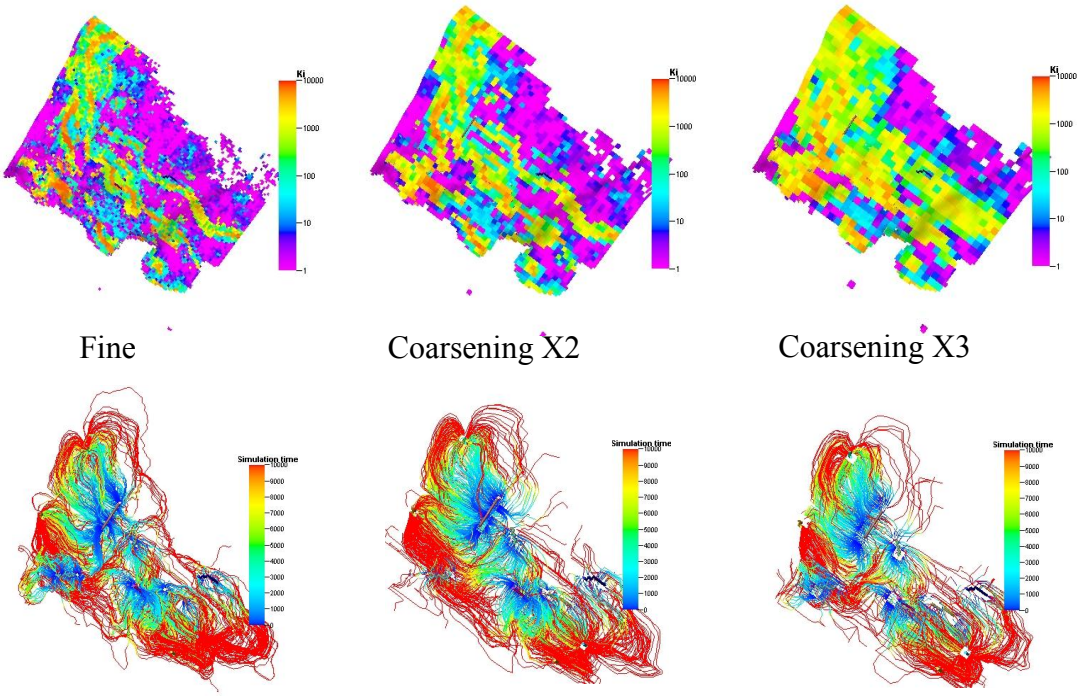

Fig. A. 9 Examples of streamlines traced in different scales of coarsened grids

- **Tracing module run setting**. To run the tracing module of DESTINY we provide a standalone GUI and executable as it is shown in Fig. A. 10. The launcher is used to set the desired work and make it run. The details about setting are explained below.

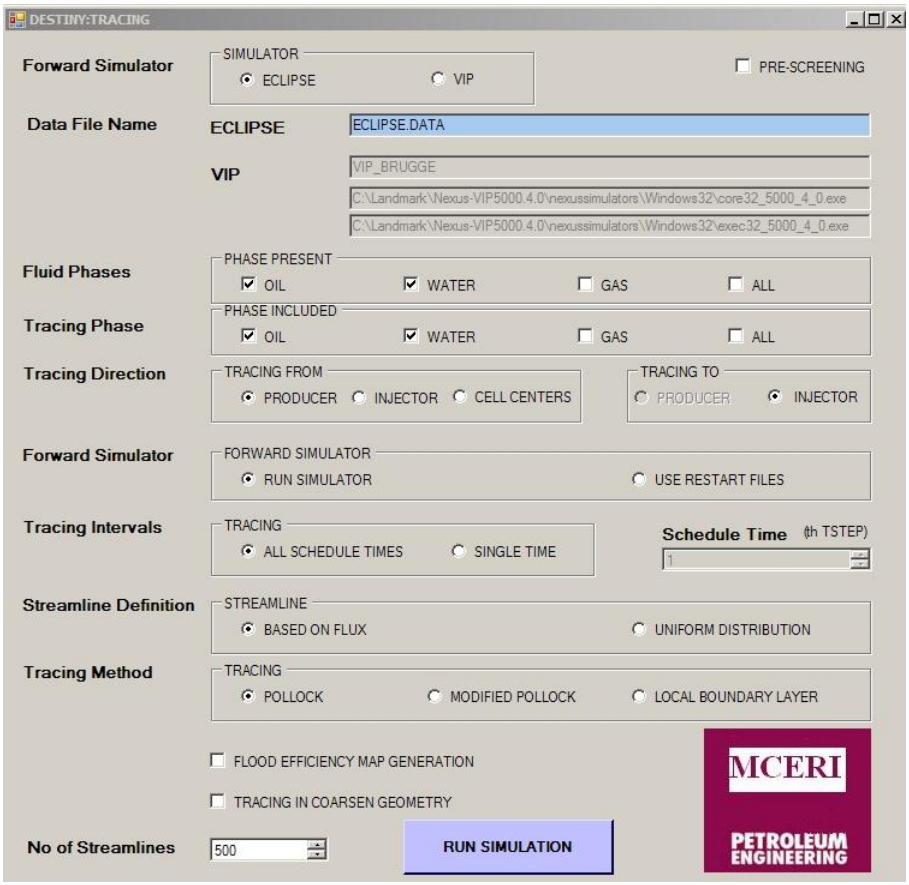

Fig. A. 10 DESTINY tracing launcher (GUI)

Followings are instructions about this launcher.

- Forward Simulator: choose ‘Eclipse’ or ‘VIP as simulator
- Data File Name: Enter data file name which calls simulator to run
- Fluid Phases: Select reservoir phases.
- Tracing Phases: Select phases to be included tracing.
- Tracing Direction: Default is tracing from producers to injectors. We can choose opposite direction to trace. In addition, we can trace from cell centers toward both directions.

- Forward Simulator: Choose ‘Run Simulator’ if simulation output file is not there. If there are already output files, choose ‘Use Restart Files’ to save time.
- Tracing Intervals: If we want tracing only for one single time step, we can choose ‘Single Time’ and gives Scheduled time in the box beside.
- Streamline Definition: Define if the number of streamlines per completion is defined based on flux *(‘Based on Flux’)* or should be uniformly *(‘Uniform Distribution’)* distributed. Default is defined based on fluxes, even if the keyword is not included in DIP file.
- Tracing Method: Choose one of ‘Pollock’, ‘Modified Pollock’ and ‘Local Boundary Layer’. About these keywords are found in previous section.
- Flood Efficiency Map: if we want to generate flood efficiency maps, we can check this box.
- Tracing in Coarsen Geometry: if the model is based on coarsen grid, we can check this box so that we can trace streamline in coarsen grid.
- No. of streamlines: we can specify number about how many streamlines in the field we want.

- **Tracing application (1): Tracing from producers to injectors**. Following setting in the launcher is to trace streamlines from producers to injectors. We applied it to Brugge field.

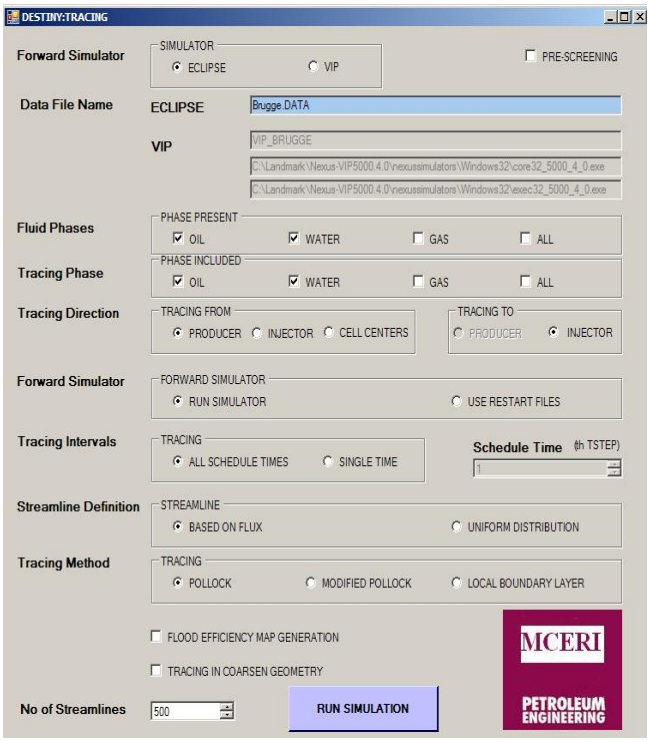

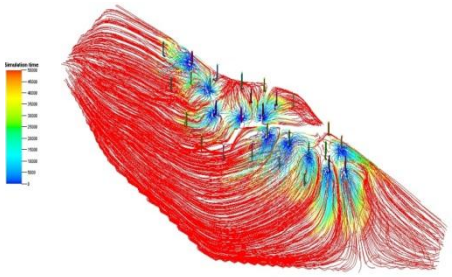

Time of flight from producers

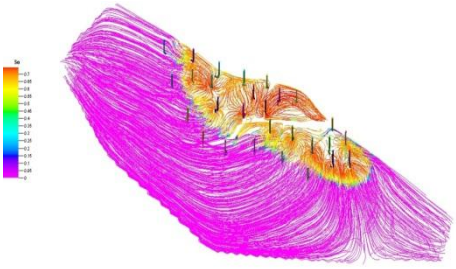

Oil saturation along streamlines

Fig. A. 11 Default tracing setting (trace from producers to injectors) and results

- **Tracing application (2): Tracing from injectors to producers**. Following launcher gives example on how to set launcher to trace streamlines from injectors to producers for the Brugge field.

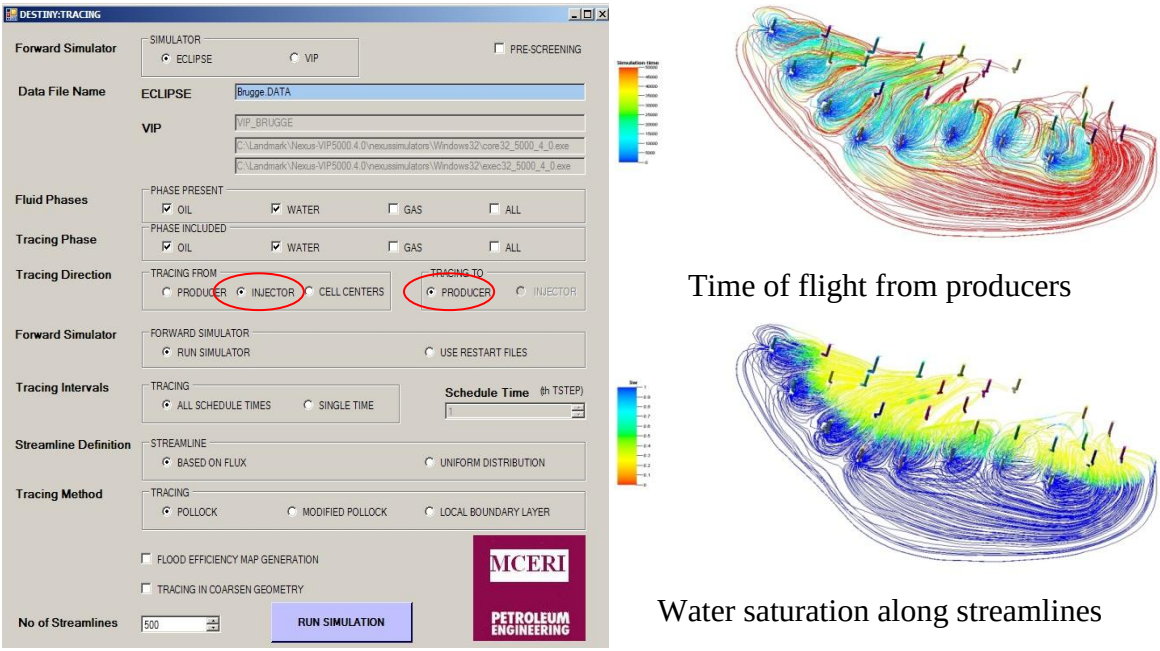

Fig. A. 12 Tracing setting (trace from injectors to producers) and results

- **Tracing application (3): Tracing from cell centers to producers**

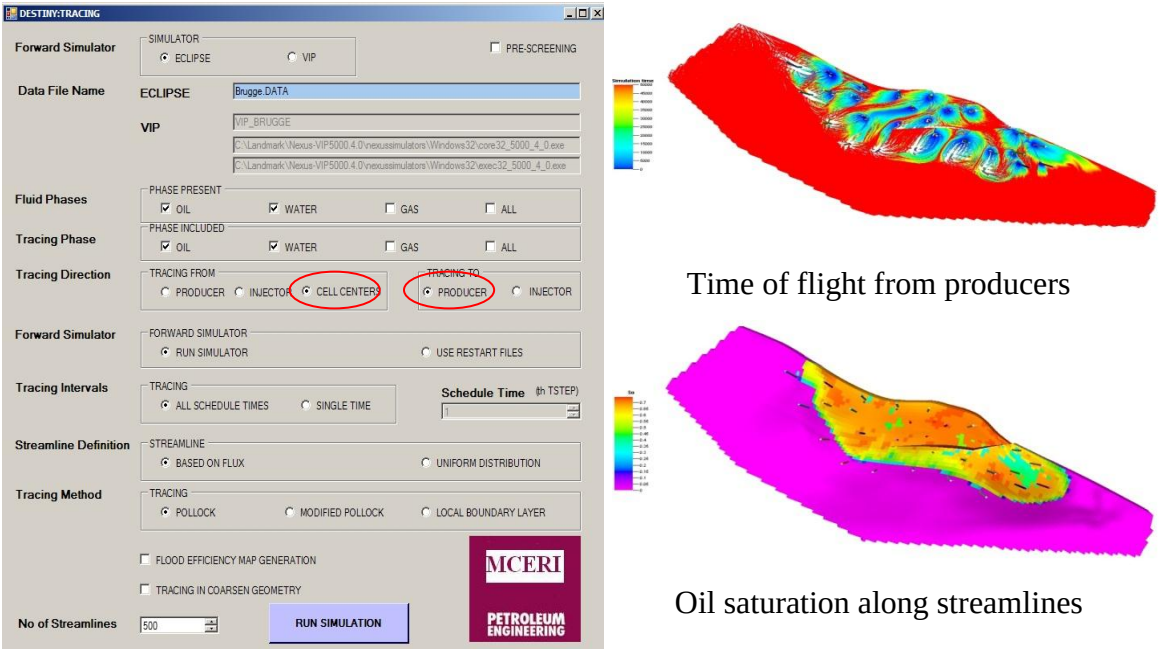

Fig. A. 13 Tracing setting (tracing from cell centers to producers) and results

- **Tracing application (4): Flood efficiency maps generation**

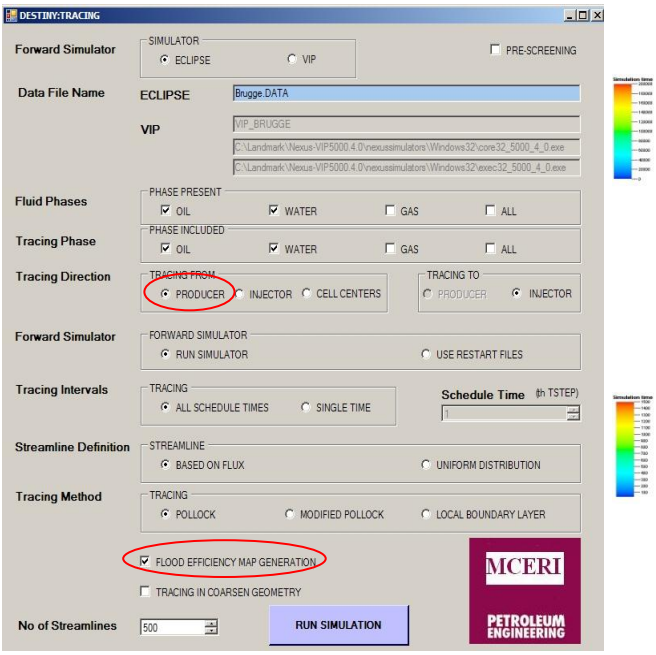

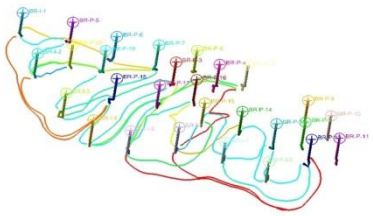

TOF distribution map

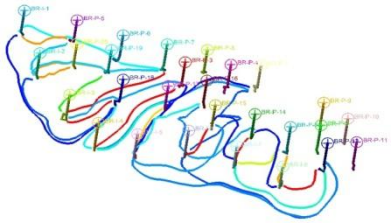

Flux distribution map

Fig. A. 14 Flood efficiency maps and results

- **Tracing application (5): Tracing in coarsened grids**

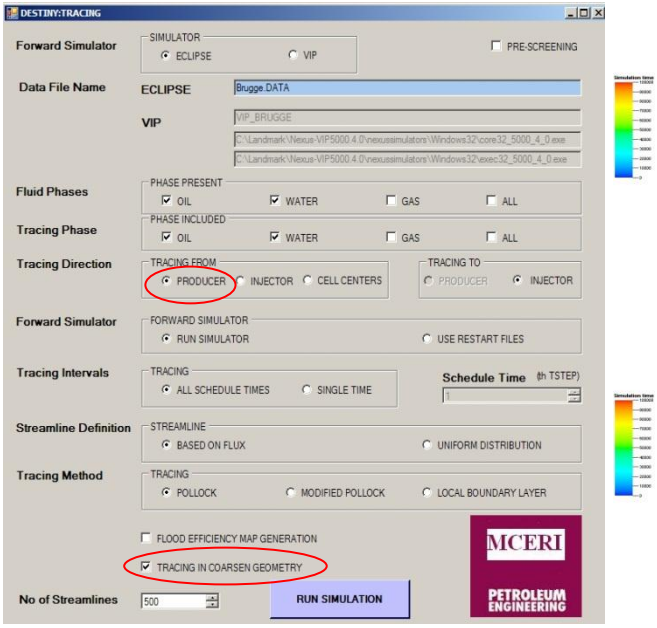

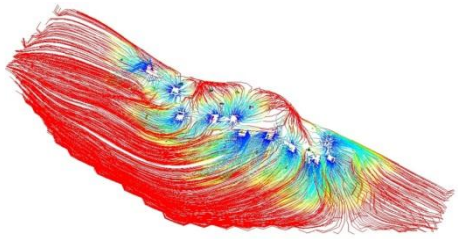

Tracing in coarsened grid (X2)

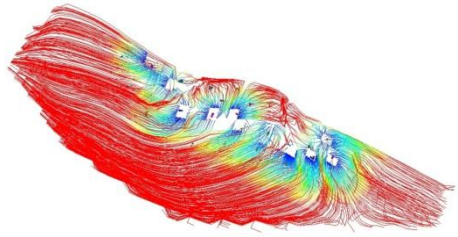

Tracing in coarsened grid (X3)

Fig. A. 15 Coarsened tracing and results

A.5.2 Inversion module

Inversion module contains many capabilities as shown in Fig. A. 16, which include water cut inversion, GOR inversion, and bottom hole pressure inversion. This inversion module is designed to incorporate with tracing module. Streamlines are generated by tracing module. This inversion module makes use of those streamlines to obtain sensitivities of production data to reservoir parameters.

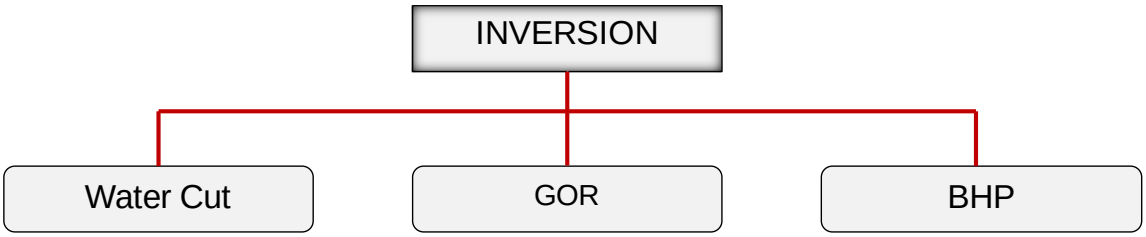

Fig. A. 16 Inversion features in DESTINY

- Water cut inversion: It follows the generalized travel-time inversion method (He et al. 2002), which reconciles geological model to production data using streamline technique. This approach is very robust, computationally efficient, and particularly well-suited for large-scale field applications. The sensitivities of the generalized travel time with respect to reservoir properties are computed analytically using a single forward simulation run.
- GOR inversion: An approach to history matching three-phase flow using a compressible streamline formulation and streamline-derived analytic sensitivities is used in this module, which was proposed by (Cheng et al. 2007).
- BHP inversion: Bottom hole pressure sensitivity is used based on the proposed formulation (Vasco et al 1999). Zero frequency of the pressure is integrated. Model parameter sensitivities (relating changes in pressure to changes in permeability) computed with the equivalent of steady state pressure calculations.

- **Inversion module run setting.** We can use a standalone GUI, called 'Inversion launcher', to run DESTINY inversion module. Following shows the interface of the launcher, which is followed by the description of keywords and examples to illustrate how to set up the launcher.

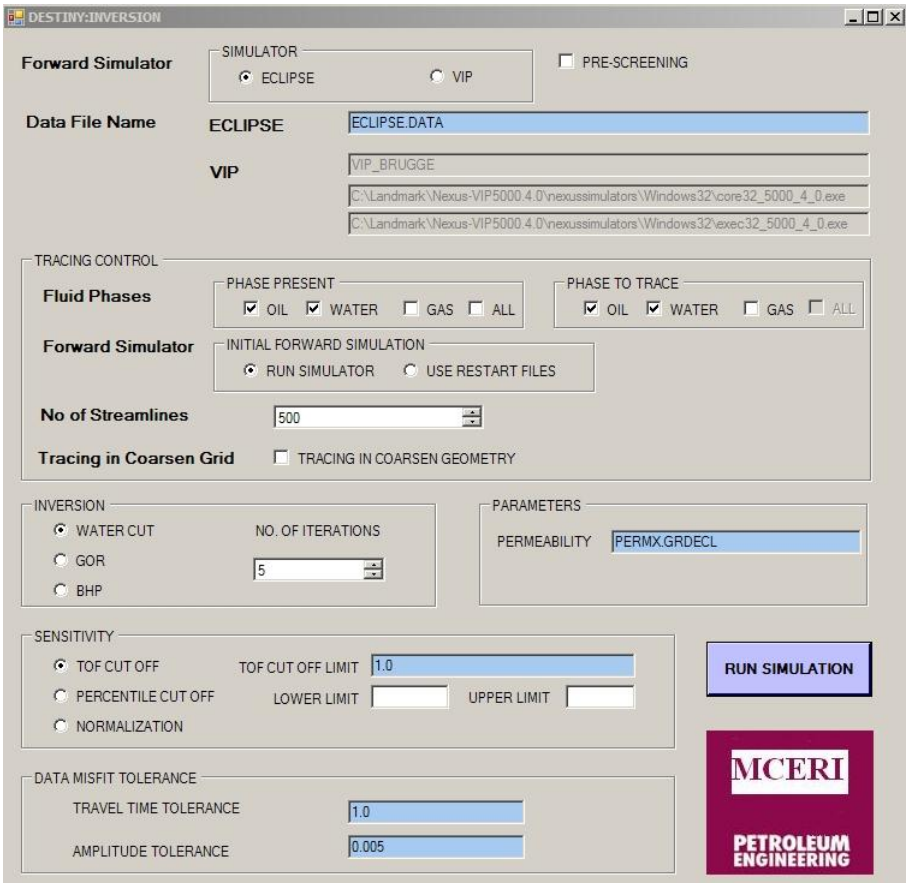

Fig. A. 17 DESTINY inversion launcher

The most of keywords in this launcher are same as those in tracing launcher, which can be found in previous section. Here are explanations about keywords used only for inversion.

- Inversion: Choose one of 'Water Cut', 'GOR', 'BHP' for history matching

- No. of Iterations: History matching is highly non-linear problem. It typically requires multiple iterations to get satisfactory solutions. Here we need to enter how many iterations we want to run.
- Parameters: The inversion algorithm calibrates reservoir cell property (permeability). Calibrated permeability replaces initial one. In the text box, we need to put permeability data file name in order for DESTINY to update it with new permeability.
- Sensitivity: TOFCUTOFF is default. A time of flight (TOF)-based cutoff will be applied to WWCT sensitivities on a well-basis. Used to eliminate the sensitivities in stagnation region which may cause distort inversion performance. TOF cutoff limit is defined as the threshold of the time of flight for the water cut sensitivity cut-off. This Maximum Time of Flight cut off value is automatically calculated by multiplication of actual production time period with user input multiplier value.
- Data Misfit Tolerance: Enter tolerance for travel time misfit and amplitude misfit.

Once this setting is done, we can hit 'Run Simulation' to run it. After it is finished, we can find outputs (tracing and inversion output) from the working folder.

- *SLNXXX Files*: When the binary output is selected, DESTINY will generate **.sln* files for every simulation time step. ECLIPSE users can use the restart files and the **.sln* files to load the entire simulation workspace to PETREL.
- *Updated permeability files*: After running the first inversion iteration this file will be modified and to the end of the each iteration. The updated permeability will be written out as initial permeability file name (the updated files will have a suffix with the iteration number in which the permeability was updated).
- *resinv.obj*: This file has the objective function behavior through all iterations. It has two columns representing the travel time and amplitude misfit defined at all producing wells included in the data integration

- *resInv.wwctX*: It contains the simulated and observed production water cut for all wells included in the project. At the header of each well the travel time misfit will be written out. This file is generated at the end of the each iteration.
- *dynamic.bin*: Binary files contain the production sensitivities. This file is used by LSQR to perform the objective function minimization.
- *dynamic.ascii*: An ASCII file contains the production sensitivities. This file is provided for history matching applications where streamline-based sensitivities are used as complementary information.

- **Inversion application (1): Water cut inversion applied to synthetic model**. Following shows how we set up for the water cut history matching.

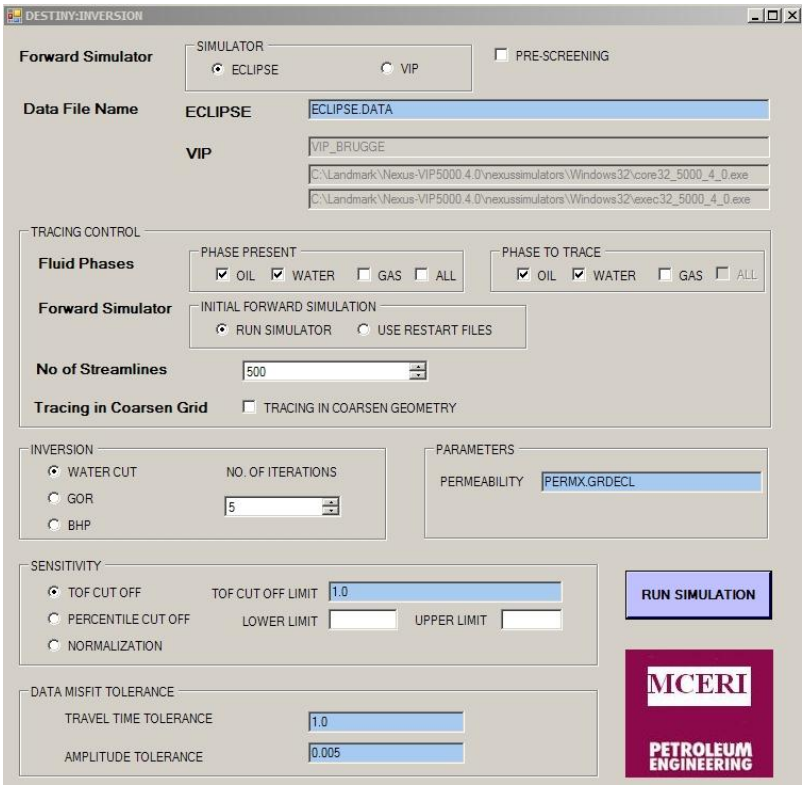

Fig. A. 18 Water cut inversion setting

We can find both travel time and water cut misfit at the output file (resinv.obj).

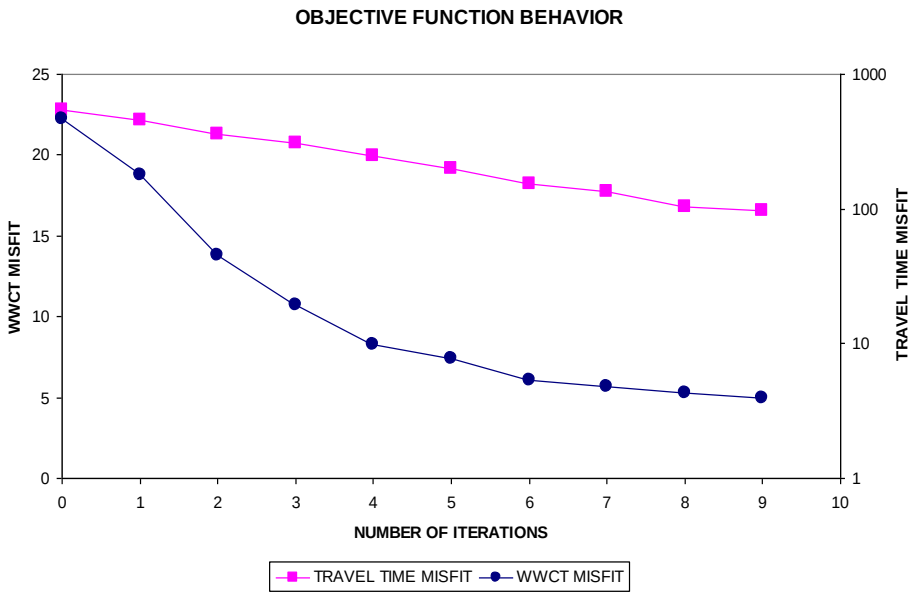

Fig. A. 19 Objective function by iteration

To check the updated responses of individual well, we can open ‘resinv.wwct’ file where we can find production responses (initial, updated, history) for all wells. We can plot it for analyzing the results as shown below.

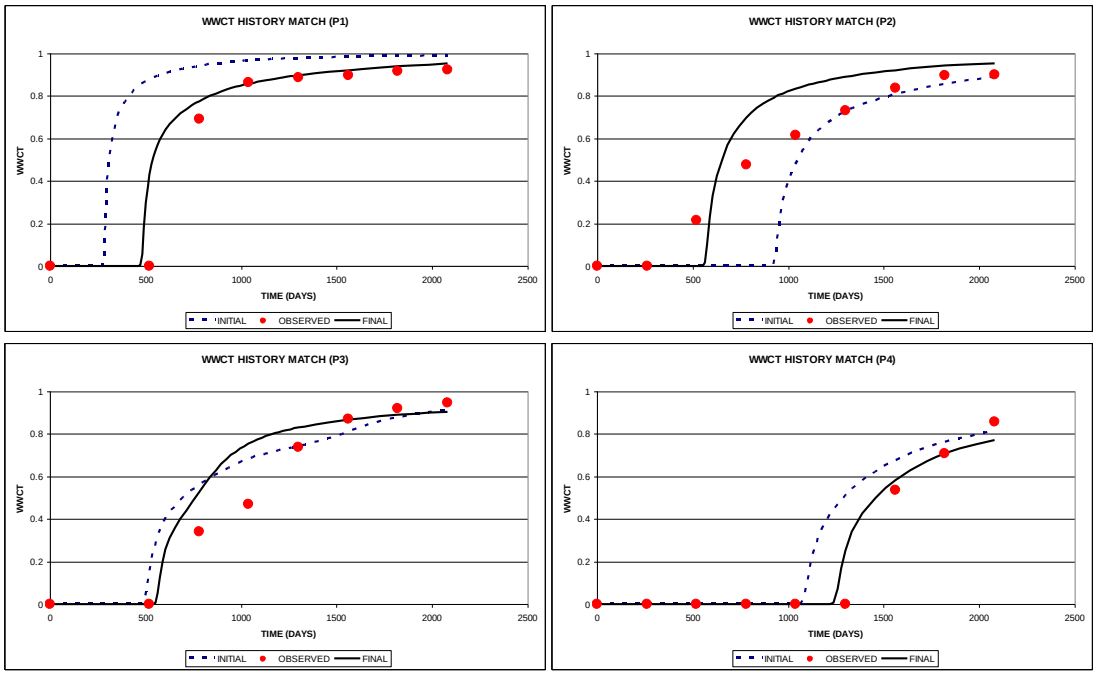

Fig. A. 20 Water cut history match before and after inversion

Updated permeability field is compared with initial model. The changed cells shows that model calibrations have been made along flow paths, keeping heterogeneity.

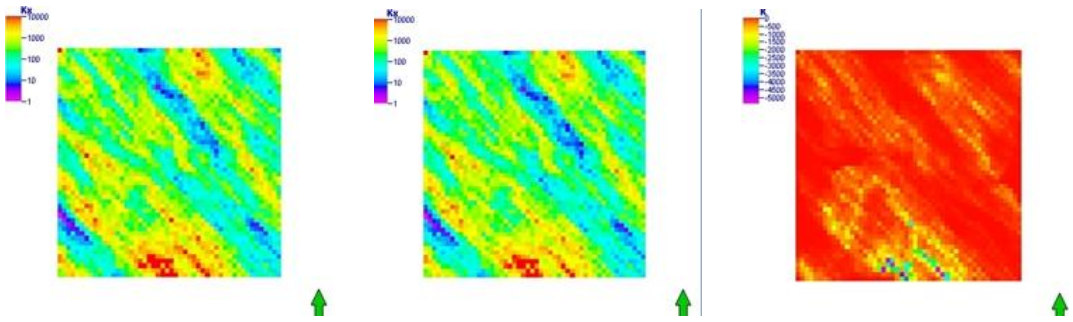

Fig. A. 21 Initial / Updated / Change of permeability field after inversion

- **Water cut inversion applied to field models**. For water cut history matching, we have applied to many field cases and showed good history matching results. Here we show one of them. Following shows the history matching results for one offshore field. History matched model is compared by manually matched model. No artificial change such as box multipliers is used. The updated model is matched to production history without loss of geologic realism.

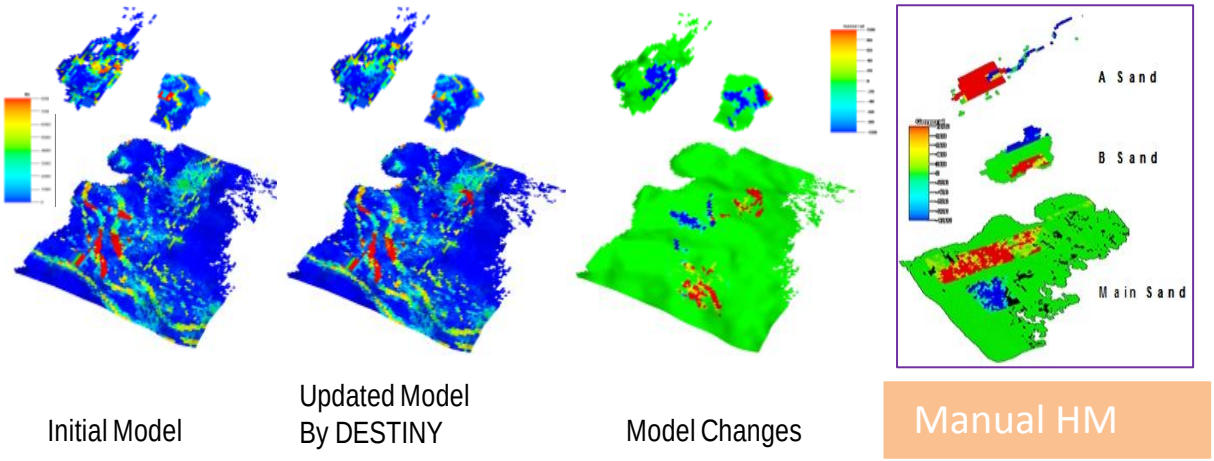

Fig. A. 22 History matched model compared with initial model and manually updated model

- **Multiscale water cut inversion: Application to large-scale offshore field model**. History matching large-scale reservoir model using current assisted history matching techniques is challenging because of extensive computation time. The use of multiscale approach is effective in history matching a large reservoir model because of desirable multiscale features: computational efficiency, effective iterative minimization, and avoiding local minima. The developed multiscale streamline-assisted history matching workflow is shown in Fig. A. 23. To use multiscale inversion feature in DESTINY we set the launcher as shown in Fig. A. 24. Make

sure that the tracing in coarsen geometry is checked and the simulation data is consistent for coarsen simulation.

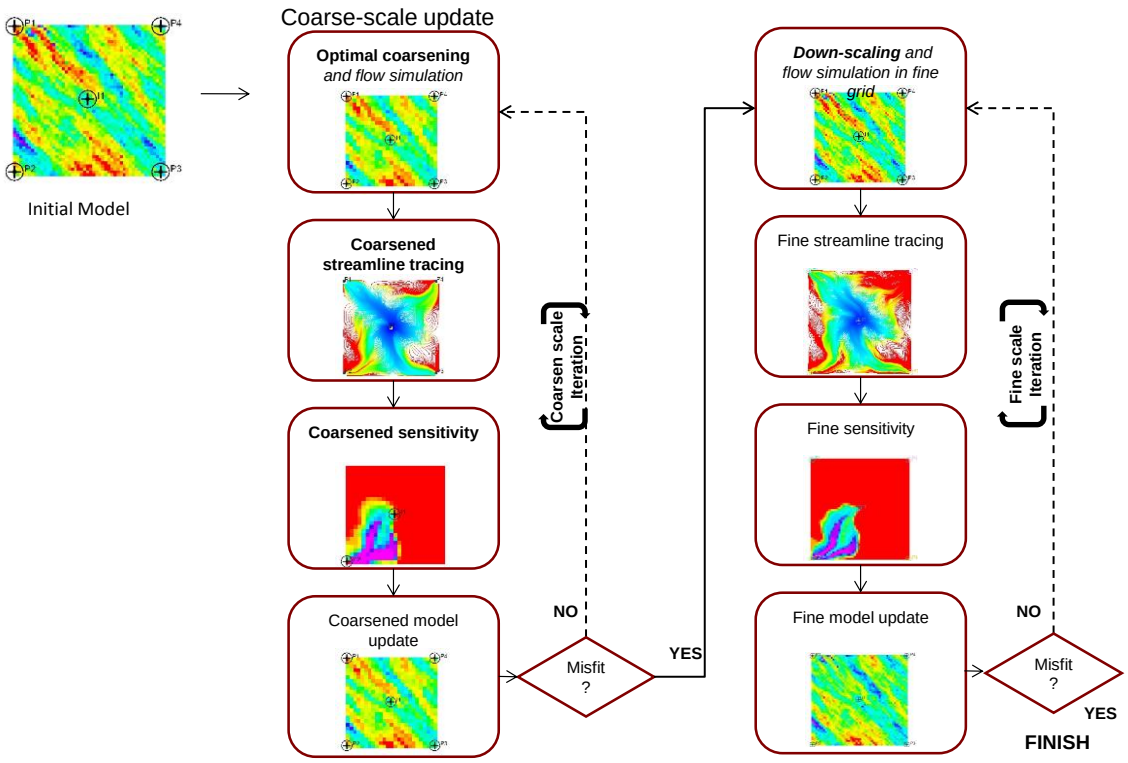

Fig. A. 23 Multiscale streamline-assisted inversion workflow

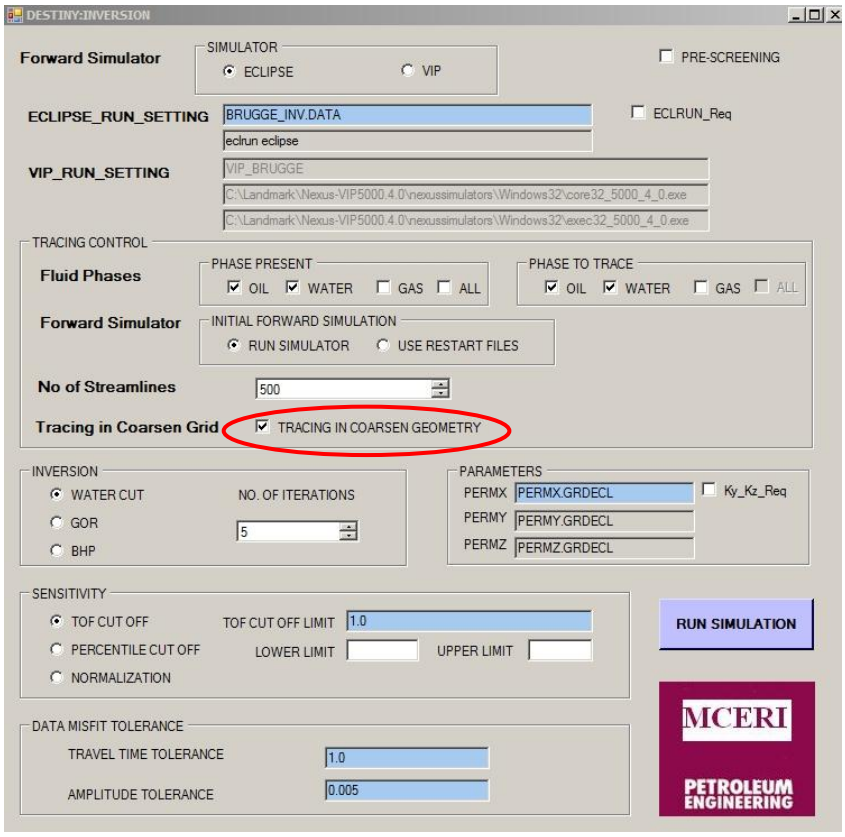

Fig. A. 24 Example setting for multiscale inversion

A.5.3 Reservoir management module

Reservoir management module in DESTINY includes following features

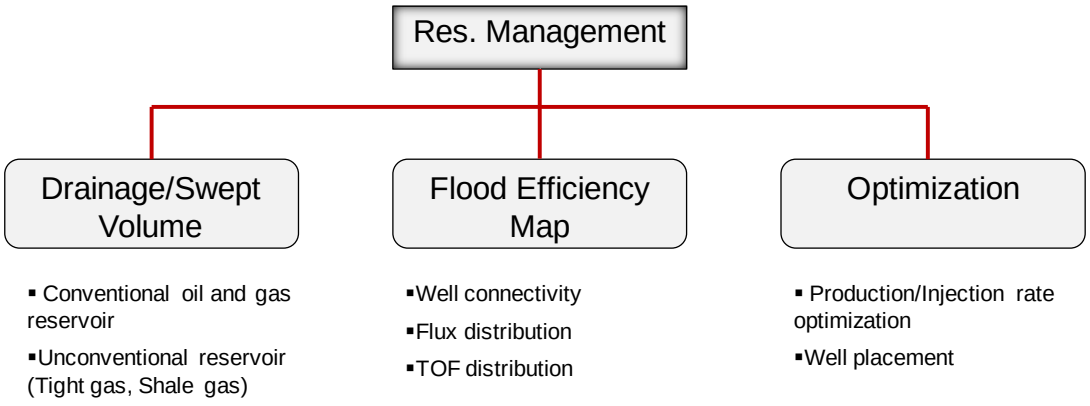

Fig. A. 25 Features in reservoir management module in DESTINY

- Drainage and swept volume: Cell center tracing is performed for drainage and swept volume calculations. Time of flight to either producers or injectors are converted to physical time using fractional flow and saturation velocity. The converted time is then mapped to grid cells. The mapped property is used to define swept and drainage area and to compute the volume.
- Flood efficiency map: We display the key information related to flow patterns and reservoir sweep with the flood efficiency map. It includes a flux distribution map and an average TOF distribution map that enable us to optimize waterflood management. The streamlines connecting each injector-producer pair is depicted with a single representative streamline along the fastest streamline. The TOF distribution map displays the 'average TOF' between the well pairs. The average TOF is calculated by a simple arithmetic average of time of flight associated with all the streamlines for each connection. The flux distribution map display volumetric flux between connecting wells computed by summing the fluxes carried by the streamlines. The flux distribution map is colored by the total flux connecting the wells while the color in TOF distribution map displays the average TOF. Thus, the flood efficiency map is a compact representation of the reservoir flow pattern and the flood front advancement.
- Production rate optimization: The main idea for production rate optimization is that we maximize sweep efficiency in reservoir by equalizing average time of flight between wells and reducing time of flight variance. We alter production target rate such that average time of flight be equalized and variance of time of flight be minimized. The detail refers to a paper (Park and Datta-Gupta 2011).
- Injection rate optimization: We introduce 'coefficient of TOF variance' to use it as injection efficiency. Based on the calculated injection efficiency for injectors, we reallocate injection rates that give reduced time of flight variance in the field and at the same time it gives maximized sweep. Details are found in the paper (Park and Datta-Gupta 2011).

- Well placement optimization: The approach (Taware et al. 2012) utilizes a dynamic measure based on the total streamline time of flight combined with static parameters to identify potential regions for infill drilling. Areas having high value of the dynamic measure (sweet spots) are both poorly drained and poorly swept, making them attractive for drilling infill wells.

- **Reservoir management module run setting**. We can use a standalone GUI, called 'Reservoir management launcher', to run DESTINY reservoir management module. Following shows the interface of the launcher, which is followed by the description of keywords and examples to illustrate how to set up the launcher.

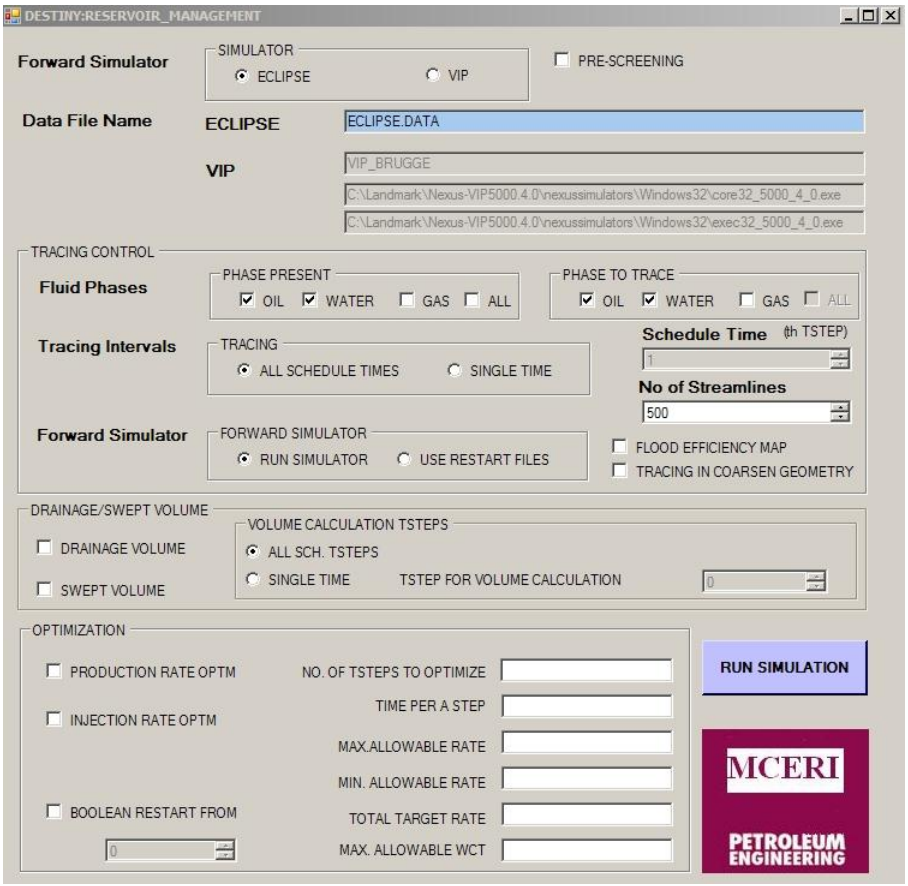

Fig. A. 26 DESTINY reservoir management launcher

The most of keywords in this launcher are same as those in tracing launcher, which can be found in previous section. Here are explanations about keywords used only for reservoir management.

- Drainage/Swept volume: Choose and check a box of either ‘Drainage volume’ or ‘Swept volume’
- Volume calculation tsteps: Check either ‘All sch. Tsteps’ or ‘Single time’. If ‘Single time’ is chosen, choose a timestep for volume calculation at ‘Tstep for volume calculation’.
- No. of Iterations: History matching is highly non-linear problem. It typically requires multiple iterations to get satisfactory solutions. Here we need to enter how many iterations we want to run.

- **Application (1): Drainage volume calculation**. Following shows setting in launcher for drainage volume and drainage area map.

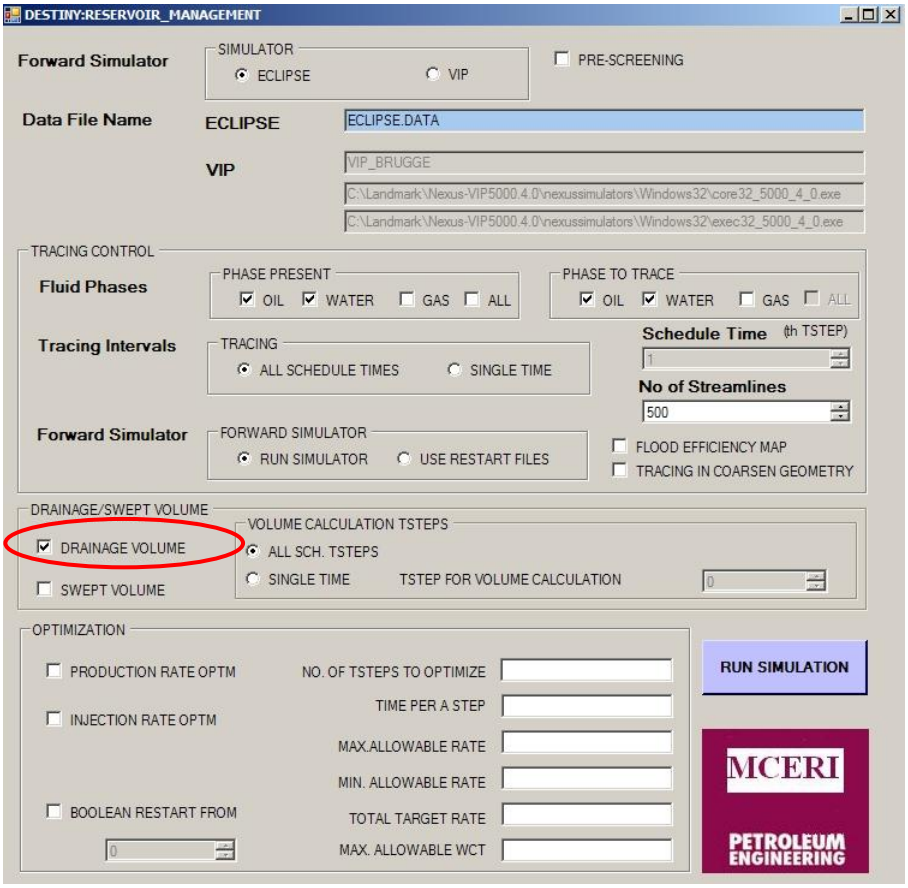

Fig. A. 27 DESTINY reservoir management launcher

The output files include ‘AREA_DRAIN(TOF2PROD)_time.GRDECL’ and ‘DRAIN(TOF2PROD)_VOL_time.dat’ and ‘Well_Prod_Indx_time.GRDECL’. If we open ‘AREA_DRAIN’ map and it will give drainage area at time. From ‘DRAIN_VOL’ file we can get exact amount of volume drained at the time. Lastly, from the ‘Well_Prod_Indx’ file we can visualize regional classification based on the area affecting to producers. Following shows the different drainage area at two different times.

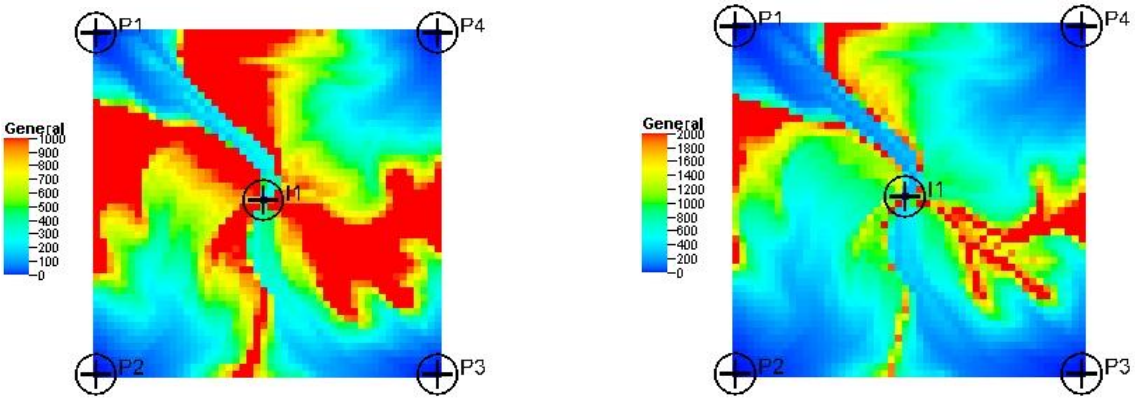

[Drainage area @1000days] [Drainage area @2000days]

Fig. A. 28 Drainage area at different time

We can find exact amount of volume drained from DRAIN_VOL.dat file.

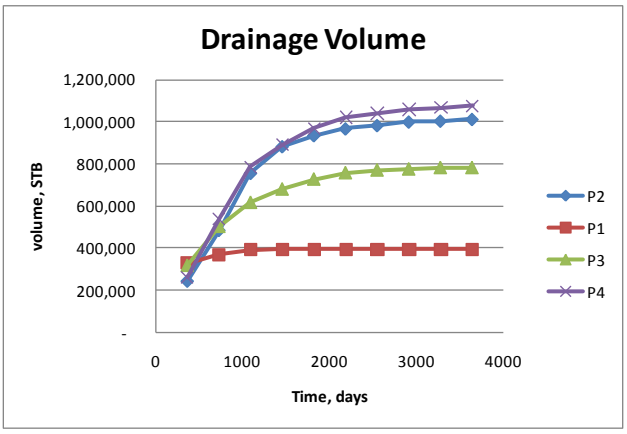

Fig. A. 29 Calculated drainage volume

Also, we can find region affecting producers from AREA_DRAIN.GRDECL file.

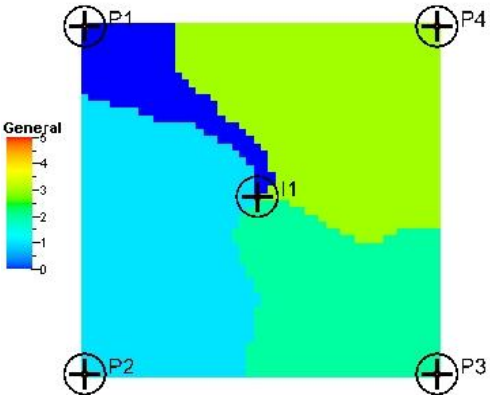

Fig. A. 30 Regional classification map

- **Application (2): Swept volume calculation**. Following setting shows for swept volume calculation.

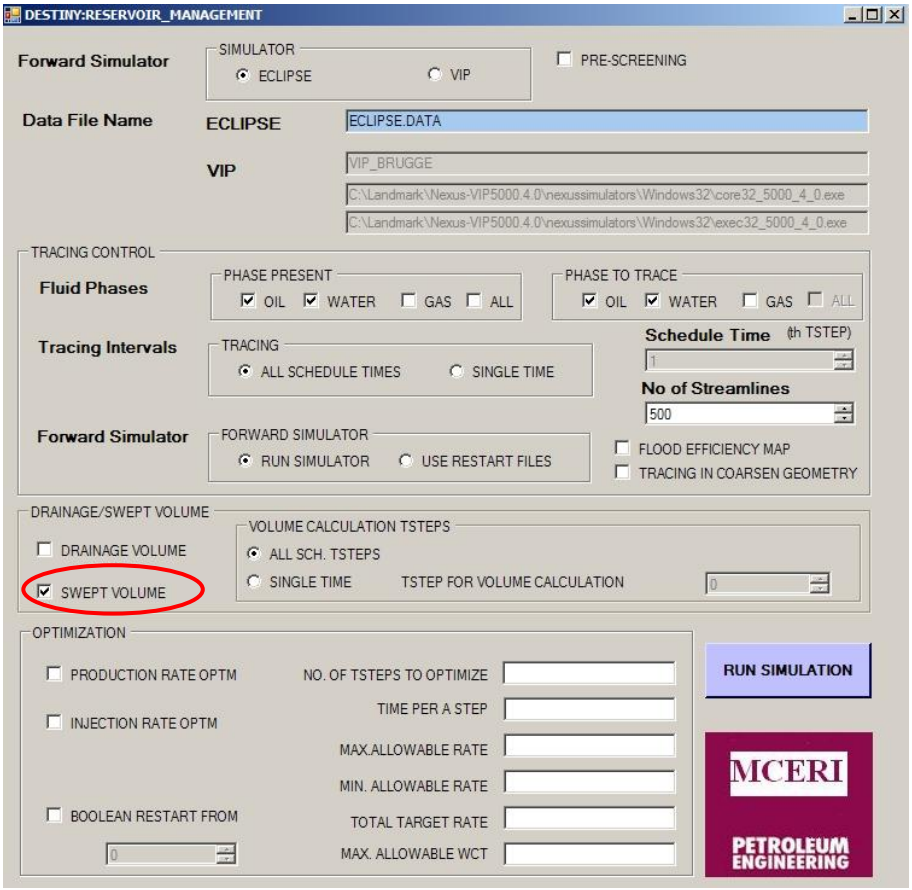

Fig. A. 31 Example setting for Swept volume calculation

The output files include ‘AREA_SWEPT(TOF2INJ)_time.GRDECL’ and ‘SWEPT(TOF2INJ)_VOL_time.dat’ and ‘Well_Inj_Indx_time.GRDECL’. If we open AREA_SWEPT map and it will give swept area at time. We import it to Petrel to visualize as shown in Fig. A. 32. From SWEPT_VOL file we can find estimated amount of volume swept at the time. Lastly, from the ‘Well_Inj_Indx’ file we can visualize region affecting injectors.

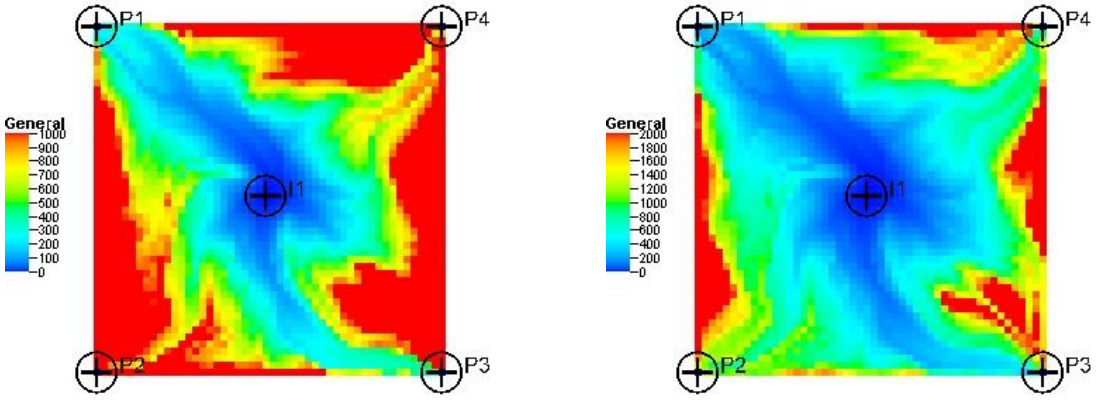

[Swept area @1000days] [Swept area @2000days]

Fig. A. 32 Swept area at different times

We can check the swept volume by simulation time. The figure below shows swept volume with time.

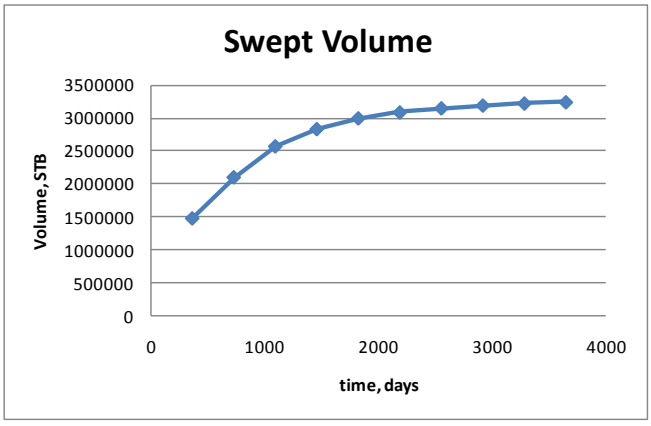

Fig. A. 33 Swept volume for a injector

- **Application (3): Production rate optimization**. Following setting in launcher gives how to set the production rate optimization for synthetic model. We check 'Production rate optimization' and enter the specific values to the required boxes in the right. Then click the 'Run Simulation' and we will see DESTINY reservoir management module running.

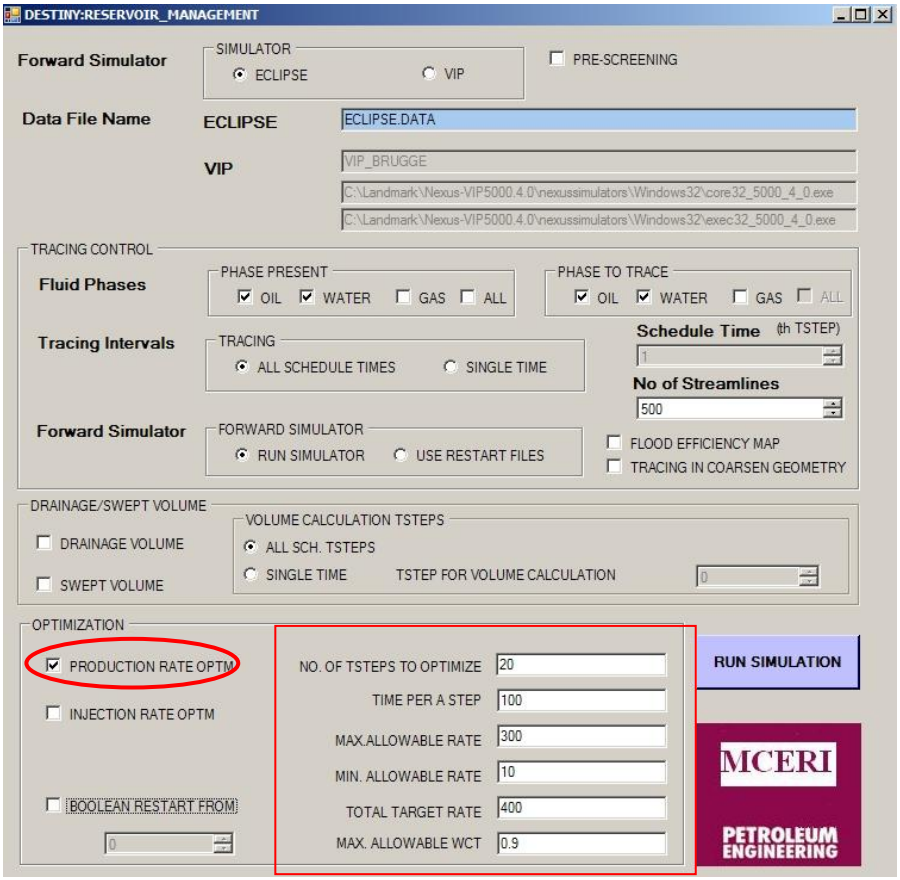

Fig. A. 34 Example of Production rate optimization setting

Importantly, it is noted that we need an input file, a schedule file where we update schedule as optimization proceeds. In specific, it should be 'sch.dat' as file name where there are included file names. The example of 'sch.dat' file is below.

Example of ‘sch.dat’:

INCLUDE

tstep.dat0/

/

As a result, we can check optimized model results showing maximized sweep efficiency and increased oil recovery.

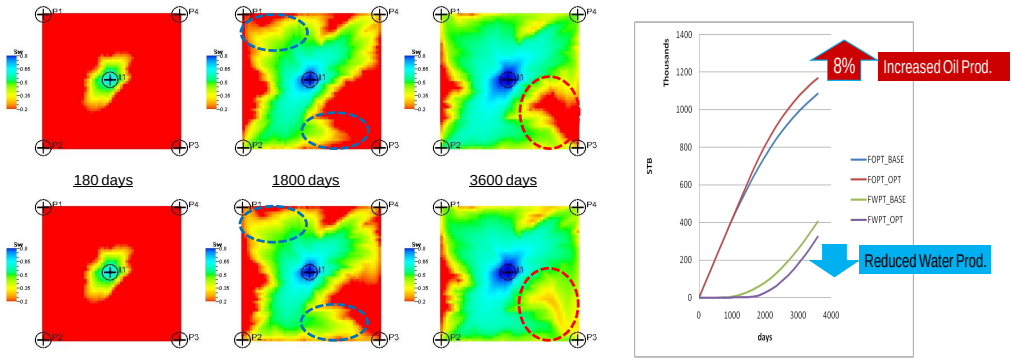

Fig. A. 35 Increased sweep efficiency; base (top) and optimized (bottom), Cumulative oil and water production (right)

- **Application (4): Injection rate optimization**. Following setting example shows how to set the injection rate optimization for a synthetic model.

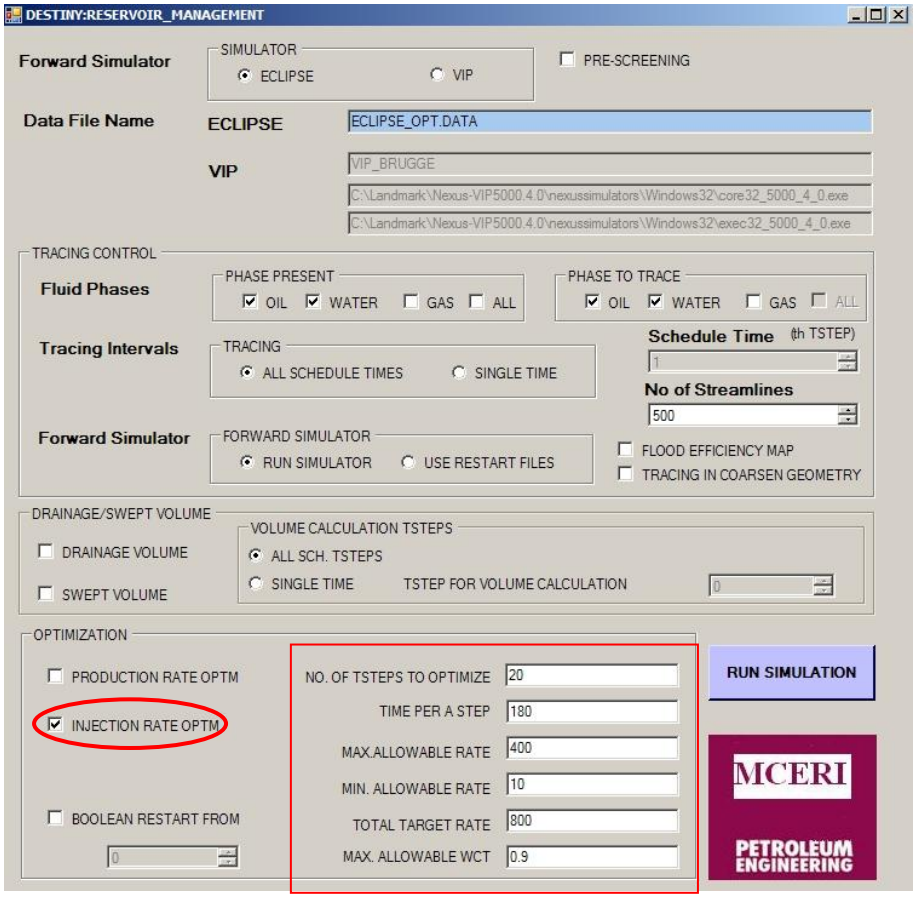

Fig. A. 36 Example setting for injection rate optimization

We check ‘Injection rate optimization’ and enter the values required in the right. Then click the ‘Run Simulation’ and we will see DESTINY reservoir management module run and then we find updated results. This injection optimization needs ‘sch.dat’ file as same as it is used in production rate optimization. The figure below shows the example for injection rate optimization for the model that has 9 producers and 4 injectors.

Increased sweep efficiency and improved oil recovery can be found using saturation displacement and production data.

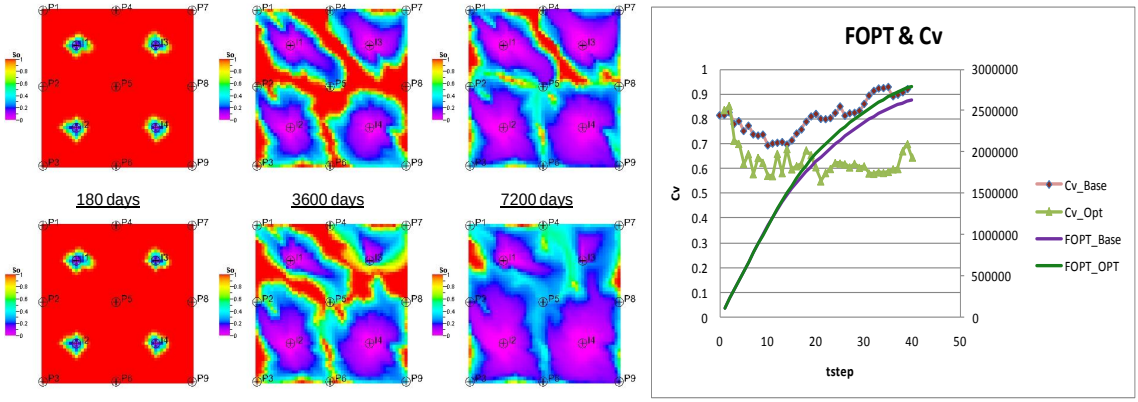

Fig. A. 37 Increased sweep efficiency (Left): base(top) and optimized(bottom), Cumulative oil production (right)

A.6 Simulator data file setting: Necessary keywords to run DESTINY

Followings show how to set simulator (ECLIPSE) keywords needed to run DESTINY. Because DESTINY reads the necessary information from the restart file and summary files of the forward simulator, it is important to include specific keywords in the forward simulation setting.

A.6.1 ECLIPSE Settings for Tracing

SECTION	EECLIPSE SETTING	REASON
SOLUTION	RPTSOL 'RESTART=2' /	Print output to the Restart files
	REMOVE “UNIFOUT” & “FMTOUT”	Destiny use separate binary file for each time step
SUMMARY	WOPR / WGPR / WWPR / WOPT / WWPT /	Read production rate base on tracing phase
SCHEDULE	RPTRST 'BASIC=2' FLOWS PRESSURE ALLPROPS/	Control restart file written data for computation

A.6.2 ECLIPSE Settings for Inversion (History Matching)

SECTION	EECLIPSE SETTING	REASON
GRID	INCLUDE 'PORO.GRDECL' / INCLUDE 'PERMX.GRDECL' /	Use "INCLUDE" as separate porosity and permeability files for iterative parameter update
SOLUTION	RPTSOL 'RESTART=2' /	Print output to the Restart files
SUMMARY	WOPR / WGPR / WWPR /	Print out production rate base on tracing phase
	WWCT / WWCTH /	Print out water cut data and history for water cut match
	WOPT / WWPT / WGPT / WOPRH / WWPRH / WGPRH /	Print out oil, water and gas production rate
SCHEDULE	RPTRST 'BASIC=2' FLOWS PRESSURE ALLPROPS /	Control restart file written data for computation
	WCONHIST P1 1* LRAT 69.87 559.09 1* / P2 1* LRAT 168.62 460.34 1* / P3 1* LRAT 163.53 465.43 1* / P4 1* LRAT 628.97 0 1* / / WCONINJH I1 WATER 1* 2515.92 / /	Use "WCONHIST" for production target and "WCONINJH" for injection target instead of "WCONPROD" and "WCONINJ" for history match. DESTINY use history target.

A.6.3 ECLIPSE Settings for Reservoir Management

SECTION	EECLIPSE SETTING	REASON
SOLUTION	RPTSOL 'RESTART=2' /	Print output to the Restart files
	REMOVE “UNIFOUT” & “FMTOUT”	Destiny use separate binary file for each time step
SUMMARY	WOPR / WGPR / WWPR / WOPT / WWPT /	Read production rate base on tracing phase
SCHEDULE	RPTRST 'BASIC=2' FLOWS PRESSURE ALLPROPS/	Control restart file written data for computation
OTHERS	Need to prepare ‘sch.dat’ for rate optimization Need to prepare’tstep.dat0’ for rate optimization	Update rate schedule from base schedule data

A.7 Acknowledgement to Previous Developers

I would like to take this opportunity to express my thanks to previous DESTINY developers, especially Eduardo Jimenez, Jonguk Kim, and Jichao Yin.

VITA

Name: Han-Young Park

Address: 3116 TAMU – 701 Richardson Building, College Station, TX77843-3116

Email: tamupe10park@gmail.com

Education: B.S., Mineral & Petroleum Engineering, Hanyang University, Seoul, Korea, February 1996

M.S., Petroleum Engineering, Texas A&M University, College Station, Texas, USA, May 2008

Ph.D., Petroleum Engineering, Texas A&M University, College Station, TX, USA, August 2012